

REPORT DOCUMENTATION PAGE			Form Approved OMB NO. 0704-0188		
<p>The public reporting burden for this collection of information is estimated to average 1 hour per response, including the time for reviewing instructions, searching existing data sources, gathering and maintaining the data needed, and completing and reviewing the collection of information. Send comments regarding this burden estimate or any other aspect of this collection of information, including suggestions for reducing this burden, to Washington Headquarters Services, Directorate for Information Operations and Reports, 1215 Jefferson Davis Highway, Suite 1204, Arlington VA, 22202-4302. Respondents should be aware that notwithstanding any other provision of law, no person shall be subject to any penalty for failing to comply with a collection of information if it does not display a currently valid OMB control number. PLEASE DO NOT RETURN YOUR FORM TO THE ABOVE ADDRESS.</p>					
1. REPORT DATE (DD-MM-YYYY) 29-03-2015		2. REPORT TYPE Final Report		3. DATES COVERED (From - To) 22-Nov-2010 - 21-Nov-2014	
4. TITLE AND SUBTITLE Final Report: Effect of Protective Devices on Brain Trauma Mechanics Under Idealized Shock Wave Loading			5a. CONTRACT NUMBER W911NF-11-1-0033		
			5b. GRANT NUMBER		
			5c. PROGRAM ELEMENT NUMBER 611102		
6. AUTHORS Ruqiang Feng			5d. PROJECT NUMBER		
			5e. TASK NUMBER		
			5f. WORK UNIT NUMBER		
7. PERFORMING ORGANIZATION NAMES AND ADDRESSES University of Nebraska @ Lincoln Research Grants & Contracts 303 Administration Bldg. Lincoln, NE 68588 -0430			8. PERFORMING ORGANIZATION REPORT NUMBER		
9. SPONSORING/MONITORING AGENCY NAME(S) AND ADDRESS (ES) U.S. Army Research Office P.O. Box 12211 Research Triangle Park, NC 27709-2211			10. SPONSOR/MONITOR'S ACRONYM(S) ARO		
			11. SPONSOR/MONITOR'S REPORT NUMBER(S) 59191-EG.16		
12. DISTRIBUTION AVAILABILITY STATEMENT Approved for Public Release; Distribution Unlimited					
13. SUPPLEMENTARY NOTES The views, opinions and/or findings contained in this report are those of the author(s) and should not be construed as an official Department of the Army position, policy or decision, unless so designated by other documentation.					
14. ABSTRACT As an effort to study the effect of primary blast on soldiers, the use of shock tube for blast testing has been evaluated experimentally. An instrumented head form with or without helmets was subjected to two blast loading conditions: a) that generated by live-fire free-field blasts, and b) that simulated using the shock tubes at the University of Nebraska-Lincoln (UNL). Surface pressures and center-of-gravity acceleration components were measured and compared for the loading conditions realized in this project. The results show that the live-fire blast loading condition can be simulated reasonably well with the blast loading generated inside UNL 28 inch shock					
15. SUBJECT TERMS Blast loading; Free field blast test; Shock tube blast test; Dummy head; Head gear; Pressure and acceleration measurements					
16. SECURITY CLASSIFICATION OF:		17. LIMITATION OF ABSTRACT	15. NUMBER OF PAGES	19a. NAME OF RESPONSIBLE PERSON	
a. REPORT	b. ABSTRACT			c. THIS PAGE	Ruqiang Feng
UU	UU	UU		19b. TELEPHONE NUMBER	
				402-472-2384	

Report Title

Final Report: Effect of Protective Devices on Brain Trauma Mechanics Under Idealized Shock Wave Loading

ABSTRACT

As an effort to study the effect of primary blast on soldiers, the use of shock tube for blast testing has been evaluated experimentally. An instrumented head form with or without helmets was subjected to two blast loading conditions: a) that generated by live-fire free-field blasts, and b) that simulated using the shock tubes at the University of Nebraska-Lincoln (UNL). Surface pressures and center-of-gravity acceleration components were measured and compared for the loading conditions realized in this project. The results show that the live-fire blast loading condition can be simulated reasonably well with the blast loading generated inside UNL 28-inch shock tube. Using the test data, the effects of loading orientation and state of protection (with or without helmets) have been studied quantitatively. The deficiencies of simulating blast loading outside a shock tube have been identified. Finally, the acceleration components related to the large post-blast head form motion observed visually in shock tube testing have been examined. The resultant dynamic effect has been found to be non-impulsive and insignificant compared to that of the primary blast loading.

Enter List of papers submitted or published that acknowledge ARO support from the start of the project to the date of this printing. List the papers, including journal references, in the following categories:

(a) Papers published in peer-reviewed journals (N/A for none)

Received

Paper

- 01/09/2014 11.00 S. Ganpule, A. Alai, E. Plougonven, N. Chandra. Mechanics of blast loading on the head models in the study of traumatic brain injury using experimental and computational approaches, *Biomechanics and Modeling in Mechanobiology*, (07 2012): 0. doi: 10.1007/s10237-012-0421-8
- 01/09/2014 9.00 Linxia Gu, Mehdi S. Chafi, Shailesh Ganpule, Namas Chandra. The influence of heterogeneous meninges on the brain mechanics under primary blast loading, *Composites Part B: Engineering*, (12 2012): 0. doi: 10.1016/j.compositesb.2012.04.014
- 01/09/2014 14.00 Maciej Skotak, Fang Wang, Namas Chandra. An in vitro injury model for SH-SY5Y neuroblastoma cells: Effect of strain and strain rate, *Journal of Neuroscience Methods*, (03 2012): 0. doi: 10.1016/j.jneumeth.2012.01.001
- 01/09/2014 12.00 N. Chandra, S. Ganpule, N. N. Kleinschmit, R. Feng, A. D. Holmberg, A. Sundaramurthy, V. Selvan, A. Alai. Evolution of blast wave profiles in simulated air blasts: experiment and computational modeling, *Shock Waves*, (07 2012): 0. doi: 10.1007/s00193-012-0399-2
- 01/09/2014 13.00 Veera Selvan, Shailesh Ganpule, Nick Kleinschmit, Namas Chandra. Blast Wave Loading Pathways in Heterogeneous Material Systems—Experimental and Numerical Approaches, *Journal of Biomechanical Engineering*, (05 2013): 0. doi: 10.1115/1.4024132

TOTAL: 5

Number of Papers published in peer-reviewed journals:

(b) Papers published in non-peer-reviewed journals (N/A for none)

Received

Paper

TOTAL:

(c) Presentations

1. Following papers were presented in National Neurotrauma Meeting and appeared as abstracts in two journals.

1) A PORCINE MODEL OF PRIMARY BLAST-INDUCED TBI: NEUROPATHOLOGICAL COMPARISONS TO HEAD ROTATIONAL ACCELERATION INDUCED TRAUMA

DK Cullen, M Skotak, C Mietus, J Frasca, F Wang, K Browne, DH Smith, N Chandra
JOURNAL OF NEUROTRAUMA 30 (15), A60-A61, 2013

2) THE ALTERATIONS OF THE CORTICAL PROTEOME IN THE RODENT MODEL OF PRIMARY BLAST TBI

M Skotak, F Wang, R Nandakumar, N Chandra
JOURNAL OF NEUROTRAUMA 30 (15), A86-A87, 2013

3) PRIMARY BLAST INDUCED OXIDATIVE AND NITROSATIVE STRESS CAUSES CEREBROVASCULAR INFLAMMATION IN ANIMAL MODEL OF MILD TRAUMATIC BRAIN INJURY

M Skotak, PM Abdul-Muneer, H Schuetz, F Wang, N Chandra, J Haorah
JOURNAL OF NEUROTRAUMA 30 (15), A142-A143, 2013

4) DO PRIMARY BLAST-SHOCK WAVES CAUSE MILD TBI? EXPERIMENTAL EVIDENCE BASED ON ANIMAL MODELS AND HUMAN CADAVERIC HEADS

N Chandra, M Skotak, F Wang, SG Ganpule, J Haorah
JOURNAL OF NEUROTRAUMA 30 (15), A80-A80, 2013

5) MECHANICS OF BLAST LOADING ON POST-MORTEM HUMAN HEADS IN THE STUDY OF TRAUMATIC BRAIN INJURY (TBI) USING EXPERIMENTAL AND COMPUTATIONAL APPROACHES

SG Ganpule, N Chandra, R Salzar
JOURNAL OF NEUROTRAUMA 30 (15), A124-A124, 2013

6) MECHANICAL STRETCH EXACERBATES THE OUTCOME IN CELLS EXPOSED TO ENVIRONMENTAL NEUROTOXINS: MITOCHONDRIAL DYSFUNCTION AND OXIDATIVE STRESS

F Wang, RF Cruz, M Skotak, N Chandra
JOURNAL OF NEUROTRAUMA 30 (15), A175-A176, 2013

7) MOUSE MODEL OF MILD TRAUMATIC BRAIN INJURY CAUSED BY AIR-BLAST WITH ULTRA-LONG-TERM ABNORMALITIES IN NEURONAL CHLORIDE AND SOCIAL AND EMOTIONAL BEHAVIOR

K Berglund, M Skotak, F Wang, N Chandra, W Liedtke
JOURNAL OF NEUROTRAUMA 30 (15), A44-A45, 2013

8) Shock loading-induced Traumatic Brain Injuries in animal models-experimental and computational studies

N Chandra, R Gupta
BRAIN INJURY 26 (4-5), 415-415, 2013

2. S. Ganpule, Y. Hua, L. Gu, N. Chandra, " Evaluation of Blast Mitigation Strategies for Taumatic Brain Injury," Proceedings of ICCE-20, the 20th Annual International Conference on Composites/Nano Engineering, Beijing, China, July 2012

Number of Presentations: 12.00

Non Peer-Reviewed Conference Proceeding publications (other than abstracts):

<u>Received</u>	<u>Paper</u>
07/27/2012 1.00	M. Nienaber, J. Lee, R. Feng , J. Lim. The Effects of Impulsive Pressurization on Human Neuronal Cell Viability and Neurite Length, 2011 BMES conference. 12-OCT-11, . . . ,
07/27/2012 2.00	J. Lim, J. Lee, I. Poudel. Neuronal Cell Patterning Using Micro-Contact Printing, 2011 BMES conference. 12-OCT-11, . . . ,
07/27/2012 3.00	S. Higgins, J. Lee, J. Lim. Mechanical Induction of SH-SY5Y Cell Neurogenesis, 2011 BMES conference. 12-OCT-11, . . . ,
TOTAL:	3

Number of Non Peer-Reviewed Conference Proceeding publications (other than abstracts):

Peer-Reviewed Conference Proceeding publications (other than abstracts):

<u>Received</u>	<u>Paper</u>
-----------------	--------------

TOTAL:

Number of Peer-Reviewed Conference Proceeding publications (other than abstracts):

(d) Manuscripts

<u>Received</u>	<u>Paper</u>
07/27/2012	6.00 Maciej Skotak, Fang Wang, Namas Chandra. An in vitro injury model for SH-SY5Y neuroblastoma cells: Effect of strain and strain rate, Journal of Neurotrauma (01 2012)
07/27/2012	7.00 L. Gub, S. Ganpule, A. Alai, N. Chandra. Role of helmet in the mechanics of shock wave propagation under blast loading conditions, Computer Methods in Biomechanics and Biomedical Engineering (06 2011)
07/27/2012	8.00 MEHDI S. CHAFI, SHAILESH GANPULE, LINXIA GU, NAMAS CHANDRA. DYNAMIC RESPONSE OF BRAIN SUBJECTED TO BLASTLOADINGS: INFLUENCE OF FREQUENCY RANGES, International Journal of Applied Mechanics (08 2011)
07/27/2012	4.00 Ishwari Poudel, Jeong Soon Lee, Li Tan, Jung Yul Lim. Micropatterning-retinoic acid co-control of neuronal cell morphology and neurite outgrowth, Acta Biomaterialia (10 2011)
07/27/2012	5.00 Matthew Nienaber, Jeong Soon Lee, Ruqiang Feng, Jung Yul Lim. Ishwari Poudel, Jeong Soon Lee, Li Tan, Jung Yul Lim, Journal of Visualized Experiments (12 2011)
TOTAL:	5

Number of Manuscripts:

Books

Received Book

TOTAL:

Received

Book Chapter

TOTAL:

Patents Submitted

Patents Awarded

Awards

Graduate Students

<u>NAME</u>	<u>PERCENT SUPPORTED</u>	<u>Discipline</u>
Kurtis Palu	1.00	
Shailesh Ganpule	0.50	
Aravind Sundaramurthy	0.50	
FTE Equivalent:	2.00	
Total Number:	3	

Names of Post Doctorates

<u>NAME</u>	<u>PERCENT SUPPORTED</u>
FTE Equivalent:	
Total Number:	

Names of Faculty Supported

<u>NAME</u>	<u>PERCENT SUPPORTED</u>	<u>National Academy Member</u>
Namas Chandra	0.08	
FTE Equivalent:	0.08	
Total Number:	1	

Names of Under Graduate students supported

<u>NAME</u>	<u>PERCENT SUPPORTED</u>	Discipline
Steve Gloor	0.50	Mechanical Engineering
FTE Equivalent:	0.50	
Total Number:	1	

Student Metrics

This section only applies to graduating undergraduates supported by this agreement in this reporting period

The number of undergraduates funded by this agreement who graduated during this period: 1.00

The number of undergraduates funded by this agreement who graduated during this period with a degree in science, mathematics, engineering, or technology fields:..... 1.00

The number of undergraduates funded by your agreement who graduated during this period and will continue to pursue a graduate or Ph.D. degree in science, mathematics, engineering, or technology fields:..... 0.00

Number of graduating undergraduates who achieved a 3.5 GPA to 4.0 (4.0 max scale):..... 0.00

Number of graduating undergraduates funded by a DoD funded Center of Excellence grant for Education, Research and Engineering:..... 0.00

The number of undergraduates funded by your agreement who graduated during this period and intend to work for the Department of Defense 0.00

The number of undergraduates funded by your agreement who graduated during this period and will receive scholarships or fellowships for further studies in science, mathematics, engineering or technology fields:..... 0.00

Names of Personnel receiving masters degrees

<u>NAME</u>	
Kurtis Palu	
Total Number:	1

Names of personnel receiving PHDs

<u>NAME</u>	
Ssilesh Granpule	
Aravind Sundaramurthy	
Total Number:	2

Names of other research staff

<u>NAME</u>	<u>PERCENT SUPPORTED</u>
Aaron Alai	1.00
FTE Equivalent:	1.00
Total Number:	1

Sub Contractors (DD882)

Inventions (DD882)

Scientific Progress

See attachment.

Technology Transfer

Shock tube design and fabrication details were transferred to Army Test Center in Aberdeen, MD.

2013

ARO/NATICK Final Report

Experimental Evaluation of Measurement Methodology for Primary Blast Loading Conditions

This report summarizes the results of spatial distribution of pressure profiles and linear/rotational accelerations of Realistic Explosion Resistant Dummy (RED) head when subjected to field testing. The RED head was then subjected to similar input profiles within the UNL shock tube, where identical measurements are made at nearly field-relevant conditions and a longer duration pulse. The RED head was also kept outside the shock tube and the same mechanical responses were measured. The effect of helmet was studied. Based on preliminary data, it is shown that the free field data can be simulated within the shock tube for the dummy head without helmet. Furthermore, the effects of helmet on data comparison with field are also illustrated. Finally, to determine the effects of performing tests outside the shock tube is also studied by comparing data with experiments inside the shock tube with long and short time duration profiles.

Submitted by:

Namas Chandra, Ph, D, P.E.
University of Nebraska-Lincoln
(NJIT since July 2013)
15 July 2013

ARO Grant:

WF911NF-08-1-0483
WBS: 2511-05001-001

Submitted to:

Dr. Larry Russell, Ph.D.
Army Research Office

Marina Carboni/Michael Maffeo

Contents

1. Introduction..... 2

2 Location of head-form for different configuration: 4

 2.1 28” shock tube..... 4

 2.2 9” shock tube..... 4

3 Instrumentation: 5

4 Incident pressure 7

5 Results and discussion 7

 5.1 Comparison between free-field blast and 28” short duration results 7

 5.1.1 Front bare head facing 7

 5.1.2 Front helmeted head..... 13

 5.2 Comparison between inside (short duration) and outside (D1) the shock tubes..... 20

 5.2.1 Front bare head 21

 5.2.2 Front helmeted head..... 27

 5.3 Comparison between two outside shots at distance D1 and D2..... 29

 5.3.1 Front bare head 29

 5.3.2 Front helmeted head..... 31

 5.4 Comparison between inside (long duration) and outside (D1) the shock tubes..... 32

 5.4.1 Front bare head 32

 5.4.2 Front helmeted head..... 34

6 Summary 35

7 Further reading..... 36

8 Appendix A – Statistical analysis 38

9 Appendix B – Velocity vector field near the exit of the shock tube..... 46

1. Introduction

In this work, the pressure-acceleration response of a well-studied head-neck human surrogate (Realistic Explosion-resistant Dummy, RED head) was evaluated in two different conditions. First, the RED head was subjected to a known live-fire field-testing and second, inside and outside of a shock tube. 11 different pressure measurements on the surface of the surrogate and linear acceleration/angular rate



measurements at the center-of-gravity (C.G.) of the head form were made in each case. In the field, controlled explosions with 4 lbs of C4 designed to produce pure planar blast waves encountered the head-neck human surrogate. Field measurements of pressure and acceleration were made with the surrogate facing towards, backwards, sideways and at an angle to the epicenter. The same specimen was then tested in our specially designed shock tube, appropriate breech conditions. Pressure and acceleration measurements from the surrogate were gathered both inside in a 28” shock tube as well as outside in a 9” shock tube.

While long duration pulses were not performed in the field due to practical reasons, they were produced in the shock tube. The pressure measurements show how the dynamic effects of the shock flow field are affected by both the blast test parameters as well as the geometry of the surrogate.

Table 1. Test matrix corresponding shot number (excluding free field blast).

28" Tube Short Duration (Refer to figure 1)	Shot Numbers
Front Facing Bare (These data were used for pressure analysis and acceleration analysis)	2651-2658
Front Facing Helmeted (Acceleration data were filtered and used to compare to free field)	2660-2665
Back Facing Bare (These data were used for pressure analysis and acceleration analysis)	2666-2672
Back Facing Helmeted (Acceleration data were filtered and used to compare to free field)	2673-2677
Acceleration/ARS mounting block rotated 45 degrees clockwise: Refer to Figure 5	
Front Facing Helmeted	2811-2815
Front Facing Helmeted 30 degrees	2816-2820
Front Facing Bare 30 degrees	2821-2824
Back Facing Helmeted	2825-2829
Side Facing Bare	2905-2908
Side Facing Helmeted	2909-2913
28" Tube Long Duration (Refer to Figure 1)	
Front Facing Bare	2830-2832;2848-2849
Front Facing Helmeted	2850-2854
Front Facing Bare 30 Degrees	2855-2858
Front Facing Helmeted 30 Degrees	2859-2862
Back Facing Bare	2863-2866
Back Facing Helmeted	2867-2870
Side Facing Bare	2872-2875
Side Facing Helmeted	2876-2878;2903-2904
9" Tube Distance 1 (Refer to figure 4)	
Front Facing Bare	2977-2980
Front Facing Helmeted	2981-2986
Back Facing Bare (after looking at the video footage we thought putting the head closer to the muzzle was appropriate)	2987-2991
Back Facing Bare (these data were used for analysis)	3047-3051
Back Facing Helmeted	3052-3056
Front Facing Bare 30 degrees	3057-3060
Front Facing Helmeted 30 degrees	3061;3119-3120
Side Facing Bare	3070-3081
Side Facing Helmeted	3082-3086



9" Tube Distance 2 (Refer to figure 4)	
Front Facing Bare 30 Degrees	3062-3065
Front Facing Helmeted 30 Degrees	3068-3069;3121
Side Facing Bare	3087-3091
Side Facing Helmeted	3092-3096
Back Facing Bare	3100-3104
Back Facing Helmeted	3105-3109
Front Facing Bare	3110-3113
Front Facing Helmeted	3114-3118

The test matrix of the performed experiments in the shock tube is shown in Table 1. A total of 208 (including free field experiments) tests with 14 measurements (11 pressures, 2 accelerations and 1 angular rate) in each test were carried out.

2 Location of head-form for different configuration:

2.1 28" shock tube

Figure 1 shows the location of the head form within the 28" inch shock tube. Location (a) was used for exposing the head to a short duration pulse and location (b) was used for exposing the head to a long duration pulse.

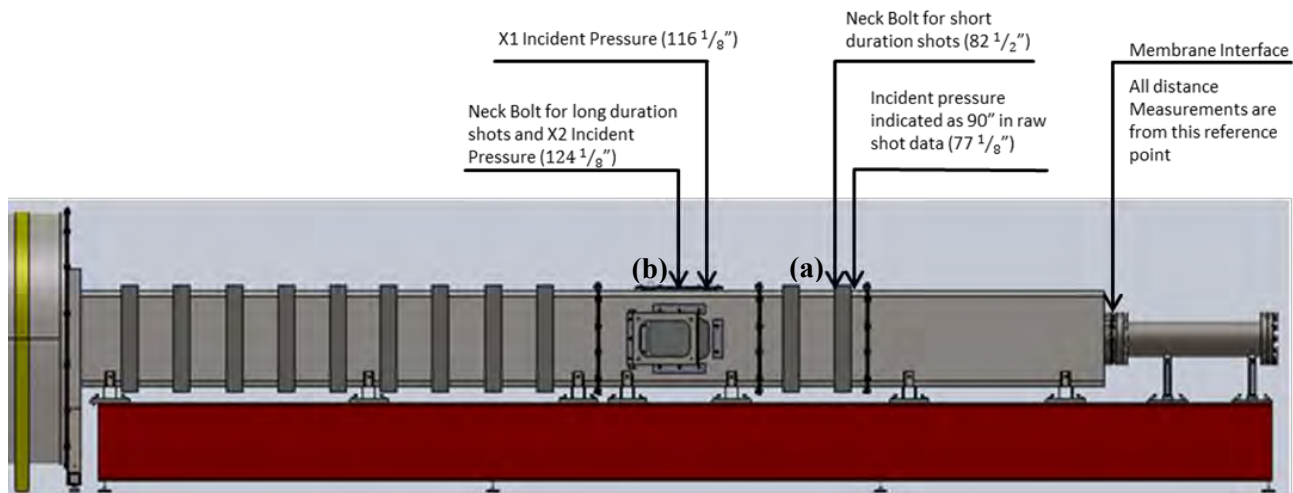


Figure 1 Locations of the head form and incident pressure measurements with respect to the location of the rupturing membranes.

2.2 9" shock tube

Figures 2 and 3 show experimental setup outside the muzzle of the 9" shock tube and the location of the head form on the testing platform just outside the muzzle of the shock tube, respectively. In all cases, the tip of the "nose" of the RED Head was centered with the midline of the 9" tube during all tests. For the 30° orientations at the 9" muzzle, the resting platform was lowered to put the center of the "nose" at the same midline.

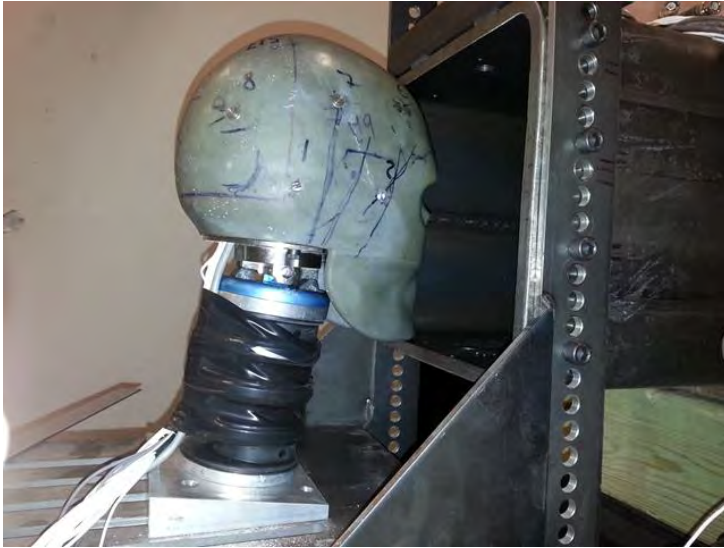


Figure 2. Photo of Red Head at 9" muzzle exit.

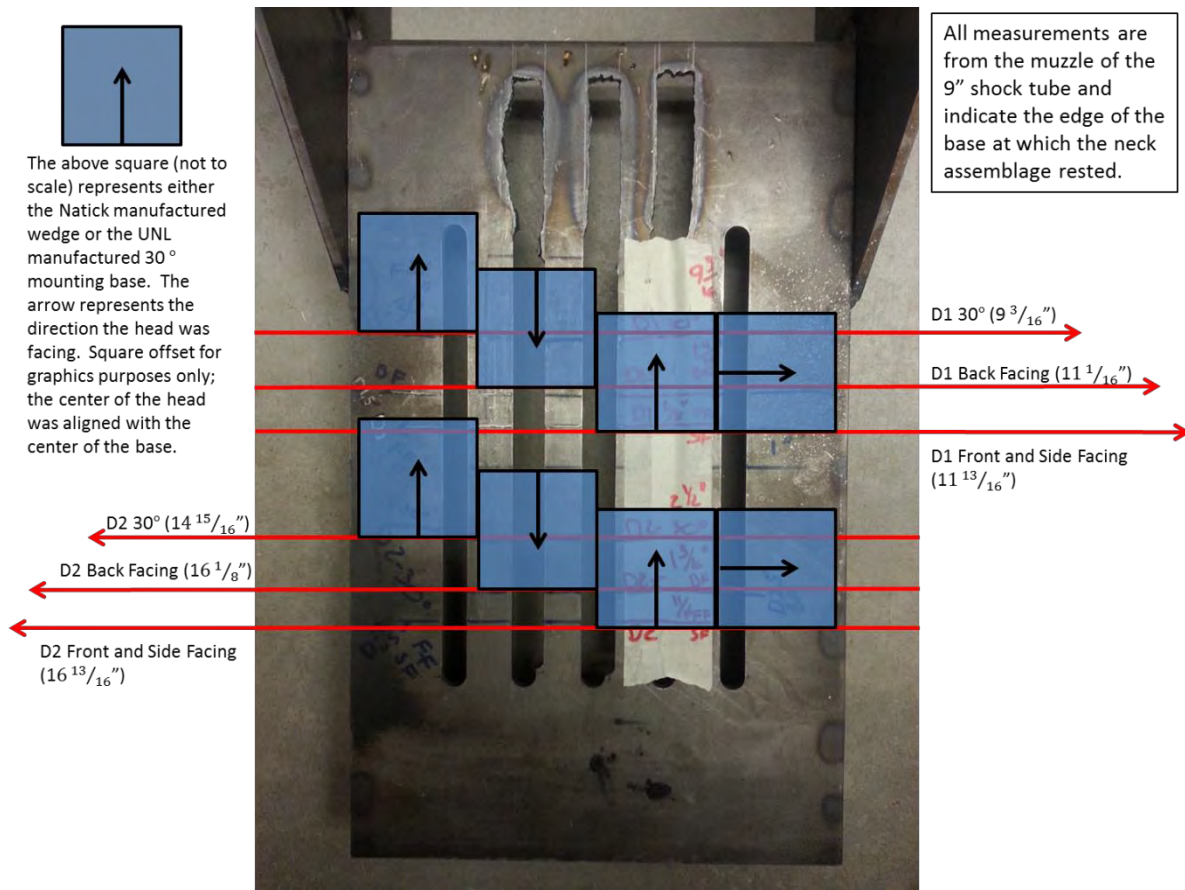


Figure 3 Locations of Red Head mounting bases for 9" tube at both Distance 1 (D1) and Distance 2 (D2).

3 Instrumentation:

The surrogate was instrumented with 11 shock-ready PCB pressure sensors (102B06), 2 linear accelerometers (Endevco 7270a) and 1 angular rate sensors (DTS ARS PRO) mounted to a tri-axial block located at the center of gravity of the 4.5 kg headform.

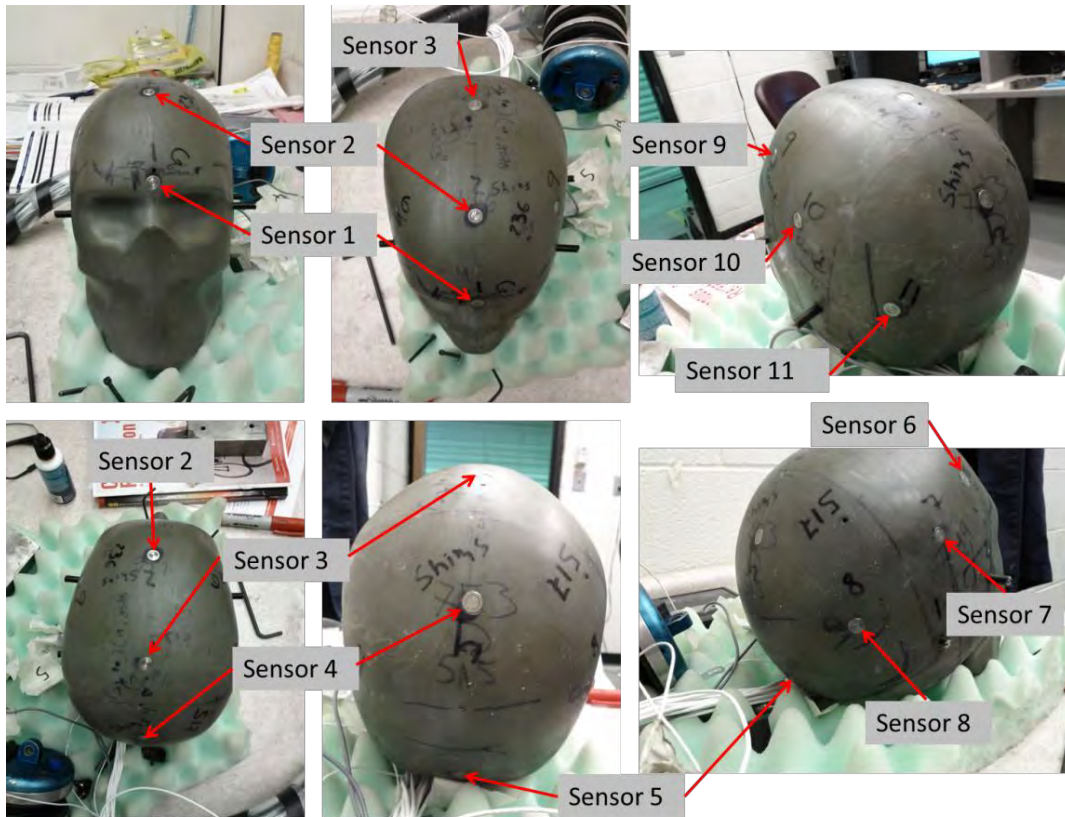
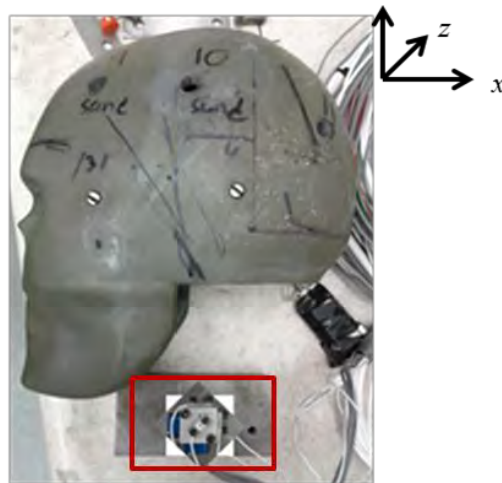


Figure 4. Location and naming convention of pressure transducers on the surface of the Red Head



Accelerometers are mounted on the CG of the dummy head

Figure 5. Locations and naming conventions of linear accelerometers and angular rate sensors placed at the center of gravity of the Red Head .

Figures 4 and 5 show the locations of the pressure transducers on the RED Head and the placement of the linear accelerometers and angular rate sensor respectively. When the head form is helmeted all the sensors except sensor 1 and 5 are covered by the helmet.

4 Incident pressure

Figure 6 shows the incident overpressures recorded in the field as well as in both shock tubes. Incident pressure varied between 25 to 34 psi, with the lowest being recorded in the field experiments.

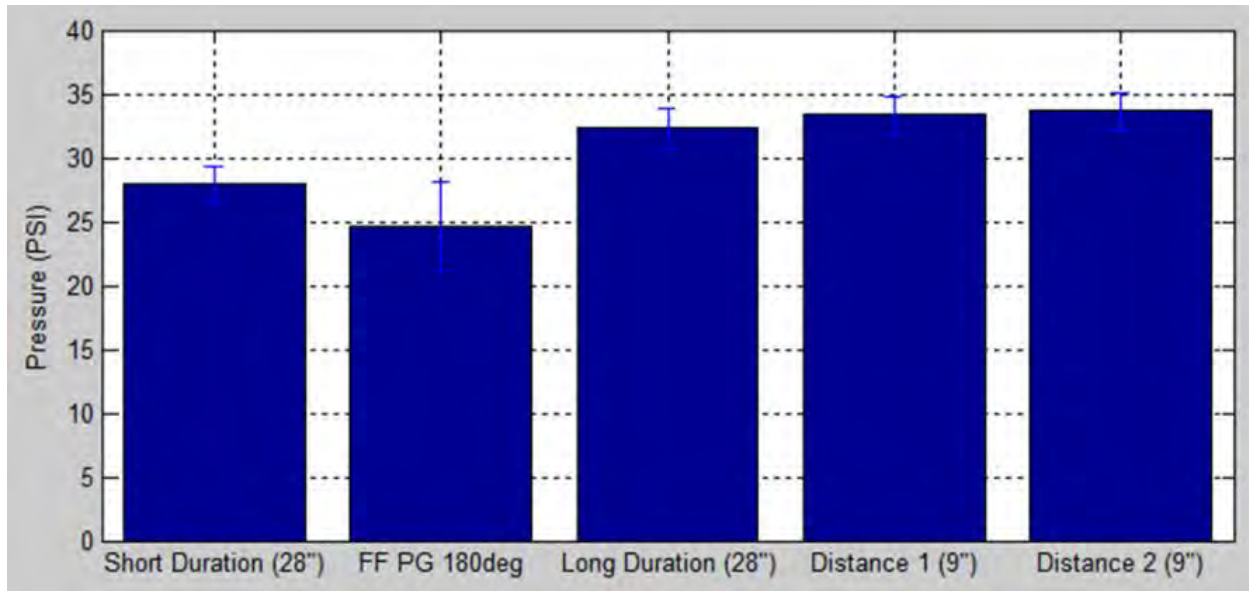


Figure 6. Comparison of the average incident overpressure between free field and shock tube shots

The variation of overpressure within the free-field shots is also high (about 9 psi) compared to shock tube (about 3 psi), which is manifested in the high standard deviation of the free field when compared to the shock tube shots. The measurement of the incident pressure for the 9” shots was taken 1.5” from the open end. Although the incident pressure measured for both D1 and D2 are similar, the pressure experienced by the head would be slightly different due to their difference in the placement location.

5 Results and discussion

5.1 Comparison between free-field blast and 28” short duration results

5.1.1 Front bare head facing

Figure 7 (a) and (b) show the comparison between maximum pressure and linear acceleration between the free-field tests and the tests performed in the 28” shock tube. In terms of magnitude, there is no significant difference between sensor 1, 4 and 11; however, while performing a power analysis on these comparison it was determined that there is a 62%, 68% and 82% chance of type II error respectively. There is a significant difference in the magnitude for all the other cases. Among them sensor 2 has the maximum average difference (17.29 psi) and sensor 7 has the minimum difference (4.87 psi). Except for the sensor location 1 and 11, the overpressure recorded in all the other sensors are higher in the case of shock tube than in the free field (statistical analysis for all sensor locations is given in appendix A).

Z

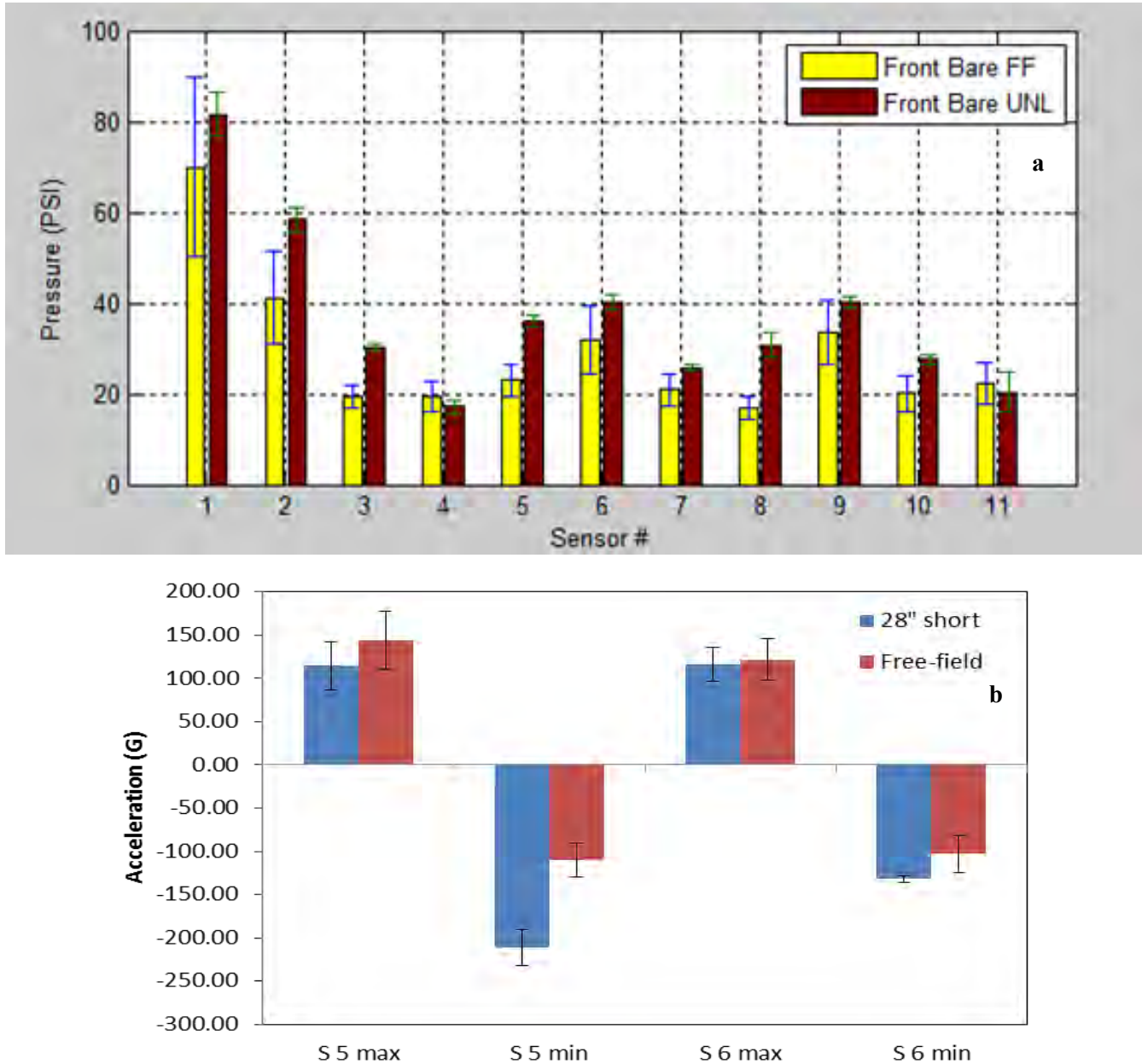
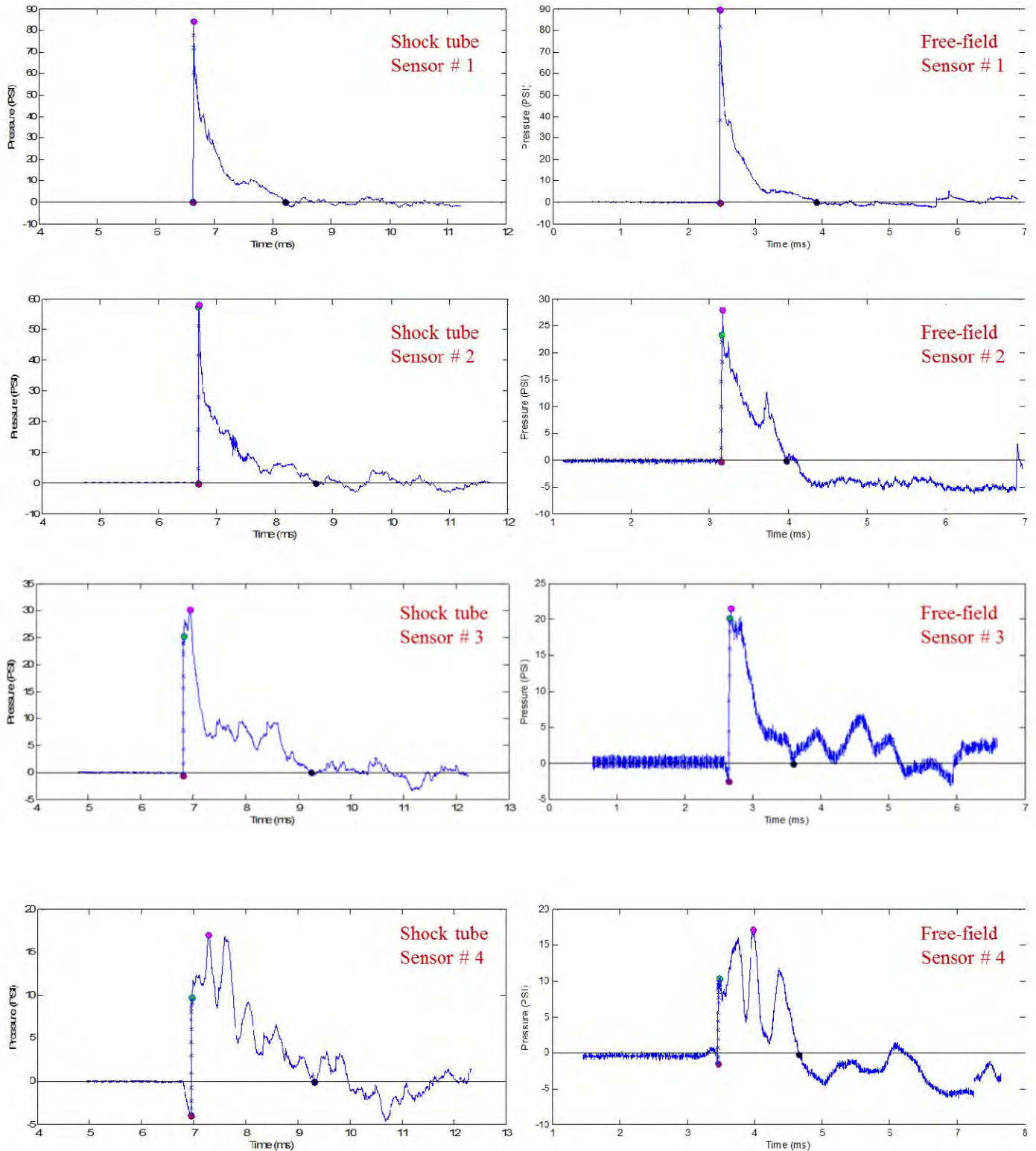


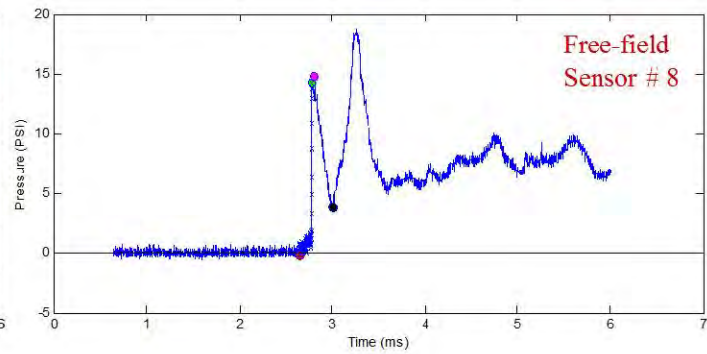
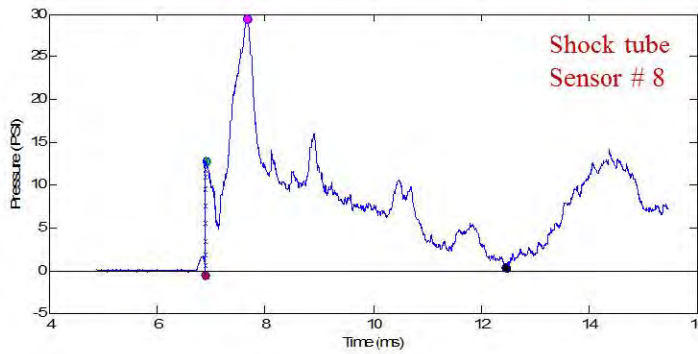
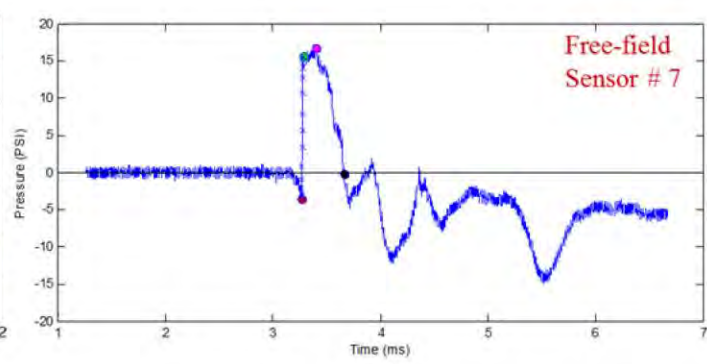
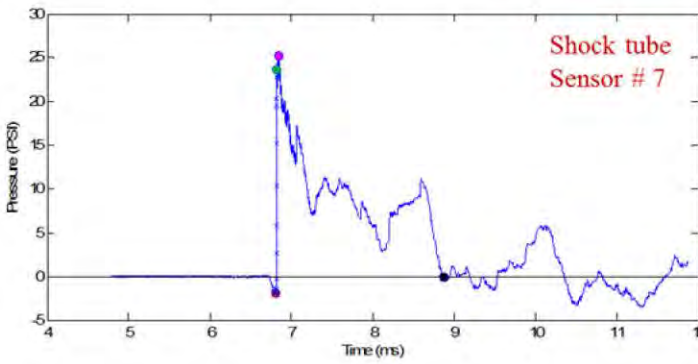
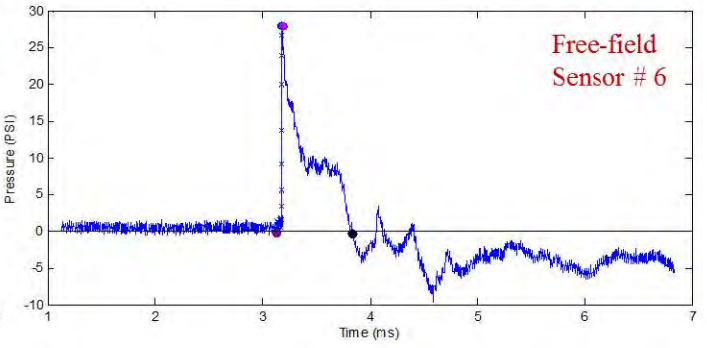
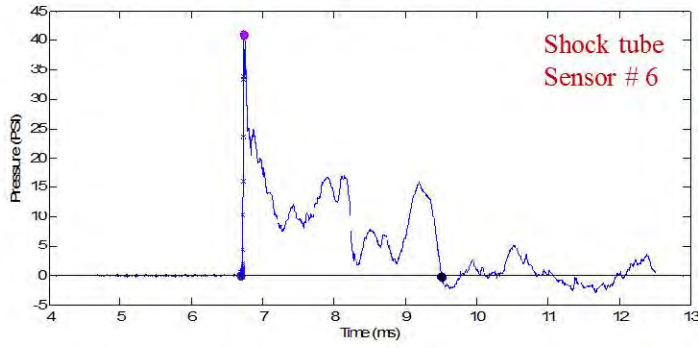
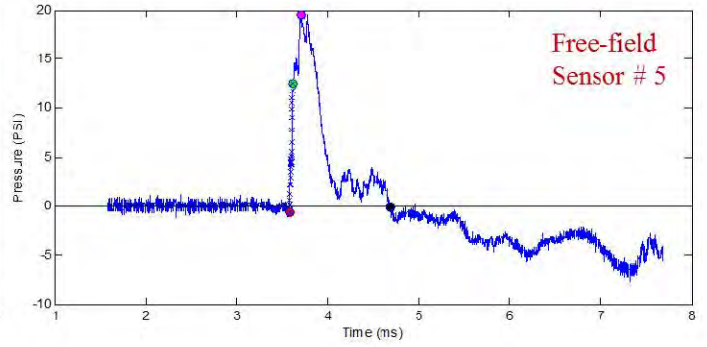
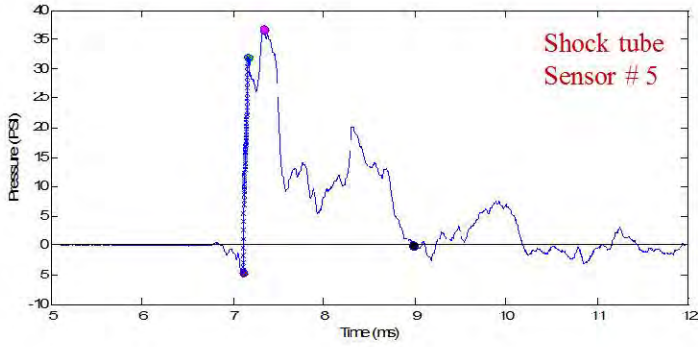
Figure 7 comparisons of (a) overpressure, (b) Minimum and maximum linear acceleration for a front facing bare head in free field and shock tube. The data in blue represent headform response inside of the 28" shock tube, duration of 3ms. Data in yellow and brown represent

Figure 8 shows the pressure profile comparison for the bare head in free field and shock tube. Looking at traces from these sensors there are not many differences in their overall profiles; positive time regions look as though they are also in good agreement. Traces with the most apparent differences are from sensor 10 and even these have similar positive time regions.

Figure 7 (b) shows the peak minimum and maximum acceleration comparisons between shock tube and free field data. From the statistical analysis, it can be seen that there no significant difference in the maximum positive acceleration recorded in sensors 5 and 6 between free field and shock tube. However, power analysis for sensor 5 and 6 proved that the probability of type II error, i.e., miss of an effect is

57% and 92 % respectively. There is a significant difference in the negative acceleration in sensor 5 and 6. In this case, the maximum and minimum in the middle of the trace are not artifacts of the sensor; it is possibly due to the existence of a force being built upon the geometry of the head. Metrics in yellow are taken from the middle of the trace.





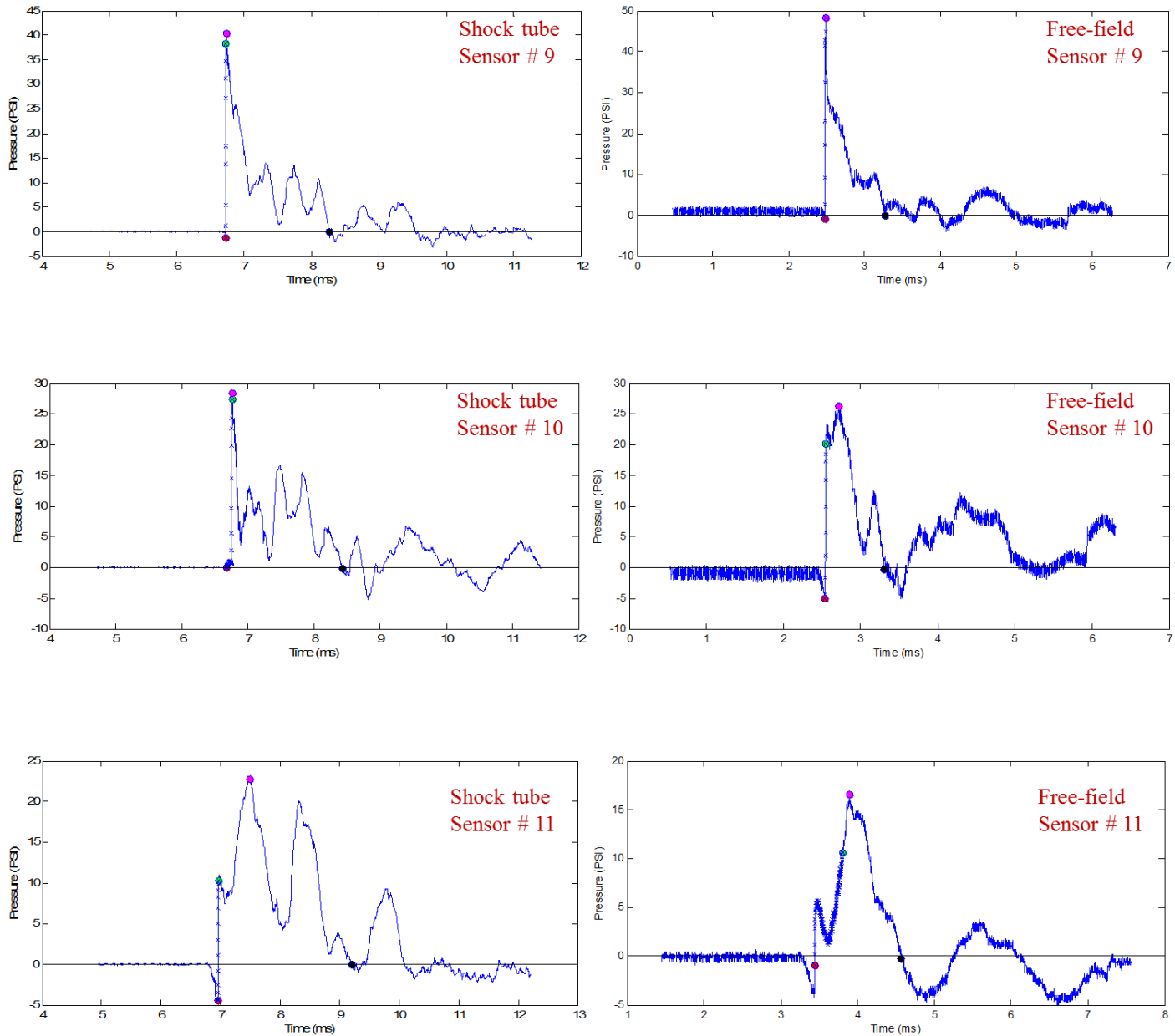


Figure 8. Comparisons between pressure profiles for bare head in free field and 28” short duration shot.

If the first peak of the acceleration, which corresponds to the shock front traverse is considered for comparison, the resulting response appear as shown in figure 9

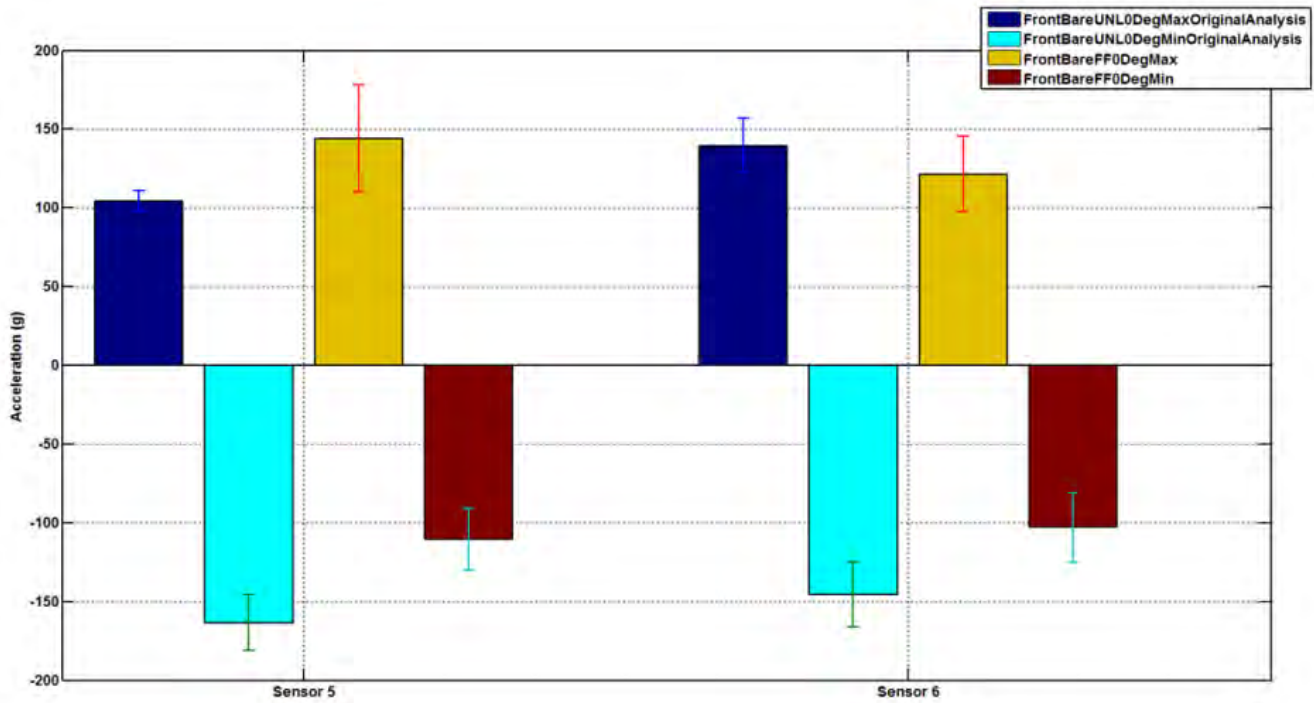


Figure 9. Comparisons of bare front facing orientation between free field and UNL 28” shock tube short duration tests; with peak values derived from the beginning of the trace.

From the analysis in Figure 9, it can be seen that positive acceleration is slightly lower for the peak maximum values from linear accelerometers 5 in the UNL shock tube. Although there is a slight difference in the response of sensor 6 it’s difficult to assign specific causative factors. There are several interesting notes with regard to the overall shapes of the linear accelerometer profiles. In both the free field and in the 28” shock tube for sensor 5, profiles exhibit a sharp rise soon after the time of arrival. Also, if one ignores the first rise in the aforementioned profiles, the time difference between the min and max peaks looks like it is in good agreement with the min value happening ~1.5 ms before the max value (Figure 10).

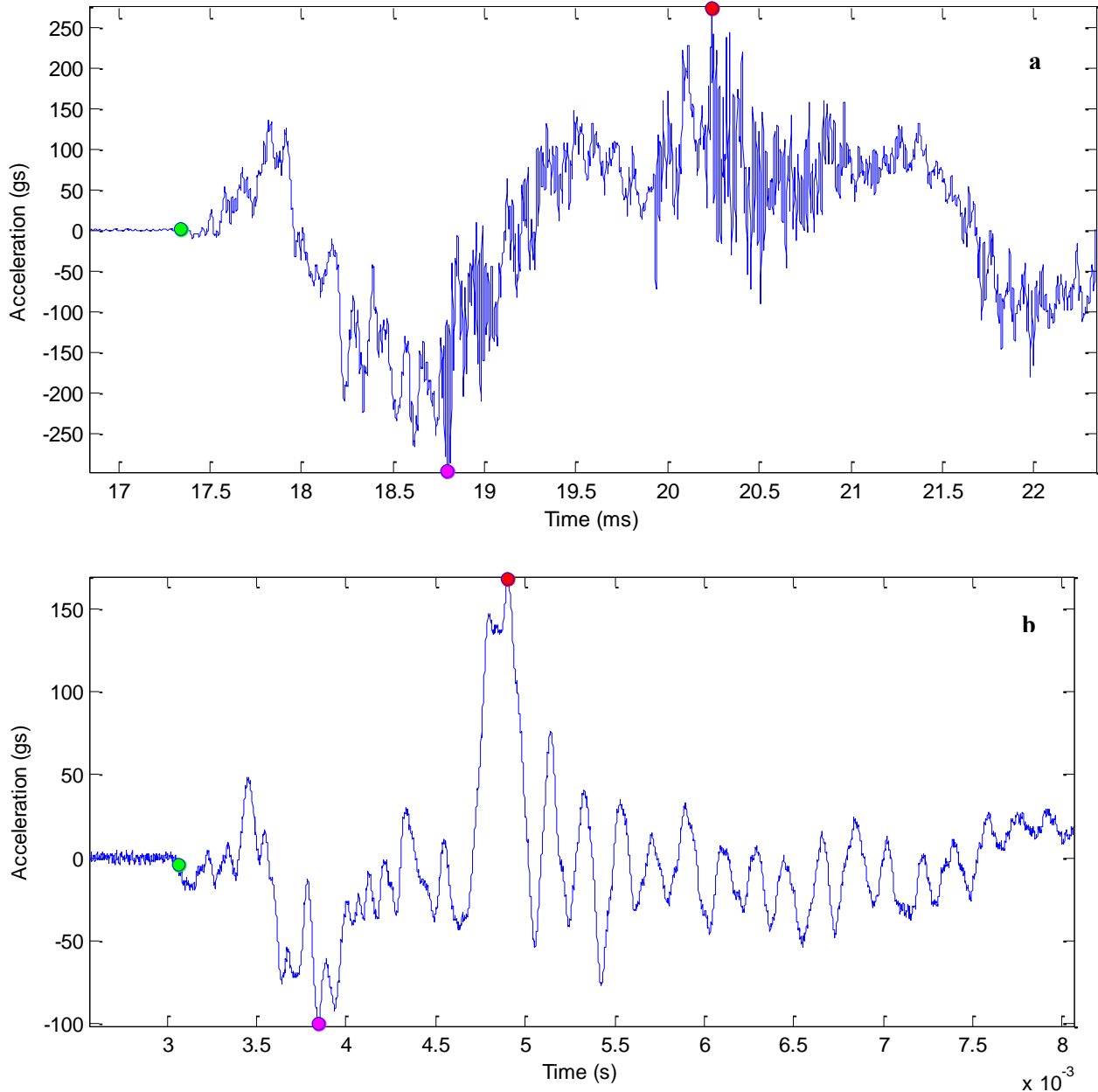


Figure 10. Comparison of acceleration profile for sensor # 5 of bare head, (a) shock tube, (b) field experiment, in this case we can clearly see the existence of maximum value well past the peak acceleration corresponding to the traverse of the shock front.

5.1.2 Front helmeted head

Figure 11 (a) shows the comparison of peak pressure between 28” short and free field when the head is helmeted. It appears that some traces from the free field seem to be attenuated with respect to the 28” shock tube tests. An exception is the response of sensor 1 and 11, in which the free field data looks larger than the UNL shock tube data. From the statistical analysis, it was determined that there is no significant difference in sensors 3, 8 and 10. However, further power analysis showed that there is 88%, 89% and 68% chance of type II error in those results respectively. Among the other sensors, sensor 5 has the maximum difference of 15.88 psi and minimum difference of 4.21 in sensor 4.

An analysis of the free field shock front planarity may be necessary to ensure the planarity of the shock front. In the shock tube, planarity has been measured and validated. Some of the pressure values seem high in the free field helmeted tests when compared to the UNL shock tube tests. This may be due to the potential curvature of the free field shock wave pushing up and underneath the helmet brim, as indicated in the Figure 12.

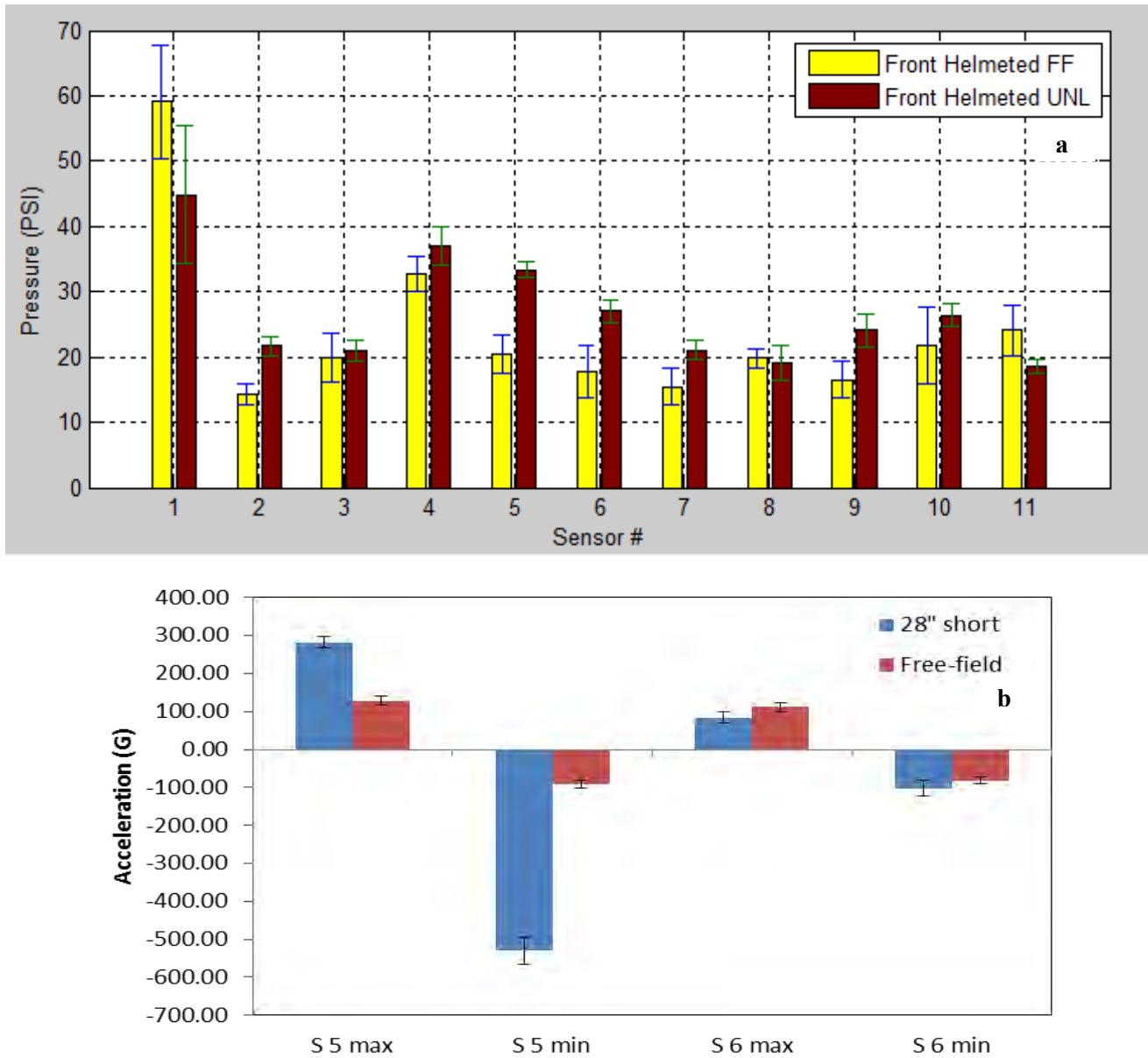


Figure 11 comparisons of (a) maximum overpressure, (b) linear acceleration for a front facing helmeted head in free field and shock tube. All the maximum values of the acceleration were obtained in the first 50 ms, there is a huge difference in the negative acceleration of sensor 5 when compared with the field.

This hypothesis may be further substantiated when looking at the traces from sensor 1 in the free field and in the 28” shock tube (Figure 13). In the free field traces of sensor 1, there is a clean rise often followed by a brief secondary peak, whereas in the 28” tube the data at the peak of the trace from sensor 1 are highly oscillatory indicating that turbulence may be occurring at this localized area. Turbulence

would be expected if the planarity of the shock front had been broken before it interacted with sensor 1 and a smooth rise would be expected if the planarity of the shock front had not been broken before it interacted with sensor 1. There are slight variations in the profiles; however, this variation may be due to several experimental factors like: (a) position of the helmet during the test, (b) variance in the shock front helmet interaction and (c) variance in the free field-testing.

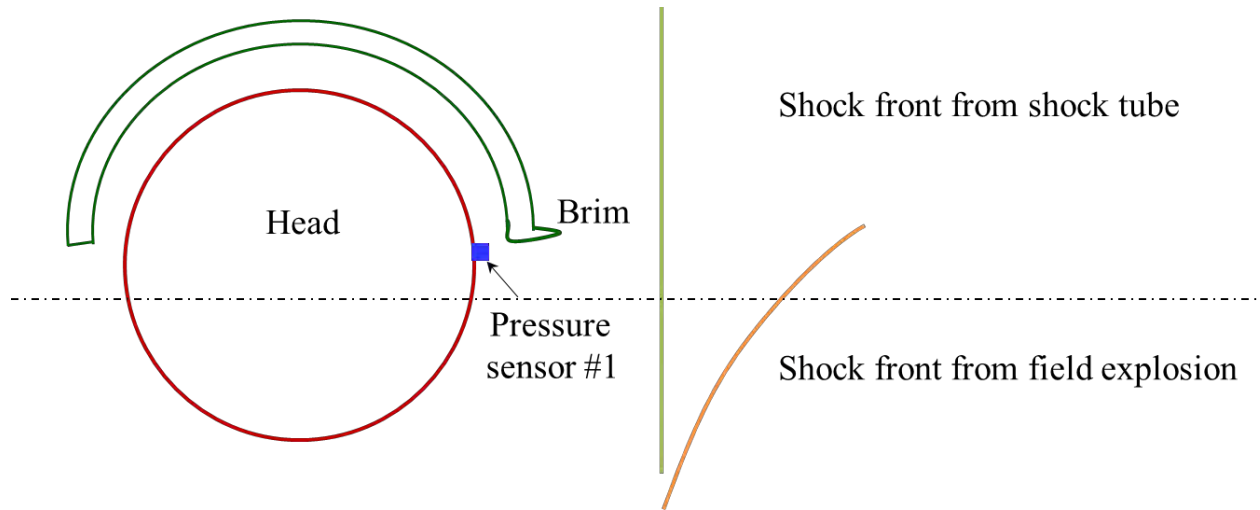
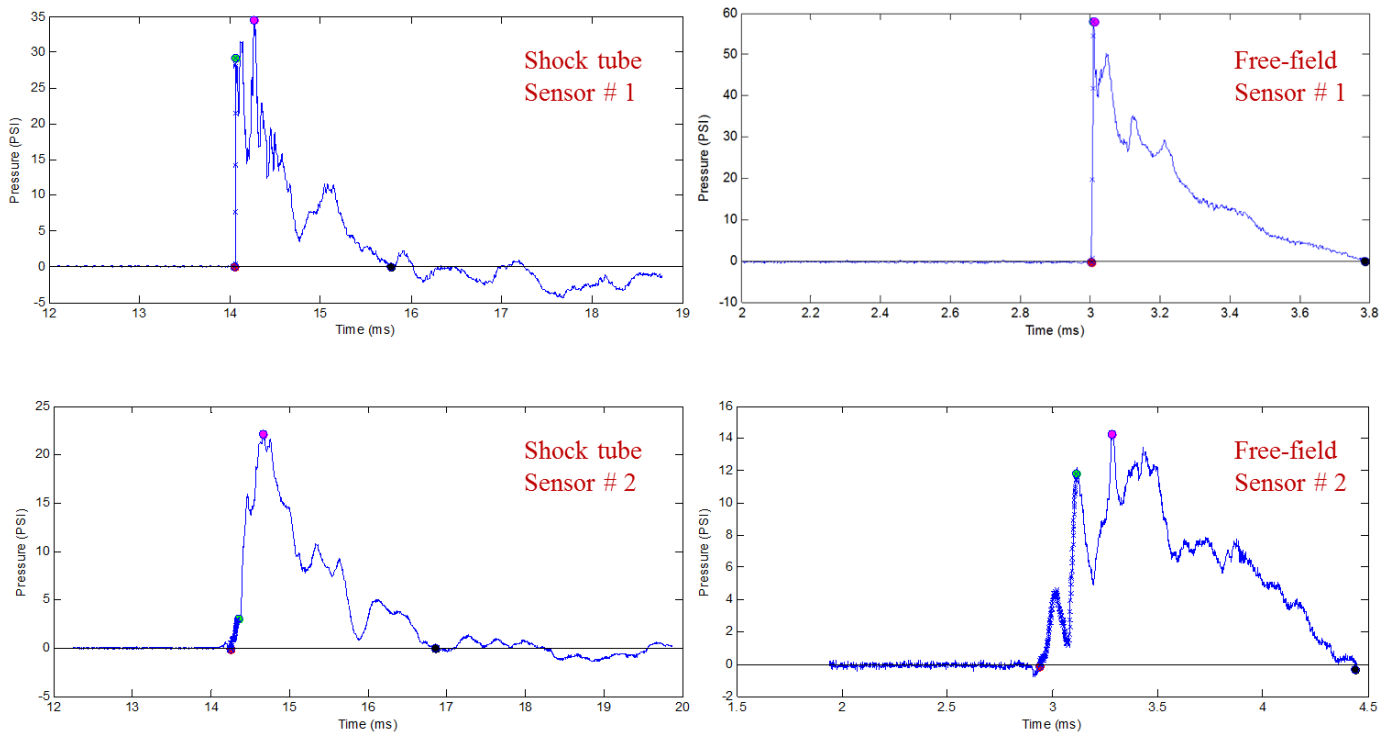
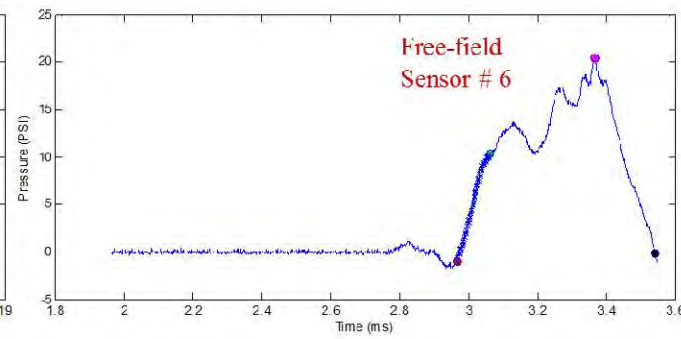
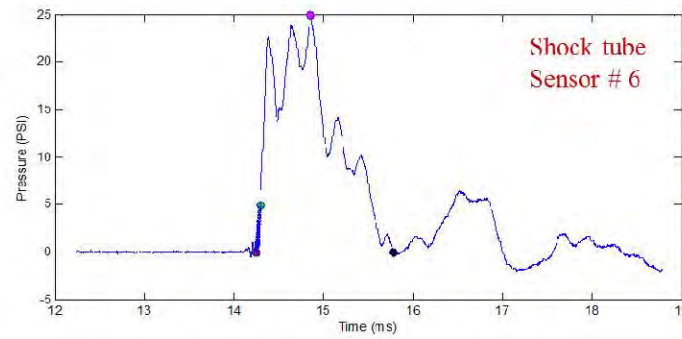
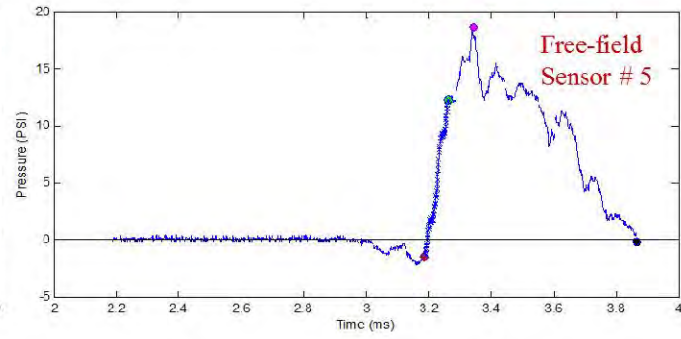
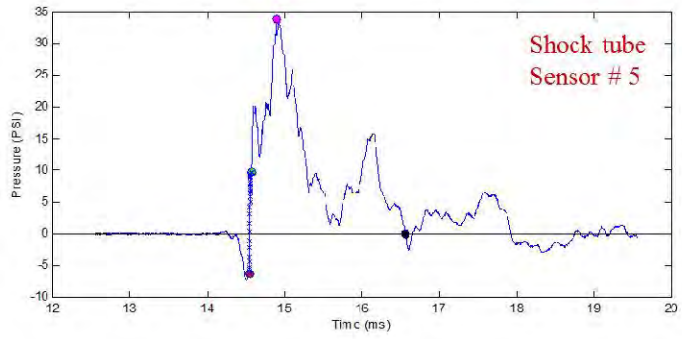
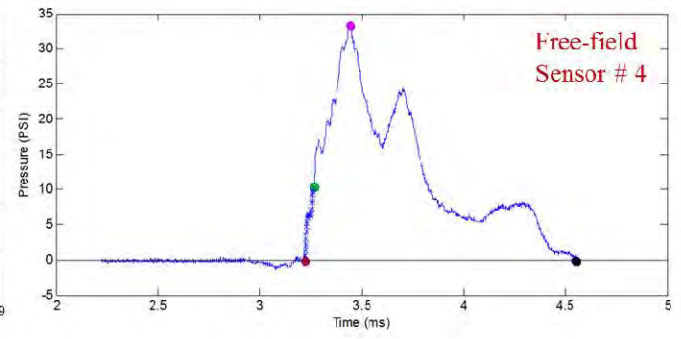
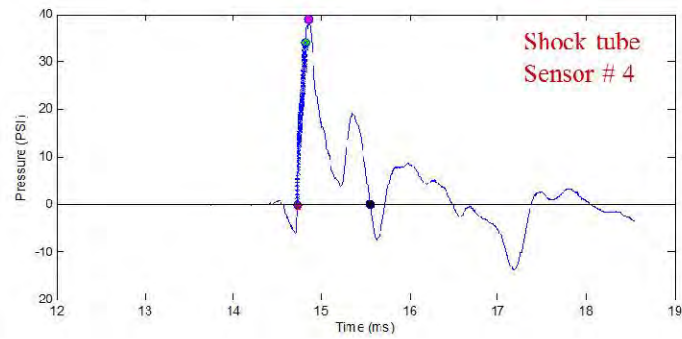
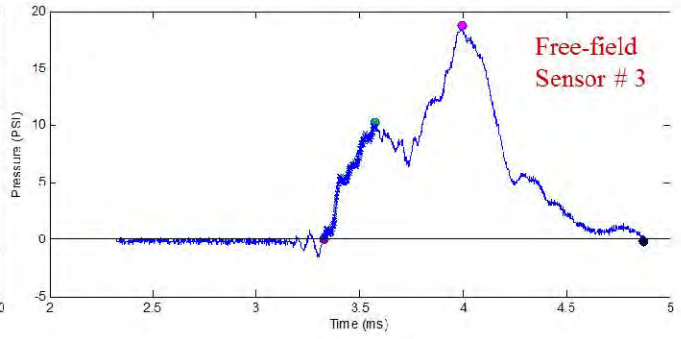
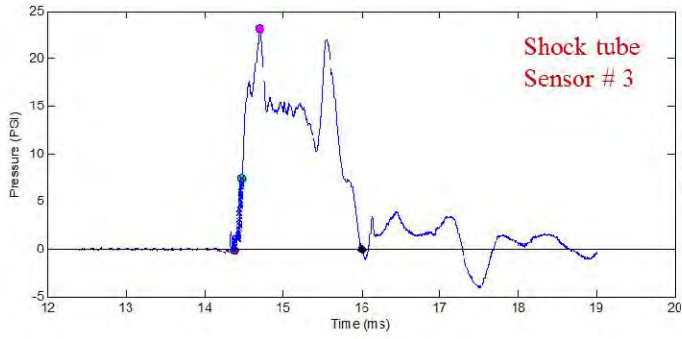
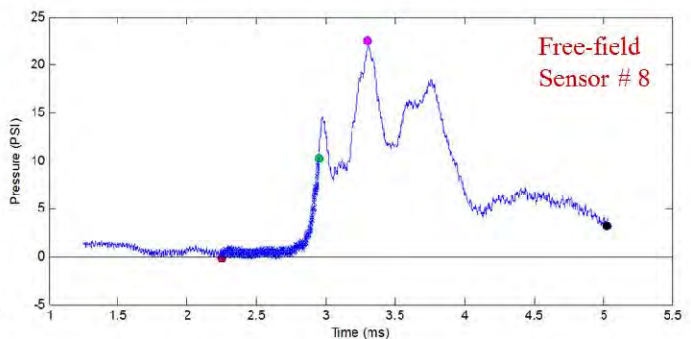
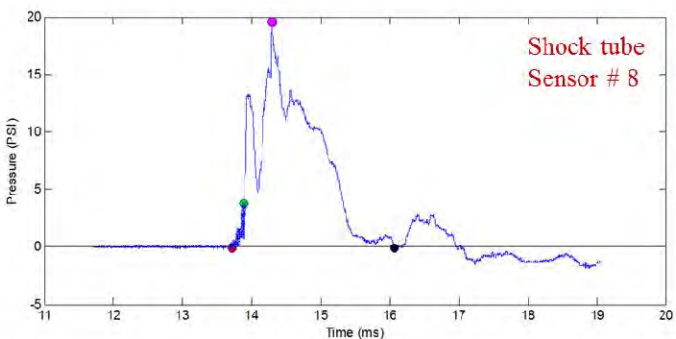
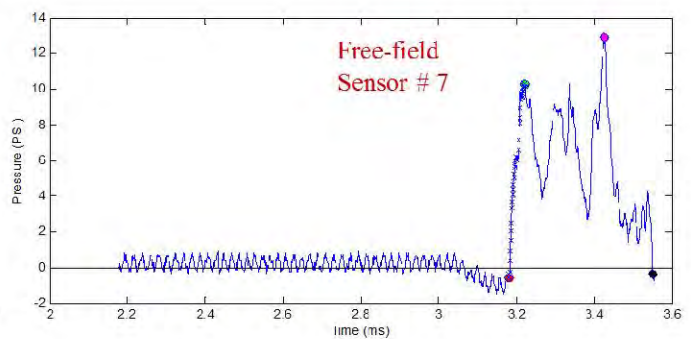
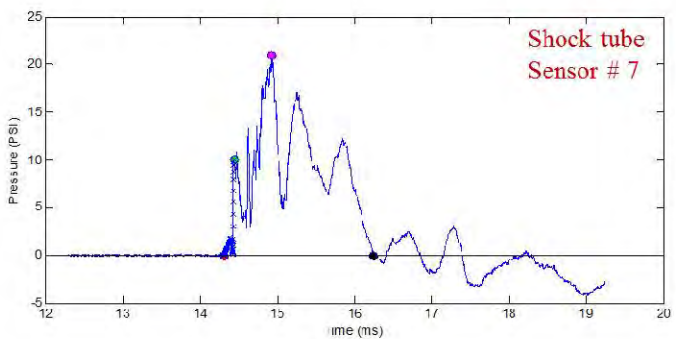
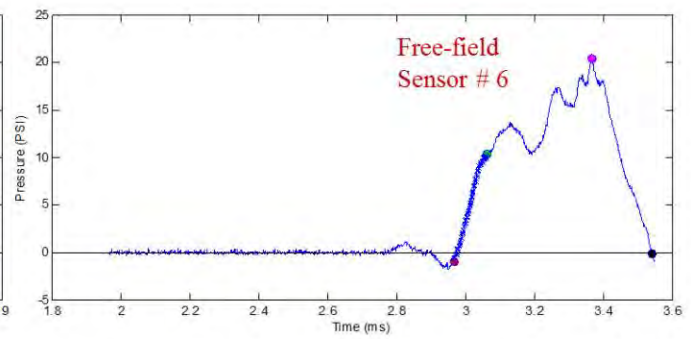
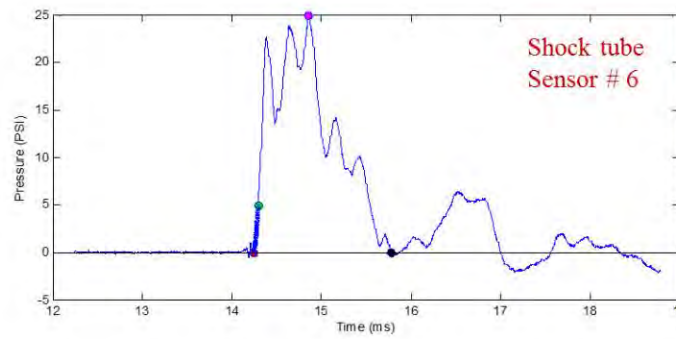
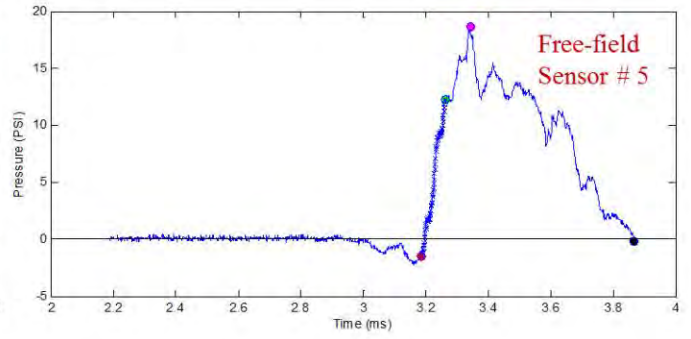
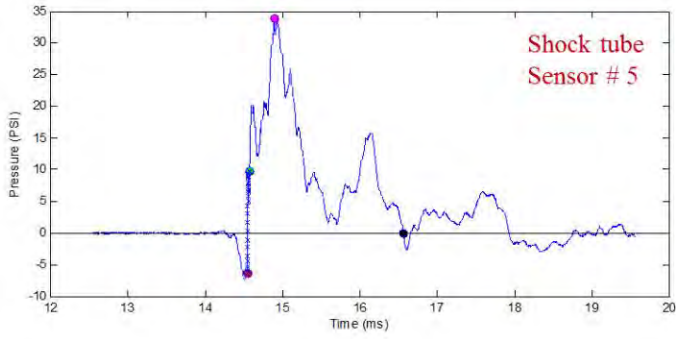


Figure 12. Diagram of head form and potential shockwave interactions. Blue square indicates location of sensor 1 with respect to the brim of the helmet. The shock fronts drawn here are exaggerated for the sake of explanation and they are not drawn to the scale







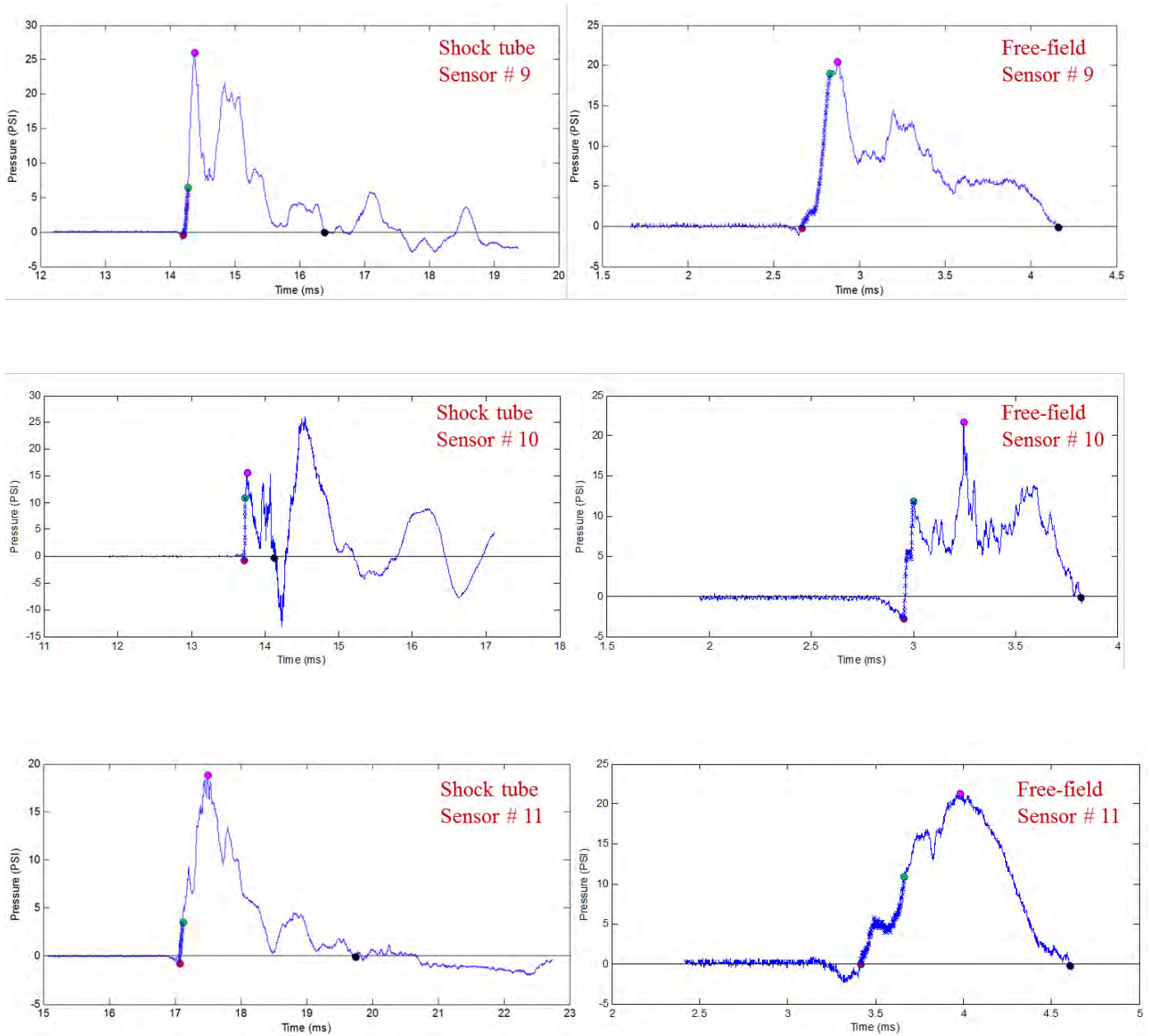


Figure 13. Comparison of pressure profiles between free field and shock tube tests for a helmeted head. From the profile for sensor 1 it can be seen that the beginning of the trace in the free field conditions is non-oscillatory indicating that the planarity of the shock front did not break from interactions with the brim of the helmet, while the trace from the shock tube is oscillatory as a result of the planarity of the shock front being broken up from interactions with the brim of the helmet before interacting with sensor 1.

Figure 11 (b) shows the linear acceleration of the helmeted head. Just as in the bare head case, linear accelerometer comparisons for the Free Field Vs. 28” Short Duration Bare Acceleration data, the maximum and minimum values were usually seen past the first peak, i.e., the acceleration values corresponding to the traverse of the shock front is not be the maximum acceleration. There is a significant difference in the acceleration in both sensors 5 and 6 with highest being the shock tube in the negative direction of sensor 5. Figure 14 shows a statistical comparison of free field and shock tube data based on maximum and minimum values garnered from the first 5ms.

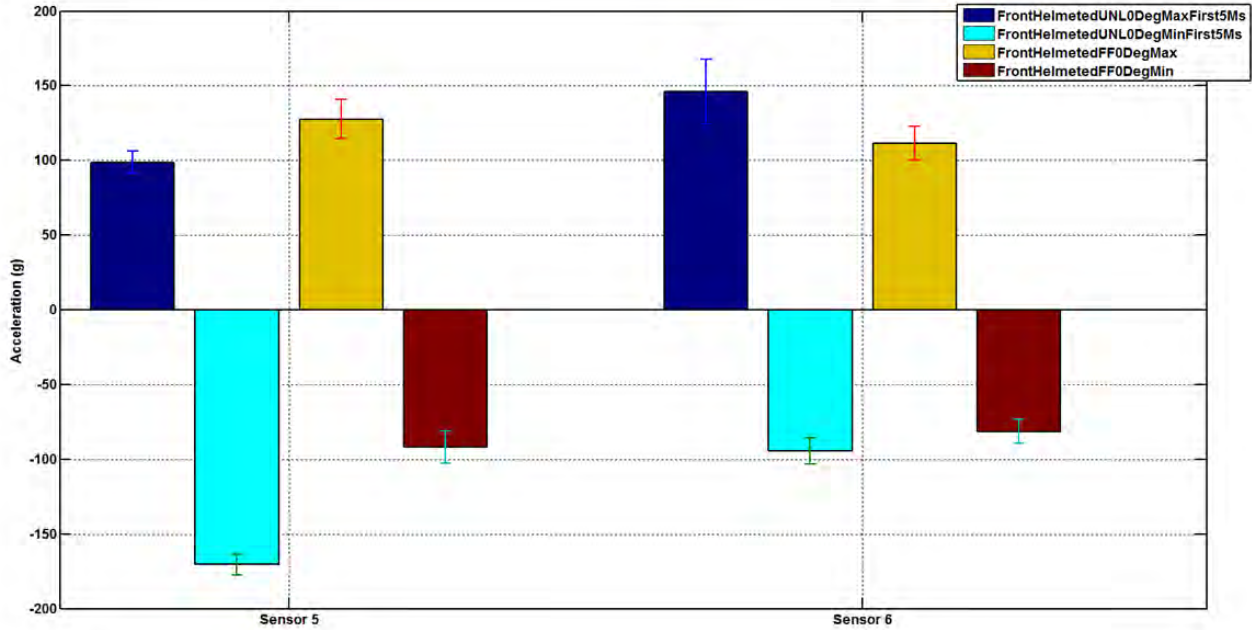
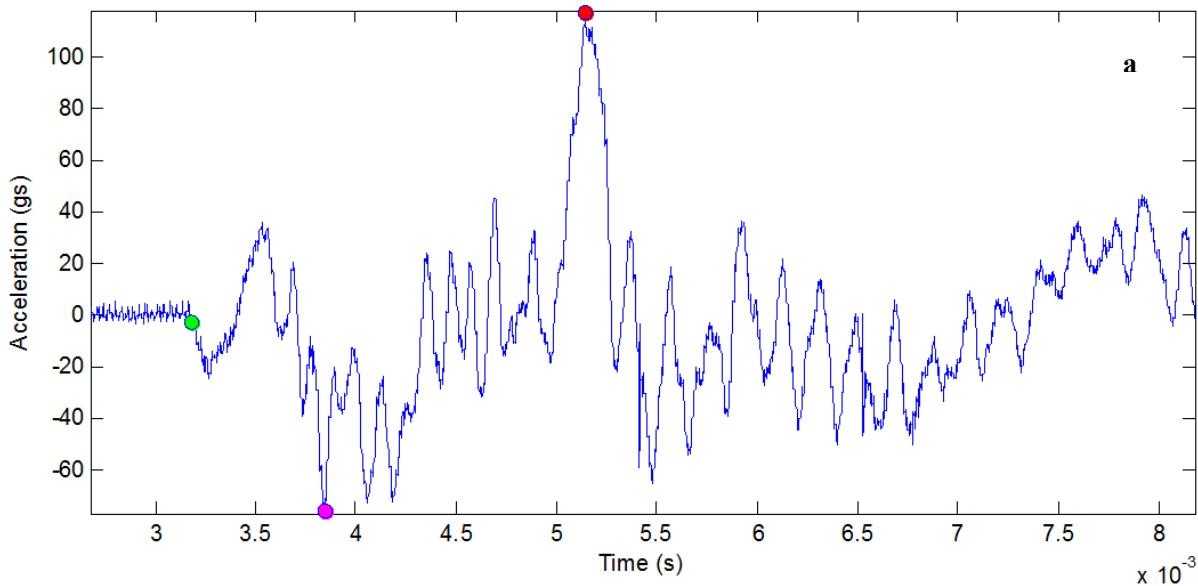


Figure 14. Comparisons between accelerometers 5 and 6 for helmeted front facing orientation in both the free field and UNL 28” shock tube short duration tests; derived from the beginning of the trace (5ms from the time of arrival). 5ms was chosen to see how comparable the accelerations are during the traverse of the shock front before buildup of energy in the anterior of the head.

Gathering the peak minimum and maximum values from the first 5ms, the shock tube data better approximates the free field data; still, discrepancies may exist between different data sets. Looking at profiles for sensor 6 the traces even exhibit a similar initial hump in the data before the majority of the profile begins to evolve.



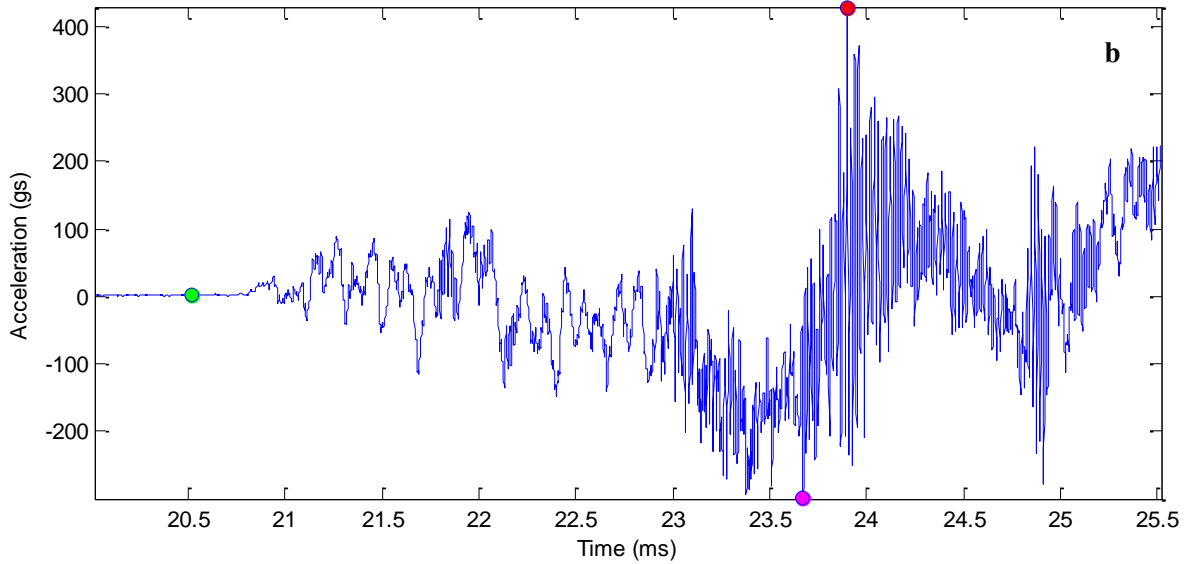
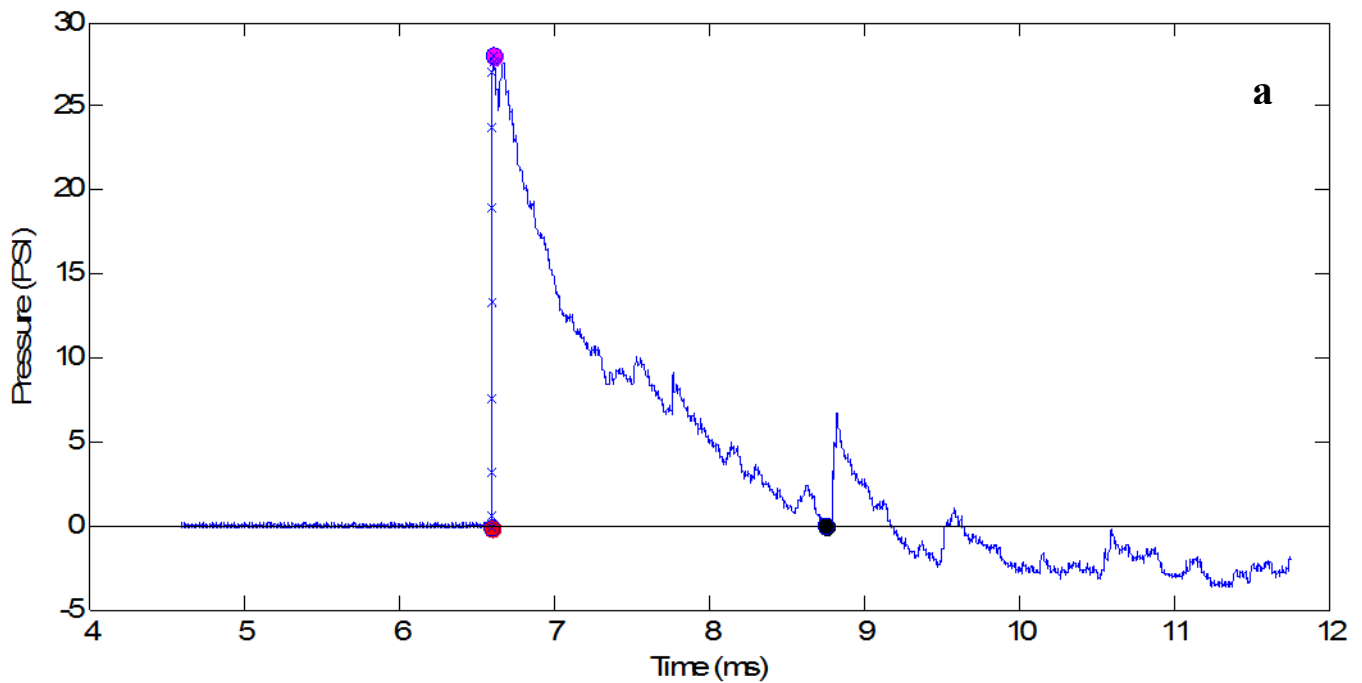


Figure 15. Comparison of acceleration profile for sensor # 5 of helmeted head, (a) shock tube, (b) field experiment.

5.2 Comparison between inside (short duration) and outside (D1) the shock tubes

Figure 16 (a) and (b) show the incident pressure profiles for 28” short duration and 9” D1 shots respectively. From the figure, it can be seen that the overpressure as well as positive time duration are significantly higher in the case of the 9” shots.



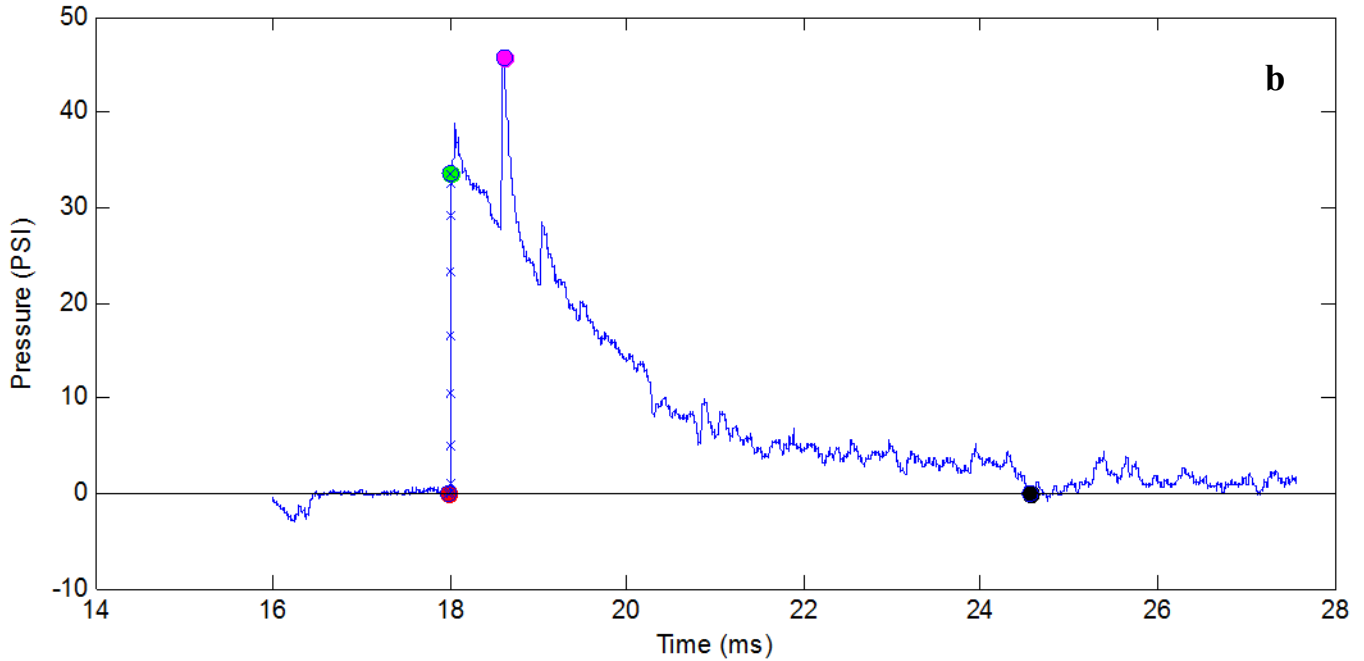
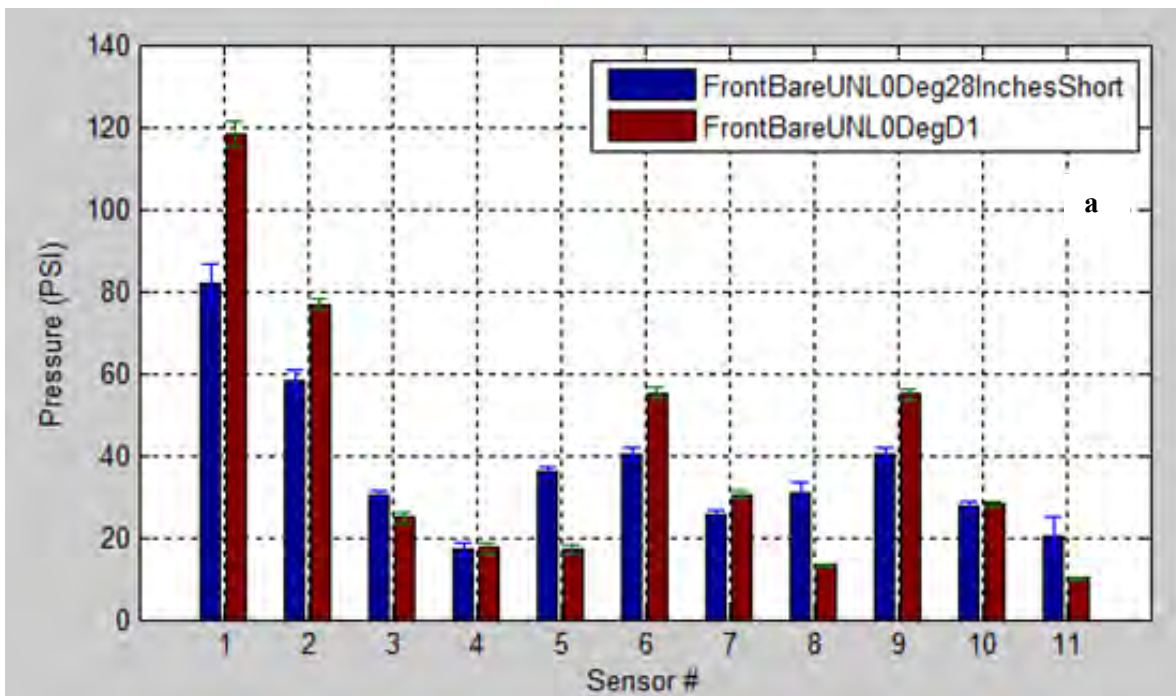


Figure 16. Incident pressures (a) 28” short duration, (b) 9” D1 shot the pink dot denote a sensor artifact due to its collision with the walls of the shock tube.

5.2.1 Front bare head

Here we compare the overpressures and linear acceleration for: (1) 28” short duration (2-3 ms) and (2) 9” shock tube at a distance D1 (11.8” from the exit). From Figure 17 (a), it can be seen that sensors 1, 2, 6 and 9 record a higher pressure in 9” D1 than in 28” short duration shot.



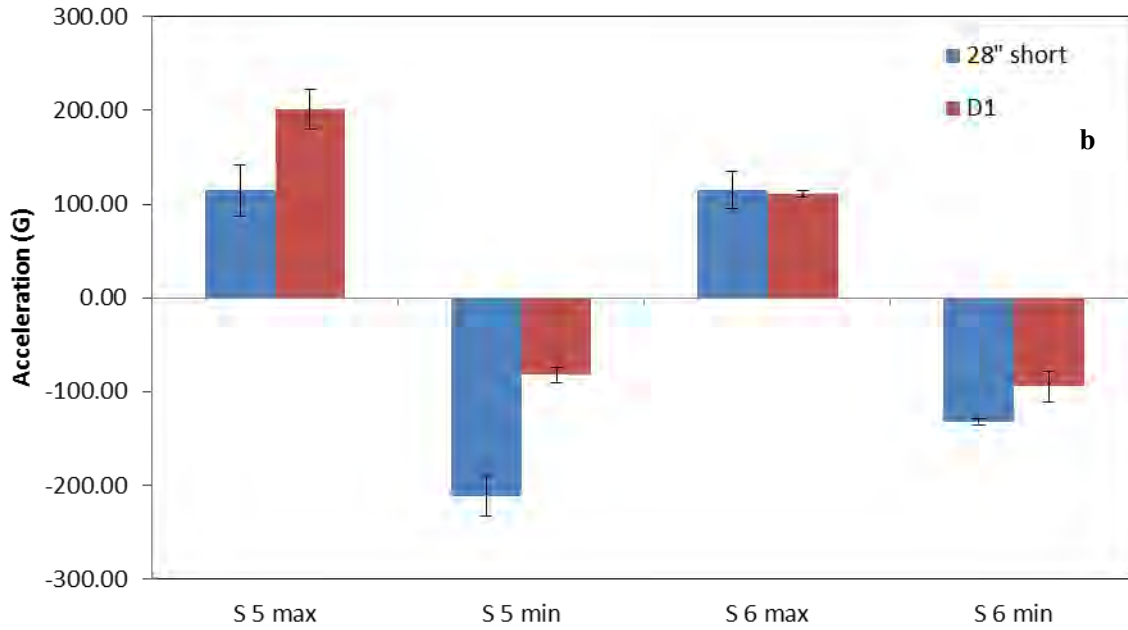


Figure 17. comparisons of (a) overpressure, (b) linear acceleration for a front facing bare head inside a 28” shock tube and outside at distance D1 in 9” shock tube.

Further statistical analysis proved that there is a significant difference in all the sensors but 4 and 10; however, power analysis showed that there is a chance of 93% and 81% respectively for those sensor comparisons to be a type II error. In sensors 3, 4, 5, 7, 8, 10, 11 the overpressure is either equal or the overpressure is higher for the 28” short duration shot. This is due to varying flow dynamics near the exit of the tube, around the RED head when placed outside, which is illustrated in the following Figure 17.

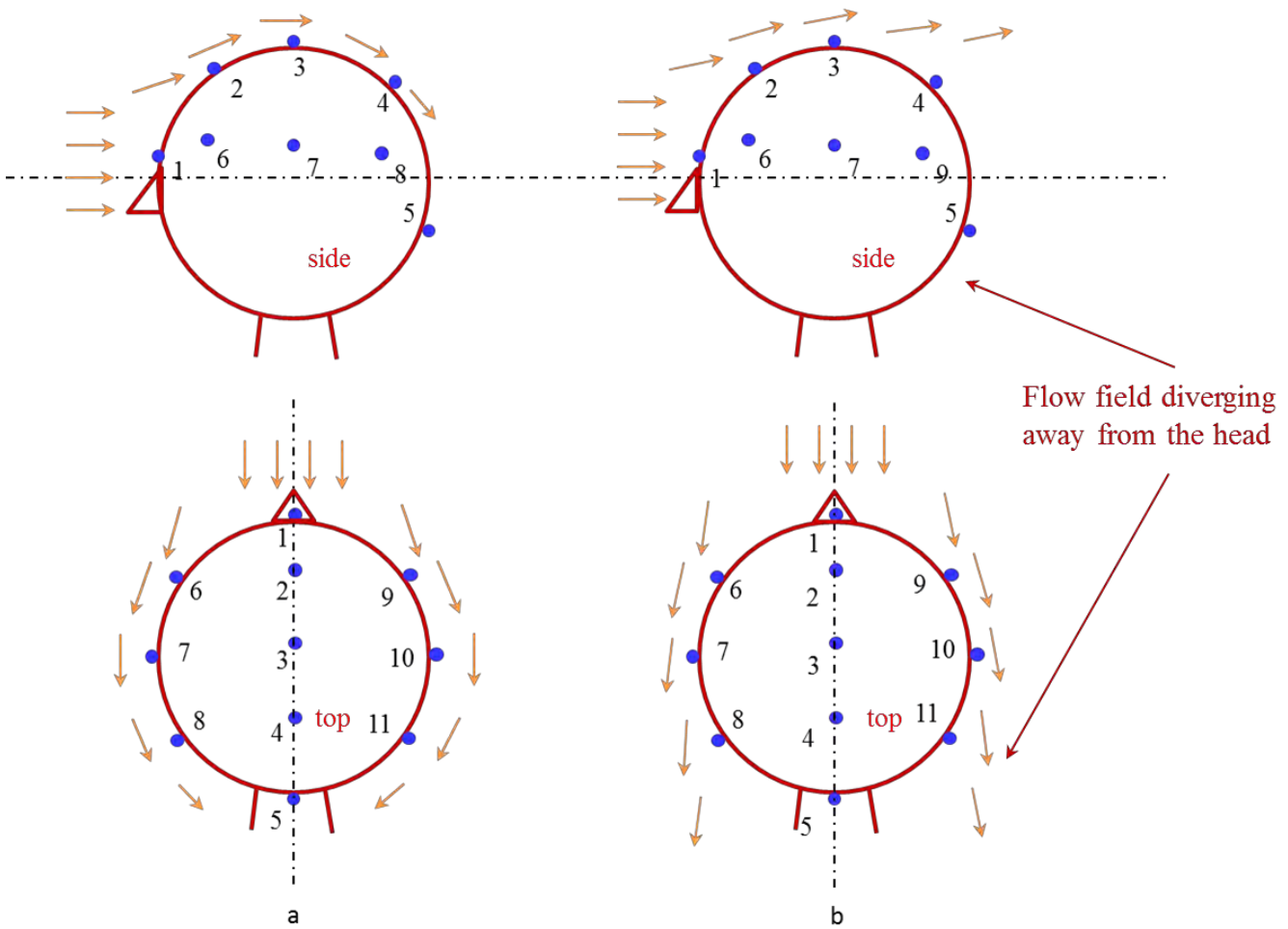
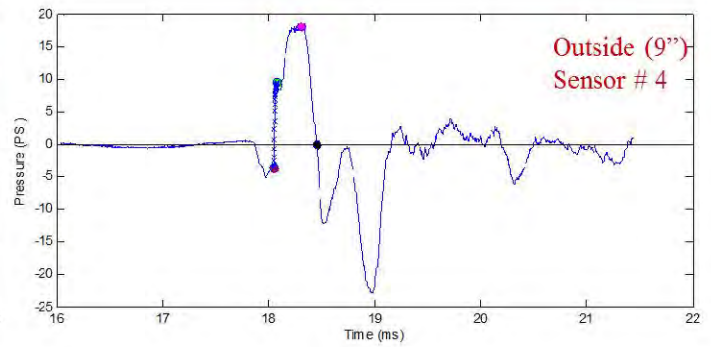
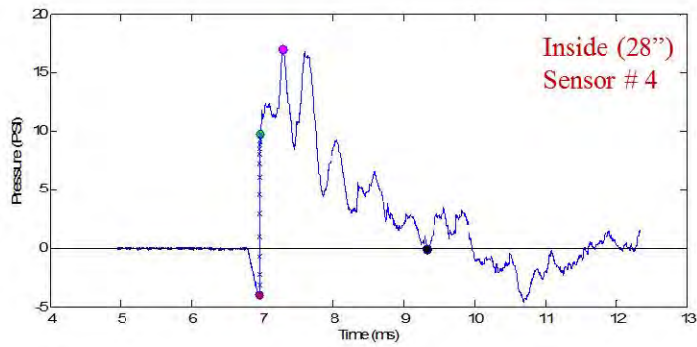
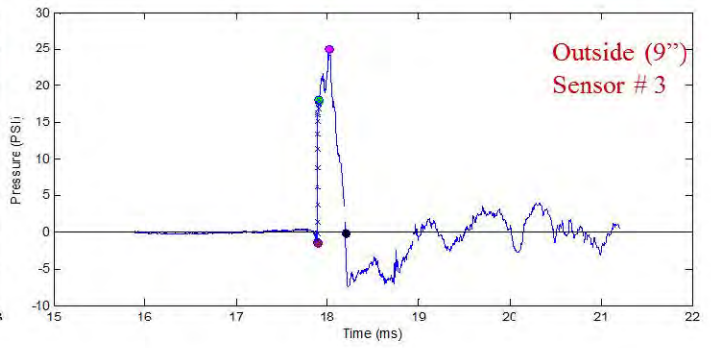
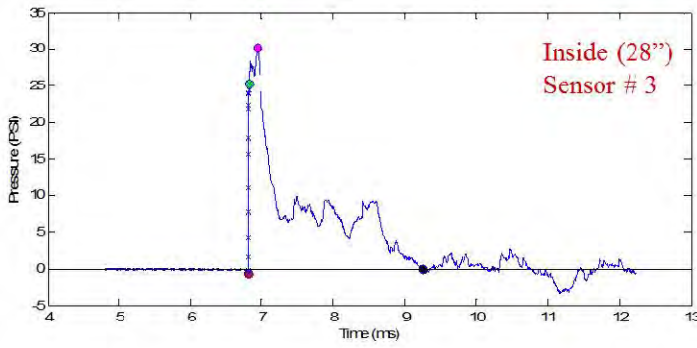
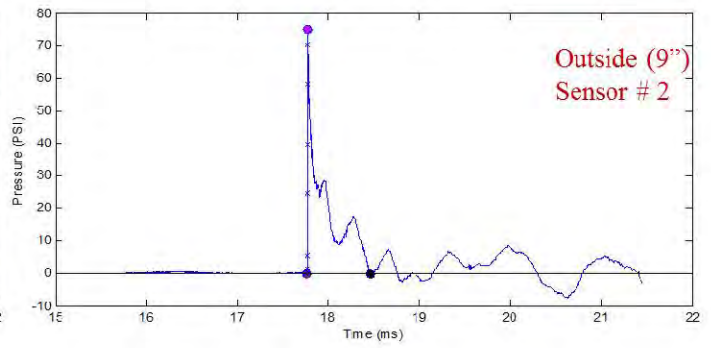
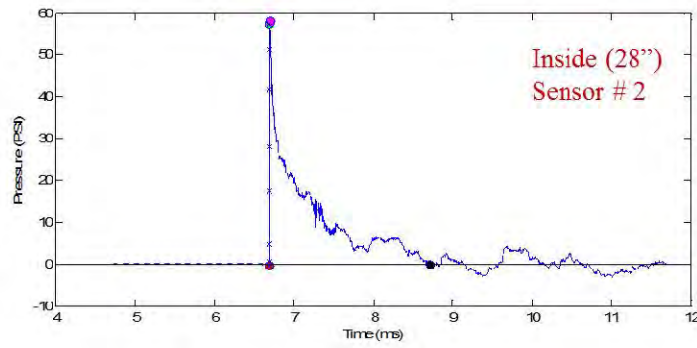
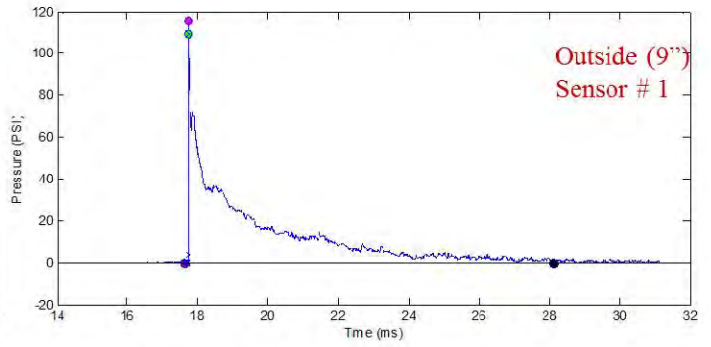
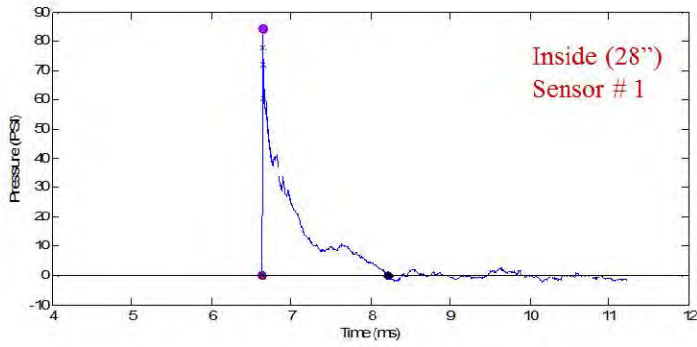
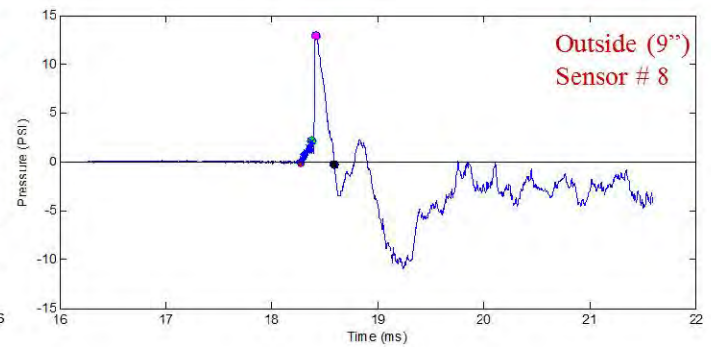
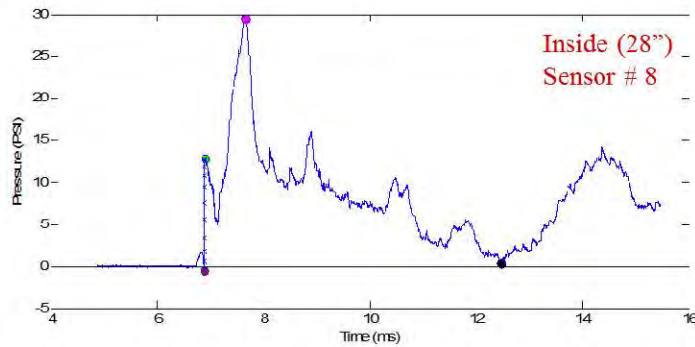
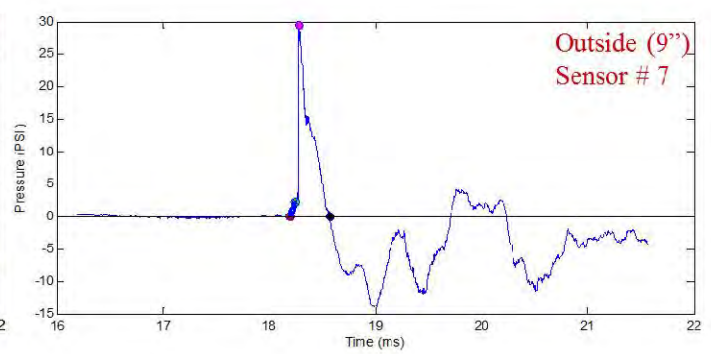
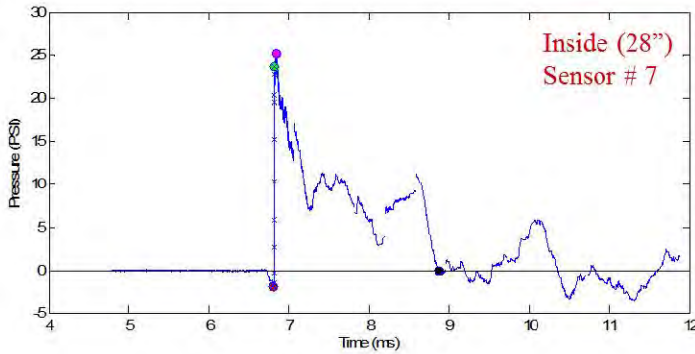
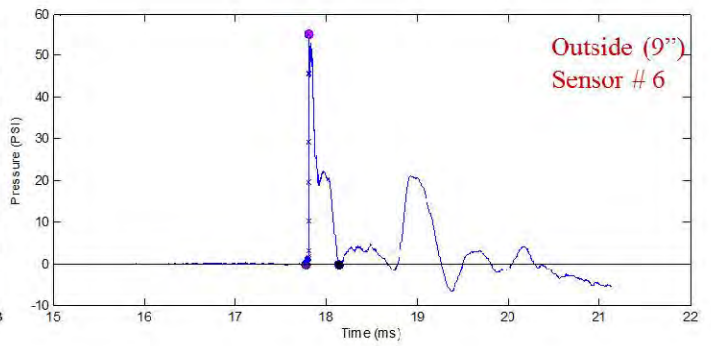
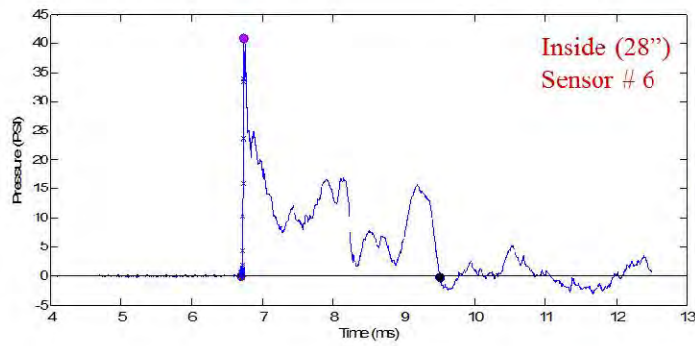
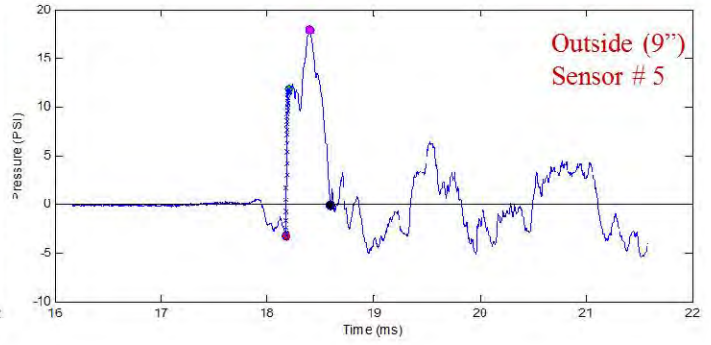
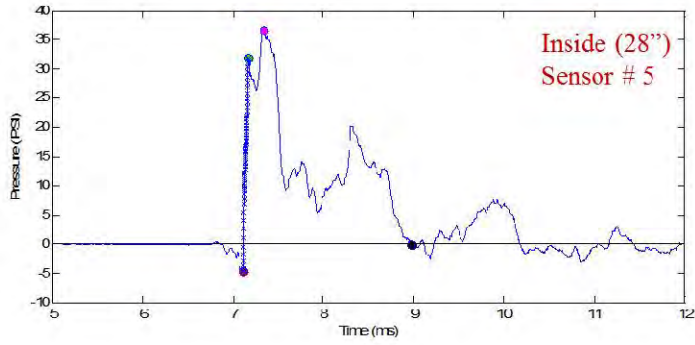


Figure 18. Flow dynamics around the head form (a) inside the shock tube, (b) outside outside the shock tube

As described above, when inside (Figure 18 (a)), the shock front after interacting with the anterior of the head diffracts and converges around the head form. However, when outside, following the interaction with the head, the flow field expands outwards due to the pressure gradient (Figure 18 (b)). This phenomenon is responsible for the reduction in the overpressure in sensors 3, 4, 5, 7, 8, 10, 11. When looking at the profiles it is evident that there is a significant reduction in the positive time duration when the head form is placed outside as opposed to inside. This behavior of the shock front losing its planarity and diverge from the exit of the shock tube is also seen through figure 1 of appendix B, where the complex nature of the shock front exiting the tube is described. Figure 17 (b) shows the comparison of linear acceleration for short duration 28” and 9” D1 shots with the RED head (bare) facing the shock front at 0°. From the statistical analysis done on sensor 5 and 6, it can be seen that there is a significant difference in both positive and negative accelerations of sensor 5 and maximum negative of sensor 6. It is interesting to notice that positive is more in 9” D1 shot whereas negative is more in the 28” shot. This might be due to the exiting jet wind in the 9” D1 shot slowing down the reaction (spring back) of the RED head. In sensor 6 maximum positive does not have a significant difference; but, power analysis shows that there is 93% chance of type II error in that comparison.





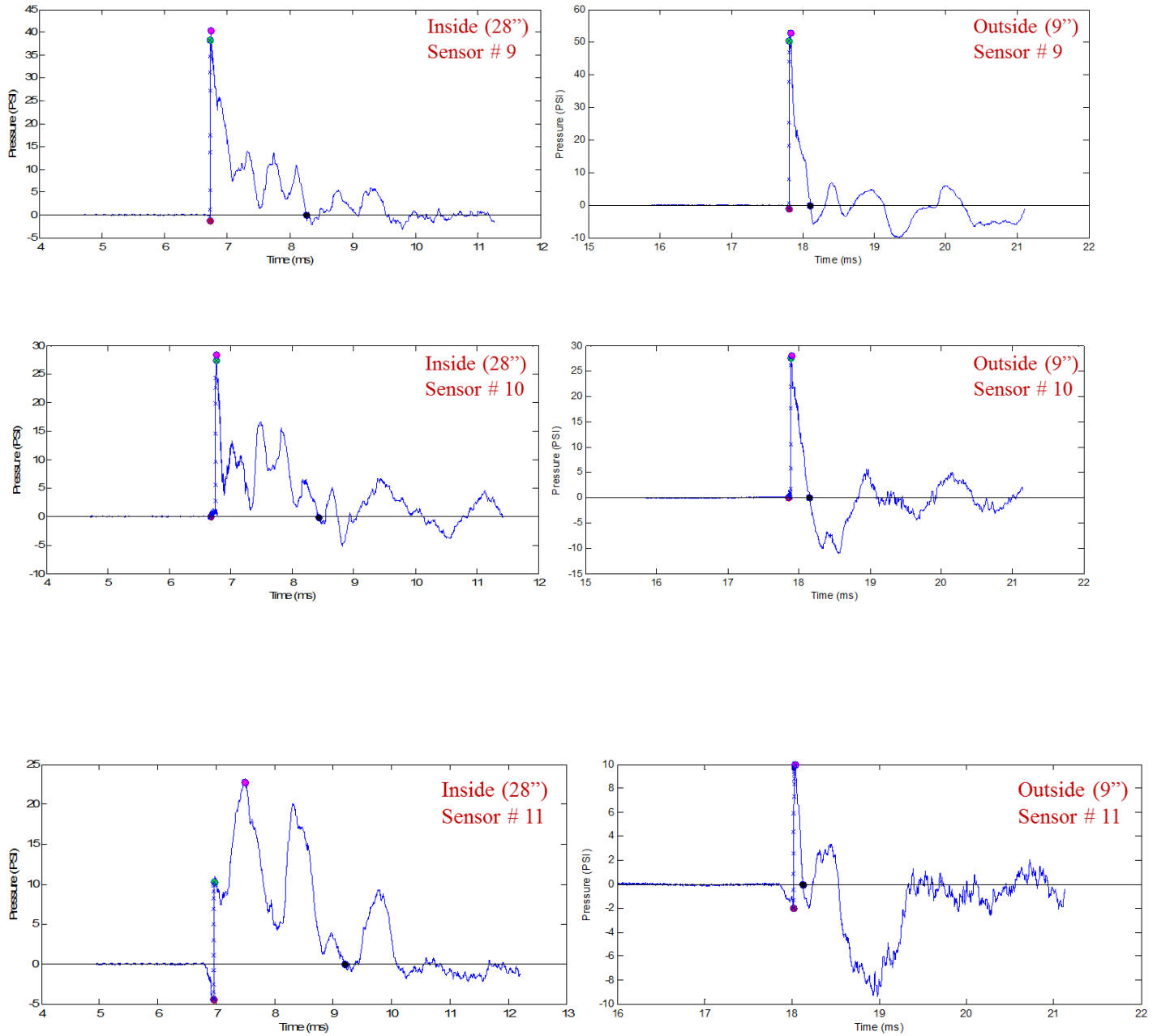


Figure 19. Shows the comparison of pressure profile between 28" short duration shot and 9" D1 shot.

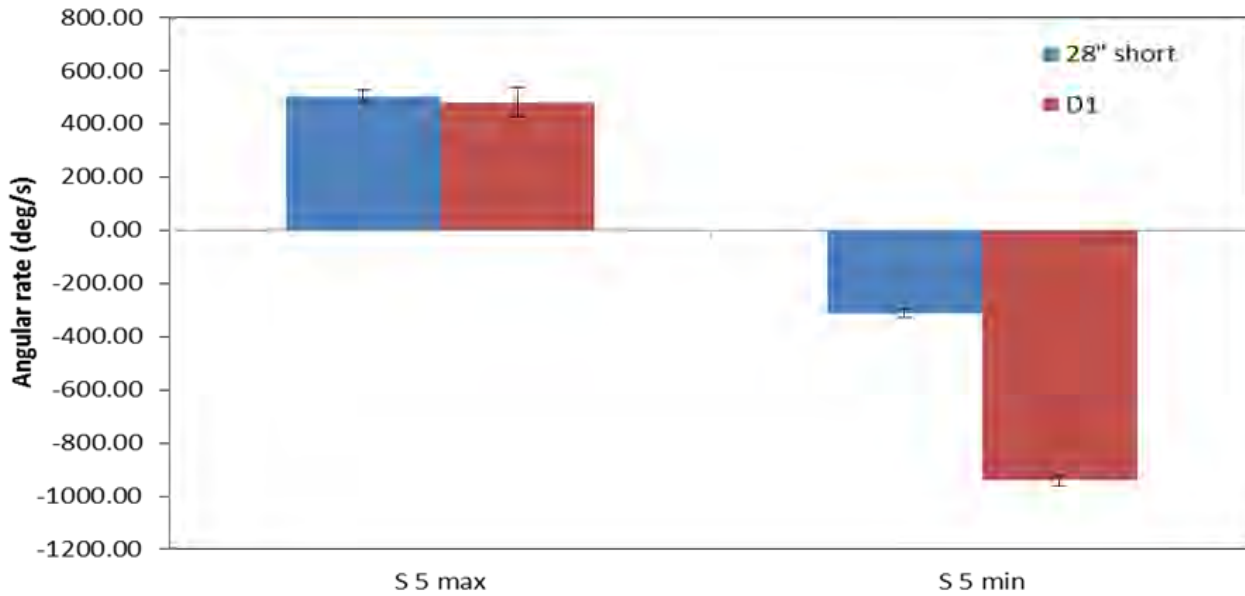


Figure 20. Shows the comparison of maximum and minimum angular rate sensor data between 28” short duration shot and 9” D1 shot.

Figure 20 shows the angular rate comparison of the maximum positive and negative angular rate values. It can be seen that there is a significant difference in negative angular velocity, i.e., 9” D1 shot has a higher negative angular velocity than the 28” shot. Further, there is no significant difference in the positive angular velocity; however, there is a chance of 84% that the result is a type II error.

5.2.2 Front helmeted head

Figure 21 (a) shows the comparison of the overpressure from a 28” short duration shot with a 9” D1 shot when the RED head was front facing at 0°. As seen in the bare head case, in sensors 1, 2, 6 and 9, the overpressure recorded in the 9” shot is significantly higher than the 28” shot (analysis attached in appendix A). There is no significant difference for sensor 7, 8, 10, and 11; however, power analysis show that there is a chance of 72%, 67%, 68%, and 65% type II error respectively. Unlike the bare head, sensor 3 and 4 seems to have significantly higher overpressures in the 9” shot than in the 28” inch shot. Conversely, in all the other sensors except 7, 8, 10 and 11, the 28” shot has a higher overpressure. Looking at the incident profiles it can be seen that the positive time durations were 8 ms and 2.5 ms for 9” shots and 28” short duration shots respectively. In spite of having a longer duration than 28” short duration shots, the 9” shots have relatively lower positive time duration in all sensors.

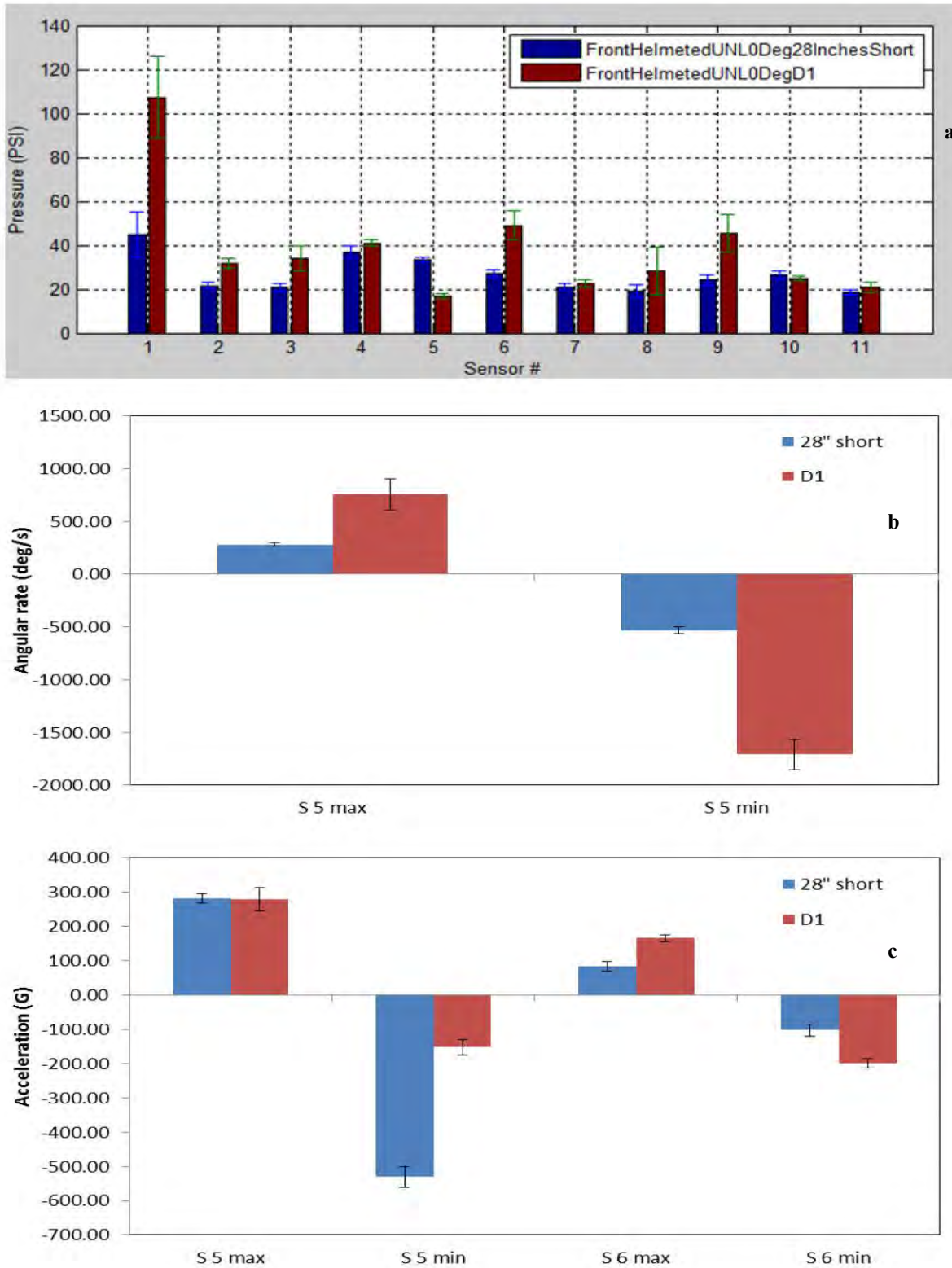


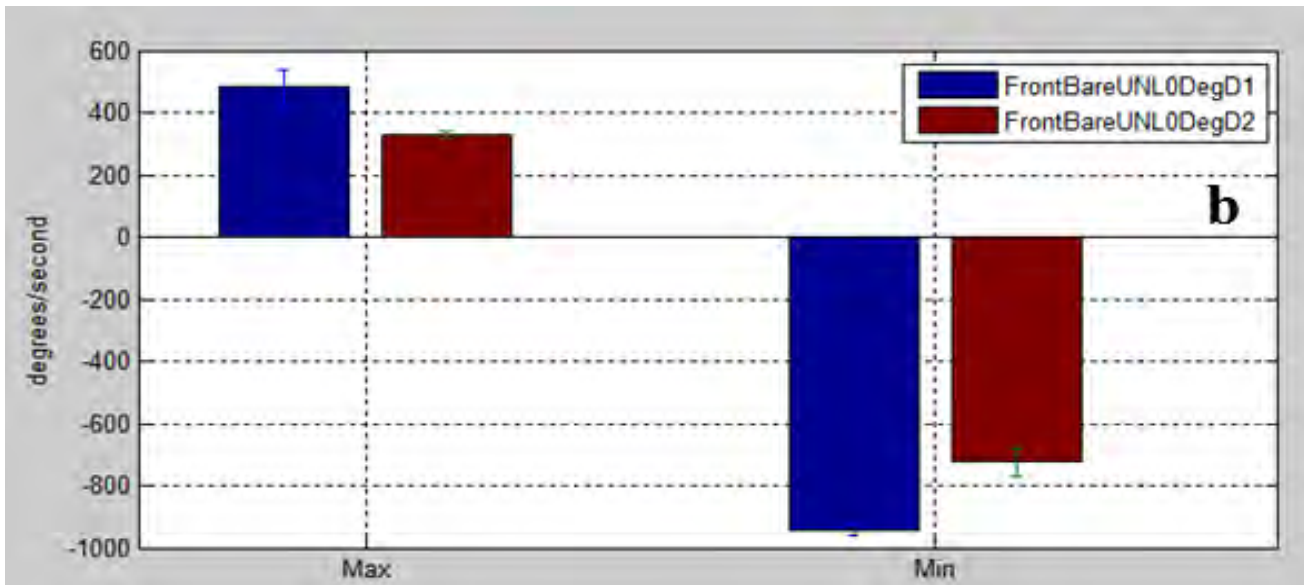
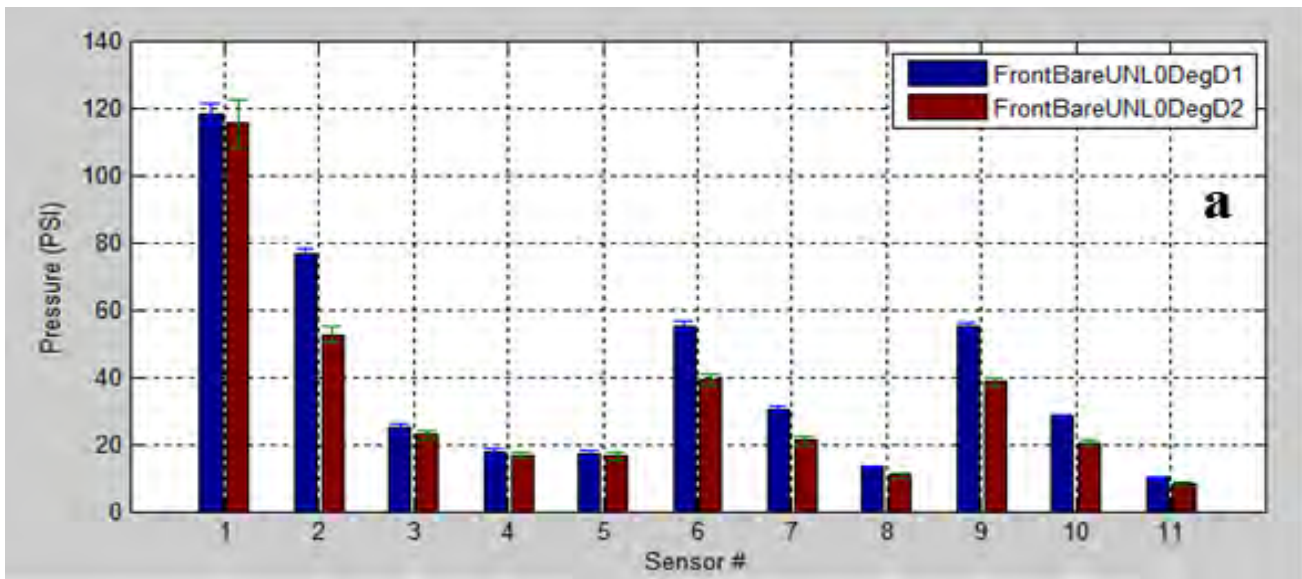
Figure 21. comparisons of (a) overpressure, (b) angular velocity for a front facing helmeted head inside a 28” shock tube and outside at distance D1 in 9” shock tube.

Figure 21 (b) shows the angular velocity comparison between the two shots, it can be seen that there is a significant difference in the angular velocity with 9” D1 shots higher in both cases when compared to the 28” short duration shots.

Figure 21 (c) shows the linear acceleration, from the statistical analysis it was determined that there is a significant difference in both positive and negative accelerations of sensor 6. However, the positive of the sensor 5 does not show any significant difference whereas the negative maximum negative does show the difference. Further, power analysis done on the comparison of sensor 5 maximum positive data showed that there is 95% chance for a type II error.

5.3 Comparison between two outside shots at distance D1 and D2

5.3.1 Front bare head



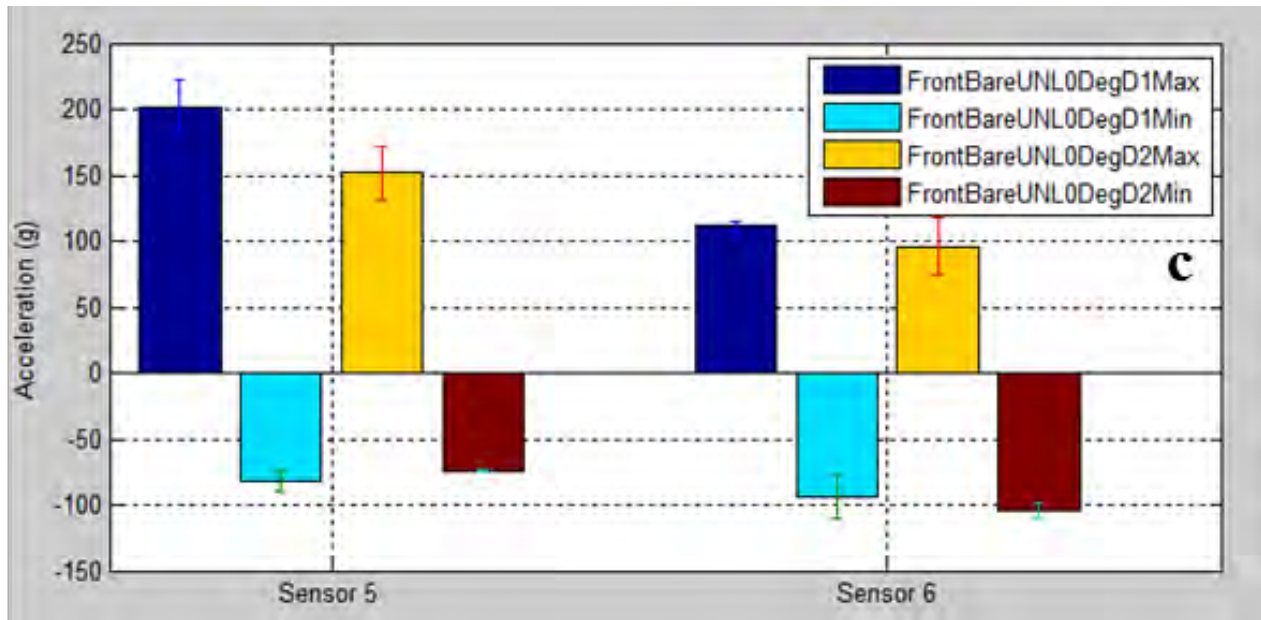


Figure 22. Comparisons of (a) overpressure, (b) angular velocity and (c) linear acceleration for a front facing bare head in 9” D1 and D2 of the shock tube.

Figure 22 (a) shows the comparison of the overpressure between two 9” shots at distance D1 and D2. There is a significant difference in the overpressure in sensors 2, 6, 7, 8, 9, 10 and 11 (9, 10 and 11 are placed symmetrically with 6, 7 and 8). In sensors 1, 3, 4 and 5 there is no significant, difference but the power analysis shows that there is chance of 90%, 65%, 82%, 86% type II error respectively. The maximum difference is 24.14 psi and seen in sensor 2 and the minimum difference is 1.74 seen in sensor 11. This indicates that the overpressure decreases drastically in sensor 2 with increase in the distance from the exit of the tube. However, the overpressure remains same in sensor 1, which is located slightly above the eye socket, which is in the line of the jet wind effect.

Figure 22 (c) shows the acceleration recorded in sensor 5 and 6. Statistical analysis shows that there is no significant difference in sensor 6 and maximum negative of sensor 5, but the power analysis show that there is a 69%, 77%, 82 % chance of type II error. There is a significant difference in the maximum positive of the sensor 5. The angular velocity is higher in the case of D1 shots as opposed to the D2 shots and this difference is significant (Figure 22 (b)).

5.3.2 Front helmeted head

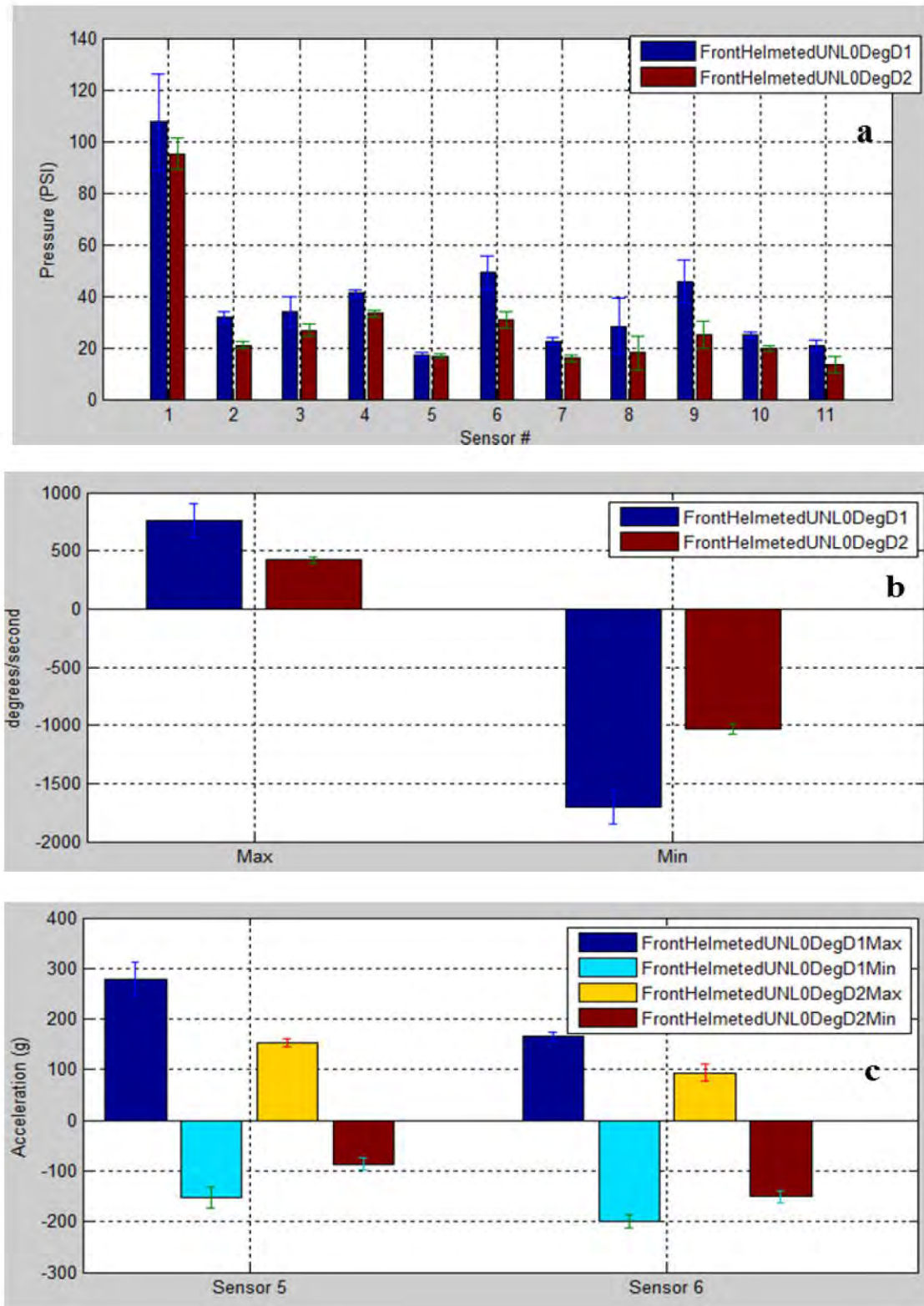


Figure 23. Comparisons of (a) overpressure, (b) angular velocity and (c) linear acceleration for a front facing helmeted head in 9” D1 and D2 of the shock tube.

Figure 23 (a) shows the comparison of the overpressure between two 9” shots at distance D1 and D2 with helmeted RED head. From the statistical analysis, it was seen that there is a significant difference in the overpressure in sensors 2, 4, 6, 7, 9, 10 and 11 and in sensors 1, 3, 5, and 8 there is no difference in the overpressure. However, the power analysis show that there is a 77%, 82%, 91% and 67% chance for type II error in comparison of those sensors. The highest difference is recorded in sensor 9 and lowest difference is recorded in sensor 10. Although sensors 8 and 11 are symmetric, the statistical analysis shows that there is a significant difference in sensor 11 and no difference in sensor 8. However, further analysis showed that this particular comparison due to its high variability has power problem ($\beta = 0.67$, 67% chance of type II error). This problem can be resolved through additional tests. Furthermore, the linear accelerations and the angular velocity is higher in D1 than in D2 when helmet is worn and all these differences are significant.

5.4 Comparison between inside (long duration) and outside (D1) the shock tubes

5.4.1 Front bare head



Figure 24. Comparisons of (a) overpressure, (b) angular velocity for a front facing bare head inside a 28” shock tube and outside at distance D1 in 9” shock tube.

Figure 24 (a) shows the comparison of the overpressure between long duration 28” and 9” D1 shots with RED head (bare) facing the shock front at 0°. In spite of having a higher incident pressure in the 9” case, overpressure values recorded in the 28” long duration shots were higher than the 9” shots. Furthermore, the statistical analysis also showed that this difference is significant. This suggests the lack of efficiency or depletion of shock front pressure due to its interaction with the rarefaction wave from the exit of the shock tube in the case of 9” shock tube. From the visual observation of the pressure profiles, it can be seen that there is a reduction in the positive time duration in all but sensor 1. From Figure 24 (b), it can be seen that angular velocity is higher in the case of the 28” long shots. Further analysis proves that this difference is significant.

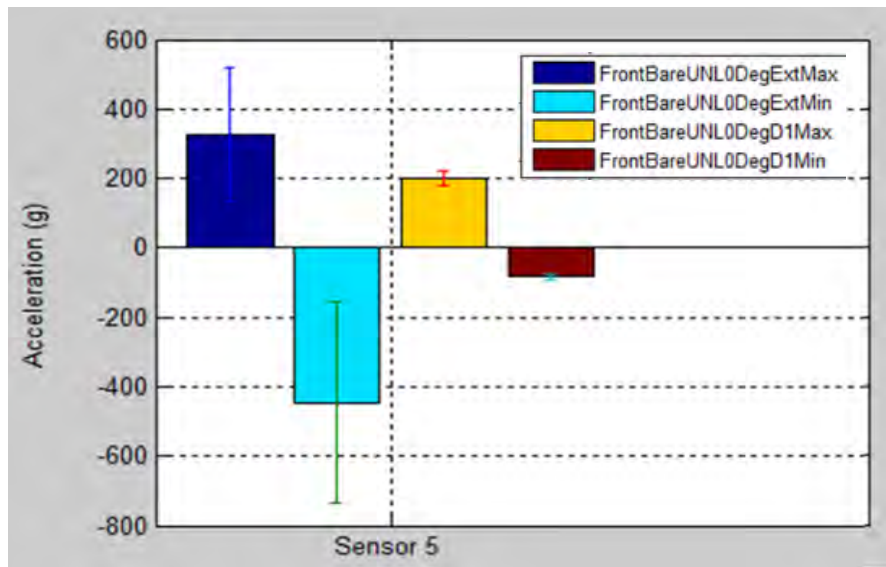


Figure 25. Comparison of linear acceleration.

Figure 25 shows the comparison of the linear acceleration between 28” long duration shot and 9” D1 shot. There is significant difference in the maximum negative acceleration. However, there is no difference in the maximum positive acceleration. A power analysis to determine the chance of type II error was performed. It was found that the chance of type II error is 63%. As observed in all the other cases the high negative acceleration inside the shock tube as opposed outside may be due to the jet wind effect. As the RED head is loaded due to the traversing shockwave, it springs back due to the energy stored in the spinal support. However, this spring back may have been reduced due to the blowing of high-speed jet winds exiting the 9” shock tube.

5.4.2 Front helmeted head

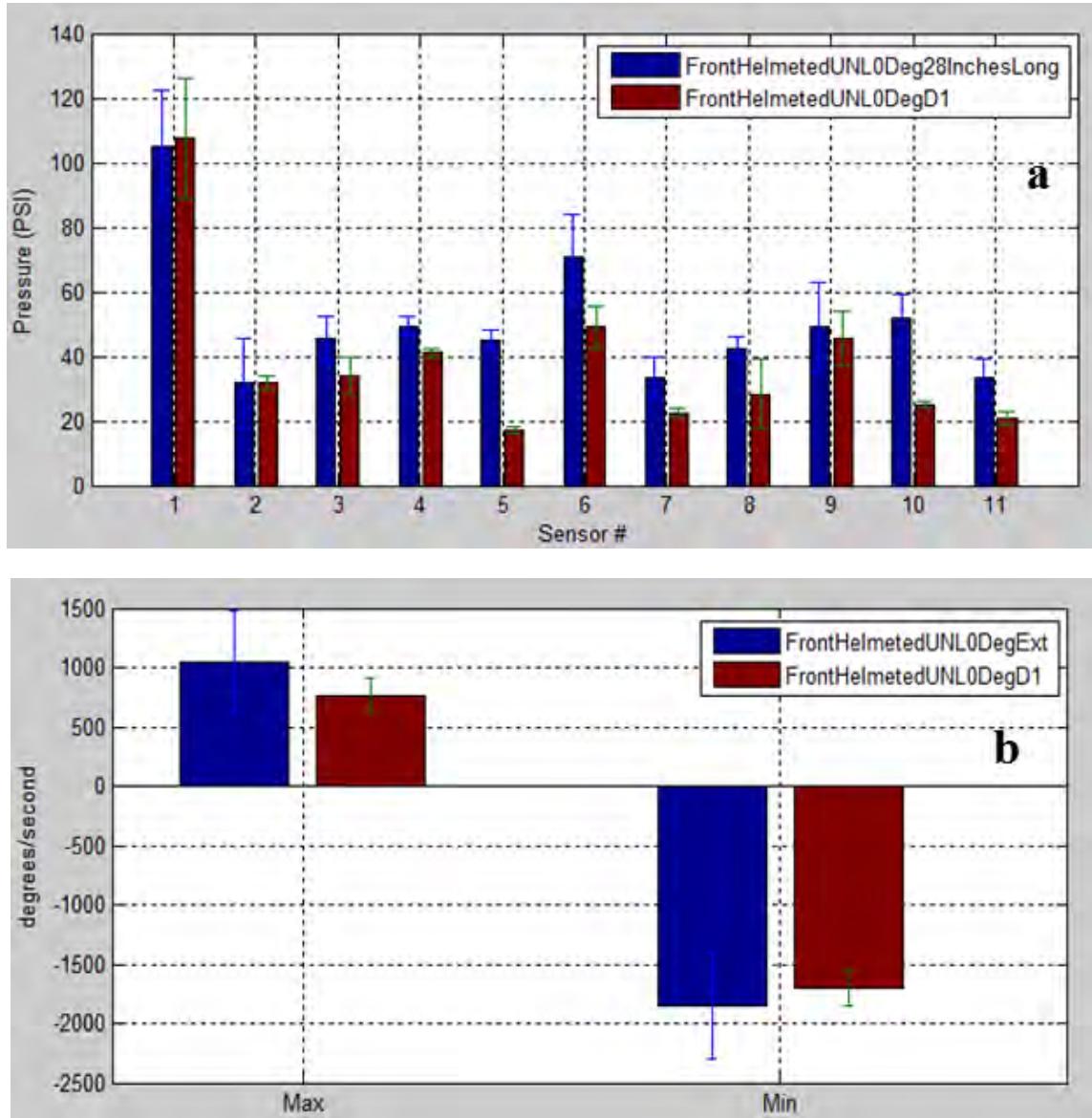


Figure 26. Comparisons of (a) overpressure, (b) angular velocity for a front facing helmeted head inside a 28” shock tube and outside at distance D1 in 9” shock tube.

Figure 26 (a) shows the comparison between overpressures of on the helmeted head for 28” long duration (inside) and 9” at distance D1 (outside) exposures. Unlike the bare head, the overpressure recorded in the helmeted head does not have a higher overpressure in all the sensors for the 28” long duration shots. From the statistical analysis, it was seen that there is a significant difference in all but sensor 1, 2 and 9. However, from the power analysis done on all these sensors indicates that the chances for a type II error are about 95%. Among the other data, Sensor 3 seems to have the highest difference (28.54 psi), with the 28” shots having a higher pressure and sensor 4 has the lowest difference (8.27 psi). This might be due to the location of the sensor and the diverging effect of the shock wave as explained in Figure 18. Having the helmet certainly seems to have increased the variability of the pressure, which is not seen in the bare head case.

Figure 26 (b) shows the comparison of angular velocity between 28” long shots and 9” D1 shot. From the statistical analysis it was determined that there is no significant difference in both the maximum positive as well as negative angular velocity.

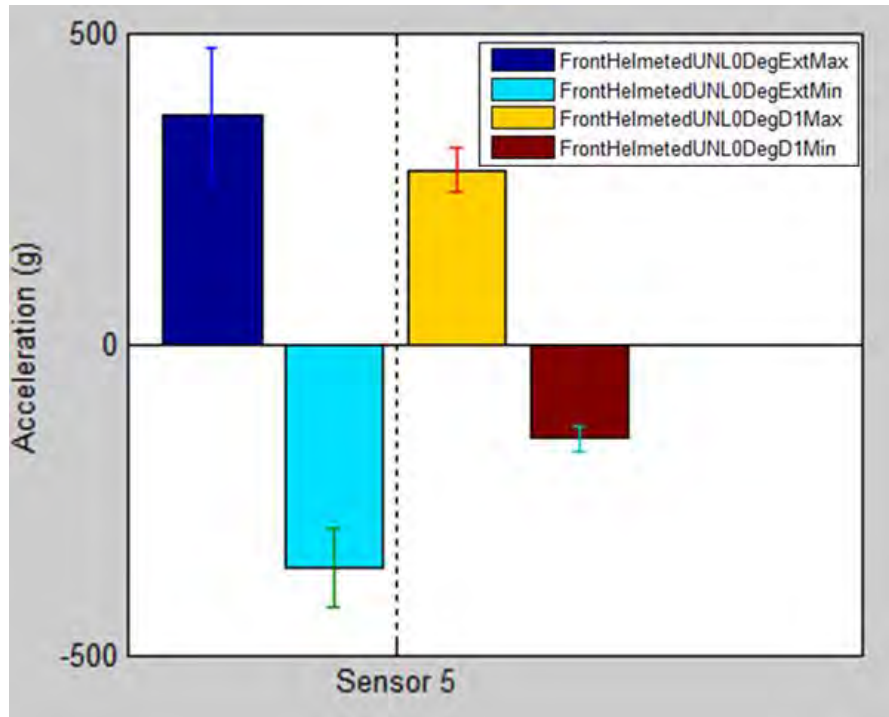


Figure 27. Comparison of linear acceleration.

Figure 27 shows the comparison between linear acceleration of the helmeted head for 28” long duration (inside) and 9” at distance D1 (outside) shots. From the analysis, it was determined that there is a significant difference in the maximum negative; however, there is no significant difference in the maximum positive acceleration. A power analysis was conducted on those quantities with p value more than 0.05 and the power was determined. In this case the maximum positive of sensor 5 and ARS had a chance of 70%, 77% and 91% for type II error. Similar to the previous analysis it can be seen that the negative acceleration is higher when inside than outside, however, there is no difference in the positive acceleration.

6 Summary

Study was conducted to compare the surface pressure, linear acceleration, and angular velocity of the RED head for various loading parameters in shock tube and free field explosive loading. Furthermore, a comparison between performing tests inside and outside of a shock tube was also done. In cases where a power problem is indicated, additional experiments with the same input shock profiles may have to be carried out to increase the power or reduce the chance of type II error. Summary of this report is as follows.

- It was determined there is some difference in the peak overpressure between 28” short duration shots and free field shots with the maximum difference being 17.29 psi in sensor 2. These

differences may be attributed to: (a) variation in the incident pressure between free field (25 psi) and 28" short (28 psi), (b) once the shock front impinges the surface of the subject, it diffracts and tends to engulf the whole head. This diffraction and pattern of fluid flow depends on the point of impingement but also on the local geometry. Consequently, this causes the variation in the maximum overpressure. There is a good qualitative match between the pressure profiles, which indicates the capture of essential physics of the phenomenon.

- Generally, the maximum positive acceleration has less difference (29.37 G, for 28" short duration shot) when compared to the field data; however, for almost all cases when the head was placed inside the maximum negative acceleration is higher in the shock tube than in the free field-testing. The exact cause of this phenomenon is still unknown.
- In the case where helmet was used, the overpressure for sensors 1, 2, 3, and 5 has the maximum variation when compared with the field data. However, this difference is not more than 14.19 psi (28" short duration inside). The acceleration of the helmeted head is higher when compared to the bare head in the shock tube. This might be due to the buildup of force in the concave helmet inner surface, which is seen in the long duration shots as well.
- When placed outside the shock tube, there is a reduction in the overpressure and positive time duration when compared with shots inside the shock tube, which can be seen in the pressure profiles comparison shown in figure 19. Especially, overpressure seems to be reduced or remain equal to that measured in the experiments conducted inside the shock tube in all but sensors 1, 2, 6, and 9, even though the 9" D1 shot had a higher incident pressure.
- It is interesting to compare the both short and long duration 28" shot with 9" D1 shot. In both cases, the positive maximum acceleration of the sensor 5 is higher in 9" than in 28"; however, the positive negative is lower in the case of the 9" when compared to 28" shot. This might be due to the high velocity jet wind in conjunction with the depleting shock front, which increases the acceleration outside. Once the head is accelerated, it reaches its peak motion and springs back to its equilibrium position. At this point, the tail end of the jet wind tries to stop this spring back motion of the RED head, which is manifested in the lower acceleration.

7 Further reading

V. Selvan, S. Ganpule, N. Kleinschmidt and N. Chandra, Blast Wave Loading Pathways in Heterogeneous Materials Systems-Experimental and Numerical Approach, **Journal of Biomechanical Engineering**, (in print 2013)

M. Skotak, F. Wang, A. Alai, A. Holmberg, H. Seth, R. Switzer III, and N. Chandra, Rat Injury Model Under Controlled Field-Relevant Primary Blast Conditions: Acute Response to a Wide Range of Peak Overpressure, **Journal of Neurotrauma**, (in print, 2013).

A. Sundaramurthy, A. Alai, S. Ganpule, A. Holmberg, E. Plougonven and N. Chandra, Blast-Induced Biomechanical Loading of the Rat: An Experimental and Anatomically Accurate Computational Blast Injury Model, **Journal of Neurotrauma**, 29:13, DOI: 10.1089/neu.2012.2413, (July 2012)

S. Ganpule, A. Alai, E. Plougonven, and N. Chandra, Mechanics of Blast Loadings on the Head Models in the Study of Traumatic Brain Injury Using Experimental and Computational Approaches, **Biomechanics and Modeling in Mechanobiology**, DOI: 10-1007/s10237-012-0421-8, (July 2012).

N. Chandra, S. Ganpule, N.N. Kleinschmit, R. Feng, A.D. Holmberg, A. Sundaramurthy, V. Selvan, A. Alai, Evolution of Blast Wave Profiles in Simulated Air Blasts: Experiment and Computational Modeling, **Shock Waves: An international journal on shock waves, detonation and explosions**, DOI: 10.1007/s00193-012-0399-2, (2012).

8 Appendix A – Statistical analysis

Max pressure comparison (yes – significant difference/ no – not significantly different based on p value)

(I) Comparison between 28” short vs. Free field (bare)

Test (bare)	Average	Std.ev	F	p	Conclusion
28" short	81.64	4.86	3.18	0.09	no
FF	70.14	20.82			
28" short	58.37	2.66	26.31	0.00	yes
FF	41.07	10.86			
28" short	30.39	0.85	192.02	0.00	yes
FF	19.17	2.54			
28" short	17.09	1.63	2.58	0.12	no
FF	18.93	3.40			
28" short	35.90	1.31	117.60	0.00	yes
FF	22.75	3.77			
28" short	40.38	1.64	11.74	0.00	yes
FF	32.10	7.85			
28" short	25.78	0.66	19.73	0.00	yes
FF	20.91	3.58			
28" short	30.73	2.73	143.85	0.00	yes
FF	17.14	2.43			
28" short	40.28	1.36	6.59	0.02	yes
FF	34.25	7.67			
28" short	27.66	1.05	34.03	0.00	yes
FF	20.12	4.15			
28" short	20.39	4.44	1.11	0.31	no
FF	22.51	4.54			

(II) Comparison between 28” short vs. Free field (Helmet)

Test (Bare)	Average	Stdev	F	p	Conclusion
28" short	81.64	4.86	189.07	0.00	yes
FF	117.98	3.20			
28" short	58.37	2.66	167.33	0.00	yes
FF	76.77	1.49			
28" short	30.39	0.85	86.23	0.00	yes
FF	24.80	1.47			
28" short	17.09	1.63	0.16	0.70	no
FF	17.45	1.24			
28" short	35.90	1.31	642.74	0.00	yes



FF	17.11	1.13			
28" short	40.38	1.64	270.17	0.00	yes
FF	55.24	1.20			
28" short	25.78	0.66	125.10	0.00	yes
FF	30.48	0.90			
28" short	30.73	2.73	153.73	0.00	yes
FF	13.33	0.35			
28" short	40.28	1.36	342.89	0.00	yes
FF	54.80	1.29			
28" short	27.66	1.05	1.26	0.28	no
FF	28.29	0.48			
28" short	20.39	4.44	20.57	0.00	yes
FF	10.07	0.20			

(III) Comparison between 28" short vs. D1 (bare)

Test (Bare)	Average	Stdev	F	p	Conclusion
28" short	81.64	4.86	189.07	0.00	yes
D1	117.98	3.20			
28" short	58.37	2.66	167.33	0.00	yes
D1	76.77	1.49			
28" short	30.39	0.85	86.23	0.00	yes
D1	24.80	1.47			
28" short	17.09	1.63	0.16	0.70	no
D1	17.45	1.24			
28" short	35.90	1.31	642.74	0.00	yes
D1	17.11	1.13			
28" short	40.38	1.64	270.17	0.00	yes
D1	55.24	1.20			
28" short	25.78	0.66	125.10	0.00	yes
D1	30.48	0.90			
28" short	30.73	2.73	153.73	0.00	yes
D1	13.33	0.35			
28" short	40.28	1.36	342.89	0.00	yes
D1	54.80	1.29			
28" short	27.66	1.05	1.26	0.28	no
D1	28.29	0.48			
28" short	20.39	4.44	20.57	0.00	yes
D1	10.07	0.20			

(IV) Comparison between 28” short vs. D1 (helmet)

Test (Helmet)	Average	Stdev	F	p	Conclusion
28" short	44.86	10.57	43.04	0.00	yes
D1	107.43	18.52			
28" short	21.69	1.48	76.98	0.00	yes
D1	31.70	2.07			
28" short	20.97	1.55	22.91	0.00	yes
D1	33.99	5.88			
28" short	36.93	2.88	8.20	0.02	yes
D1	41.09	1.51			
28" short	33.37	1.11	514.69	0.00	yes
D1	17.03	1.17			
28" short	26.99	1.83	50.80	0.00	yes
D1	49.06	6.68			
28" short	21.05	1.54	2.62	0.14	no
D1	22.59	1.48			
28" short	19.11	2.71	3.39	0.10	no
D1	28.25	10.76			
28" short	24.06	2.65	29.98	0.00	yes
D1	45.42	8.31			
28" short	26.44	1.74	3.15	0.11	no
D1	24.84	1.00			
28" short	18.60	1.03	3.71	0.09	no
D1	20.74	2.26			

(V) Comparison between D1 vs. D2 (bare)

Test (Bare)	Average	Stdev	F	p	Conclusion
D1	117.98	3.20	0.48	0.52	no
D2	115.32	7.02			
D1	76.77	1.49	280.22	0.00	yes
D2	52.63	2.47			
D1	24.80	1.47	4.71	0.07	no
D2	22.64	1.34			
D1	17.45	1.24	1.37	0.29	no
D2	16.59	0.79			
D1	17.11	1.13	0.96	0.37	no
D2	16.32	1.14			
D1	55.24	1.20	233.01	0.00	yes
D2	39.24	1.72			
D1	30.48	0.90	130.77	0.00	yes

D2	21.23	1.35			
D1	13.33	0.35	58.44	0.00	yes
D2	10.53	0.64			
D1	54.80	1.29	273.78	0.00	yes
D2	38.50	1.49			
D1	28.29	0.48	233.76	0.00	yes
D2	20.42	0.91			
D1	10.07	0.20	44.13	0.00	yes
D2	8.32	0.48			

(VI) Comparison between D1 vs. D2 (Helmet)

Test (Helmet)	Average	Stdev	F	p	Conclusion
D1	107.43	18.52	2.00	0.20	no
D2	95.10	6.10			
D1	31.70	2.07	100.71	0.00	yes
D2	21.04	1.16			
D1	16.87	19.61	1.25	0.30	no
D2	26.76	2.20			
D1	41.09	1.51	72.52	0.00	yes
D2	33.38	1.35			
D1	17.03	1.17	0.34	0.58	no
D2	16.67	0.73			
D1	49.06	6.68	31.14	0.00	yes
D2	30.64	3.14			
D1	22.59	1.48	59.84	0.00	yes
D2	15.90	1.25			
D1	28.25	10.76	3.37	0.10	no
D2	17.95	6.45			
D1	48.90	11.23	18.89	0.00	yes
D2	24.93	5.10			
D1	24.84	1.00	63.64	0.00	yes
D2	19.56	1.09			
D1	20.74	2.26	17.52	0.00	yes
D2	13.53	3.12			

(VII) Comparison between Long vs. D1 (Bare)

Test (Bare)	Average	Stdev	F	p	Conclusion
Long	153.51	13.87	24.93	0.00	yes
D1	117.98	3.20			
Long	104.52	8.40	42.32	0.00	yes



D1	76.77	1.49			
Long	52.93	1.90	546.29	0.00	yes
D1	24.80	1.47			
Long	25.17	1.10	86.30	0.00	yes
D1	17.45	1.24			
Long	58.00	3.37	528.56	0.00	yes
D1	17.11	1.13			
Long	66.96	4.42	26.19	0.00	yes
D1	55.24	1.20			
Long	51.68	3.26	157.44	0.00	yes
D1	30.48	0.90			
Long	28.86	2.58	142.84	0.00	yes
D1	13.33	0.35			
Long	67.04	5.13	21.48	0.00	yes
D1	54.80	1.29			
Long	48.11	3.37	135.49	0.00	yes
D1	28.29	0.48			
Long	21.13	1.62	184.32	0.00	yes
D1	10.07	0.20			

(VIII) Comparison between Long vs. D1 (Helmet)

Test (Helmet)	Average	Stdev	F	p	Conclusion
Long	104.95	17.45	0.05	0.83	no
D1	107.43	18.52			
Long	31.78	13.98	0.00	0.99	no
D1	31.70	2.07			
Long	45.41	7.00	9.39	0.02	yes
D1	16.87	19.61			
Long	49.36	2.95	31.07	0.00	yes
D1	41.09	1.51			
Long	45.03	3.10	357.11	0.00	yes
D1	17.03	1.17			
Long	70.57	13.15	10.64	0.01	yes
D1	49.06	6.68			
Long	33.25	6.36	13.34	0.00	yes
D1	22.59	1.48			
Long	42.49	3.42	7.95	0.02	yes
D1	28.25	10.76			
Long	49.37	13.68	0.00	0.95	no
D1	48.90	11.23			
Long	51.66	7.31	66.04	0.00	yes



D1	24.84	1.00			
Long	33.52	5.90	20.45	0.00	yes
D1	20.74	2.26			

Linear acceleration and ARS comparison (yes – significant difference/ no – not significantly different based on p value)

(I) FF vs. Short 28” (bare)

Sensor#	Test (Bare)	Average	Stdev	diff	F	p	Conclusion
Sensor 5 max	Short	114.66	27.75	-29.37	3.99	0.06	no
	FF	144.03	34.08				
Sensor 5 min	Short	-210.96	20.79	-100.60	115.25	0.00	yes
	FF	-110.36	19.72				
Sensor 6 max	Short	115.82	19.76	-5.73	0.30	0.59	no
	FF	121.55	24.20				
Sensor 6 min	Short	-132.18	3.77	-29.22	13.73	0.00	yes
	FF	-102.96	21.90				

(II) FF vs. Short 28” (Helmet)

Sensor#	Test (Helmet)	Average	Stdev	diff	F	p	Conclusion
Sensor 5 max	Short	281.83	14.14	154.09	329.95	0.00	yes
	FF	127.74	12.23				
Sensor 5 min	Short	-530.57	34.88	-438.73	1112.18	0.00	yes
	FF	-91.84	10.78				
Sensor 6 max	Short	83.70	14.35	165.03	617.49	0.00	yes
	FF	-81.34	6.00				
Sensor 6 min	Short	-102.44	19.84	-213.92	620.24	0.00	yes
	FF	111.49	9.80				

(III) Short 28” vs. D1 (Bare)

Sensor#	Test (Bare)	Average	Stdev	diff	F	p	Conclusion
Sensor 5 max	Short	114.66	27.75	-87.02	29.94	0.00	yes
	D1	201.68	21.26				
Sensor 5 min	Short	-210.96	20.79	-128.95	137.75	0.00	yes
	D1	-82.01	8.04				
Sensor 6 max	Short	115.82	19.76	4.39	0.19	0.68	no
	D1	111.43	3.33				



Sensor 6 min	Short	-132.18	3.77	-37.99	41.39	0.00	yes
	D1	-94.19	16.63				
ARS max	Short	503.51	23.40	21.80	0.98	0.34	no
	D1	481.71	54.91				
ARS min	Short	-311.88	17.83	630.21	3210.65	0.00	yes
	D1	-942.09	18.91				

(IV) Short 28" vs. D1 (Helmet)

Sensor#	Test (helmet)	Average	Stdev	diff	F	p	Conclusion
Sensor 5 max	D1	279.24	34.28	-2.59	0.02	0.88	No
	Short	281.83	14.73				
Sensor 5 min	D1	-152.62	21.80	377.96	513.41	0.00	yes
	Short	-530.57	30.27				
Sensor 6 max	D1	165.35	9.09	81.65	122.74	0.00	yes
	Short	83.70	13.75				
Sensor 6 min	D1	-199.77	13.69	-97.33	97.78	0.00	yes
	Short	-102.44	17.24				
ARS max	D1	757.34	145.87	475.52	52.59	0.01	yes
	Short	281.83	14.73				
ARS min	D1	-1707.12	144.70	-1176.55	316.70	0.00	yes
	Short	-530.57	30.27				

(V) D1 vs. D2 (Bare)

Sensor#	Test (Bare)	Average	Stdev	diff	F	p	Conclusion
Sensor 5 max	D1	201.68	21.26	50.15	11.37	0.02	yes
	D2	151.53	20.81				
Sensor 5 min	D1	-82.01	8.04	-7.73	3.65	0.10	no
	D2	-74.28	0.89				
Sensor 6 max	D1	111.43	3.33	15.47	2.05	0.20	no
	D2	95.97	21.33				
Sensor 6 min	D1	-94.19	16.63	10.33	1.34	0.29	no
	D2	-104.52	6.52				
ARS max	D1	481.71	54.91	153.16	29.94	0.00	yes
	D2	328.55	10.89				
ARS min	D1	-942.09	18.91	-217.13	86.45	0.00	yes
	D2	-724.96	42.70				

(VI) D1 vs. D2 (Helmet)



Sensor#	Test (Helmet)	Average	Stdev	diff	F	p	Conclusion
Sensor 5 max	D1	279.24	34.28	126.23	65.30	0.00	yes
	D2	153.01	6.72				
Sensor 5 min	D1	-152.62	21.80	-66.43	35.73	0.00	yes
	D2	-86.19	11.93				
Sensor 6 max	D1	165.35	9.09	71.11	65.15	0.00	yes
	D2	94.24	17.48				
Sensor 6 min	D1	-199.77	13.69	-49.20	38.76	0.00	yes
	D2	-150.57	11.18				
ARS max	D1	757.34	145.87	337.32	25.65	0.00	yes
	D2	420.03	30.00				
ARS min	D1	-1707.12	144.70	-673.10	99.91	0.00	yes
	D2	-1034.02	41.66				

(VII) Long vs. D1 (Bare)

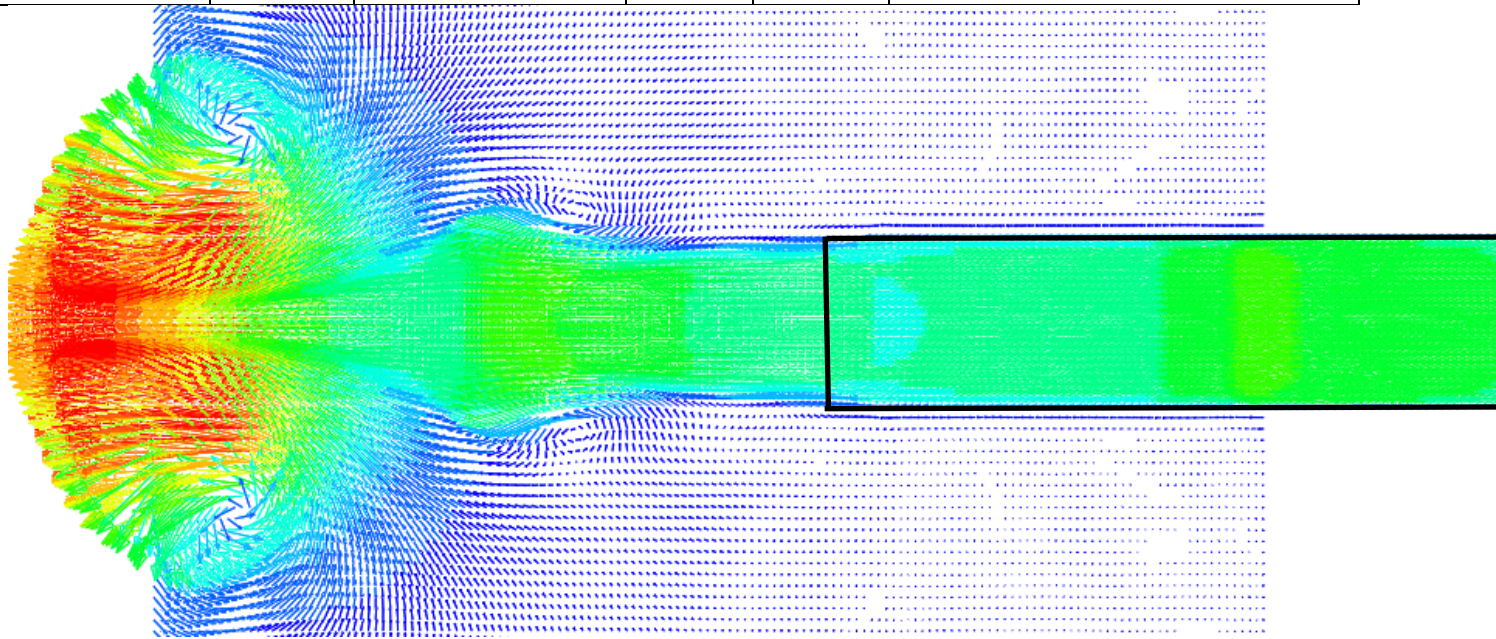
Sensor#	Test (Bare)	Average	Stdev	diff	F	p	Conclusion
Sensor 5 max	D1	201.68	21.26	-37.11	5.25	0.06	no
	Long	238.79	24.43				
Sensor 5 min	D1	-82.01	8.04	235.90	61.74	0.00	yes
	Long	-317.90	59.50				
ARS max	D1	481.71	54.91	-253.71	8.43	0.02	yes
	Long	735.42	150.16				
ARS min	D1	-942.09	18.91	293.82	7.47	0.03	yes
	Long	-1235.91	223.46				

(VIII) Long vs. D1 (Helmet)

Sensor#	Test (Helmet)	Average	Stdev	diff	F	p	Conclusion
Sensor 5 max	D1	279.24	34.28	-87.15	5.25	0.13	no
	Long	366.39	108.89				
Sensor 5 min	D1	-152.62	21.80	206.86	61.74	0.00	yes
	Long	-359.48	62.79				
ARS max	D1	757.34	145.87	-286.21	8.43	0.20	no
	Long	1043.55	435.50				
ARS min	D1	-1707.12	144.70	140.99	7.47	0.53	no
	Long	-1848.11	452.02				

9 Appendix B – Velocity vector field near the exit of the shock tube.

Naming Scheme					
Orientation	Helmet?	Experiment Location	Degrees	Shot Type	
<i>Front</i>	<i>Helmeted</i>	<i>UNL</i>	<i>0Deg</i>	<i>EXT</i>	Extended
<i>Back</i>	<i>Bare</i>	<i>FF</i>	<i>30Deg</i>		blank is Short (free field conditions)
<i>Side</i>				<i>D1</i>	D1
				<i>D2</i>	D2



ARO/NATICK Phase II Report

Evaluation of Primary Blast Loading Condition Generated by Shock Tube with That of Live-Fire Blast

This report summarizes an experimental study on the surface pressure, linear acceleration and angular rate of an instrumented Realistic Explosion-resistant Dummy (RED) head under primary blast loading. The RED head was subjected to two blast loading conditions: a) that generated by live-fire free-field blasts, and b) that simulated using the shock tubes at the University of Nebraska-Lincoln (UNL). For each loading condition, an identical set of pressure and acceleration history profiles was obtained for a duration of 0.1 second. The results show that the live-fire blast loading condition can be simulated reasonably well with the shock-induced air blast loading generated inside UNL 28-inch shock tube. The effects of performing blast tests with a sample located outside a shock tube was also studied by comparing the measurements from the tests inside the 28-inch shock tube with those from the tests with the RED head being placed at two different locations outside UNL 9-inch shock tube. From the measurements, the deficiencies of simulating blast loading outside the shock tube have been identified. Finally, the acceleration and angular rate data collected over a very long period of time enabled the study of the post-blast kinematics of the RED head in shock tube blast testing. The data show small but discernable post-blast secondary dynamic response, which can be related to the visually observed large sample motion caused by the interaction between the RED head and the expansion of pre-compressed helium driver gas behind the primary blast wave. However, this appears to be a non-impulsive event and its dynamic effects on the RED head are insignificant.

Submitted by:

Ruqiang Feng
University of Nebraska-Lincoln

ARO Grant:

WF911NF-08-1-0483
WBS: 2511-05001-001

Submitted to:

Army Research Office

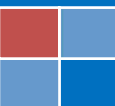




Table of Contents

1	Introduction	3
1.1	Case I	3
1.2	Case II.....	3
2	Shock Tube Experiment Protocol.....	3
3	Methodology	5
3.1	Sensor placement	5
3.2	RED head placement.....	7
3.2.1	Case I: Inside 28” shock tube	7
3.2.2	Case II: Outside 9” shock tube	7
4	Results and Discussion.....	9
4.1	Case I (a): RED head inside 28” tube with front bare head facing short pulse	10
4.2	Case I (b): RED head inside 28” tube with front bare head facing long pulse	13
4.3	Case II (a): RED head outside 9” tube at D1 position with front bare head facing.....	16
4.4	Case II (b): RED head outside 9” tube at D2 position with front bare head facing.....	20
5	Closing Remarks	24
5.1	Peak overpressure.....	24
5.2	Impulse density	25
5.3	Acceleration and angular rate.....	25
	Reference.....	26



1 Introduction

In this experimental study, the blast loadings generated by compressed-gas driven shock tubes on the Realistic Explosion-resistant Dummy (RED) head, which is a head neck surrogate, were evaluated along with comparisons of the test results with the data from the live-fire free-field explosion tests reported previously [1]. Two shock tubes in the blast facility at the University of Nebraska-Lincoln (UNL) were used in the study. The RED head was instrumented with 11 pressure sensors on the head surface, 2 accelerometers aligned respectively with in-plane X and Y axes, and an angular rate sensor sensitive to the angular velocity about out-of-plane Z axis. The accelerometers and the angular rate sensor were placed at the center of gravity of the RED head. In all the shock tube experiments presented in this report, the RED head was placed with its anterior facing the blast loading.

1.1 Case I

The RED head was exposed to two different pulse durations inside UNL 28" shock tube:

- (a) short duration pulse of 3 ms, and
- (b) long duration pulse of 5 ms.

1.2 Case II

The RED head was tested at two positions outside UNL 9" shock tube:

- (a) D1 position where the RED head front is 1.5 in. away from the tube muzzle, and
- (b) D2 position where the RED head front is 6.5 in. away from the tube muzzle.

The live-fire free-field blast tests were performed to generate 3-ms short duration blast data [1]. No long duration live-fire blast test was performed due to the practical limit.

2 Shock Tube Experiment Protocol

The instrumented RED head was exposed to blast loadings symmetric to the sagittal plane for total 17 tests. The following four types of experimental conditions were used in the tests.

- 1) Case I (a): Front bare head facing at 0° tilt inside the 28" shock tube with
 - a. **3 ms pulse duration**
 - b. sampling rate at 1 MHz
 - c. data collection for 0.1 s
 - d. no video
 - e. 5 trails
 - f. 11 pressure sensors (PCB #102B06)
 - g. 2 linear accelerometers (Endevoc #7270A)
 - h. 1 angular rate sensor (DTS ARS-Pro)



- i. 14 membranes
 - j. 5.625" breech length
 - k. helium gas driver
- 2) Case I (b): Front bare head facing at 0° tilt inside the 28" shock tube with
- a. **Long pulse duration (~5 ms)**
 - b. sampling rate at 1 MHz
 - c. data collection for 0.1 s
 - d. 4 test trails
 - e. 11 pressure sensors (PCB #102B06)
 - f. 2 linear accelerometers (Endevoc #7270A)
 - g. 1 angular rate sensor (DTS ARS-Pro)
 - h. 13 membranes
 - i. 29.625" breech length
 - j. helium gas driver
- 3) Case II (a): Front bare head facing at 0° tilt outside the 9" shock tube at **D1 position** with
- a. rear wedge base edge at 11.8125" (1.5" nose tip distance) from tube muzzle
 - b. sampling rate at 1MHz
 - c. data collection for 0.1 s
 - d. 4 trails
 - e. 11 pressure sensors (PCB #102B06)
 - f. 2 linear accelerometers (Endevoc #7270A)
 - g. 1 angular rate sensor (DTS ARS-Pro)
 - h. 5 membranes
 - i. 35.625" breech length
 - j. helium gas driver
- 4) Case II (b): Front bare head facing at 0° tilt outside the 9" shock tube at **D2 position** with
- a. rear wedge base edge at 16.8125" (6.5" nose tip distance) from tube muzzle
 - b. sampling rate at 1MHz
 - c. data collection for 0.1 s
 - d. 4 trails
 - e. 11 pressure sensors (PCB #102B06)
 - f. 2 linear accelerometers (Endevoc #7270A)
 - g. 1 angular rate sensor (DTS ARS-Pro)
 - h. 5 membranes
 - i. 35.625" breech length
 - j. helium gas driver

3 Methodology

3.1 Sensor placement

Figure 1 shows the sensor locations. The details of the sensors used are specified in Table 1.

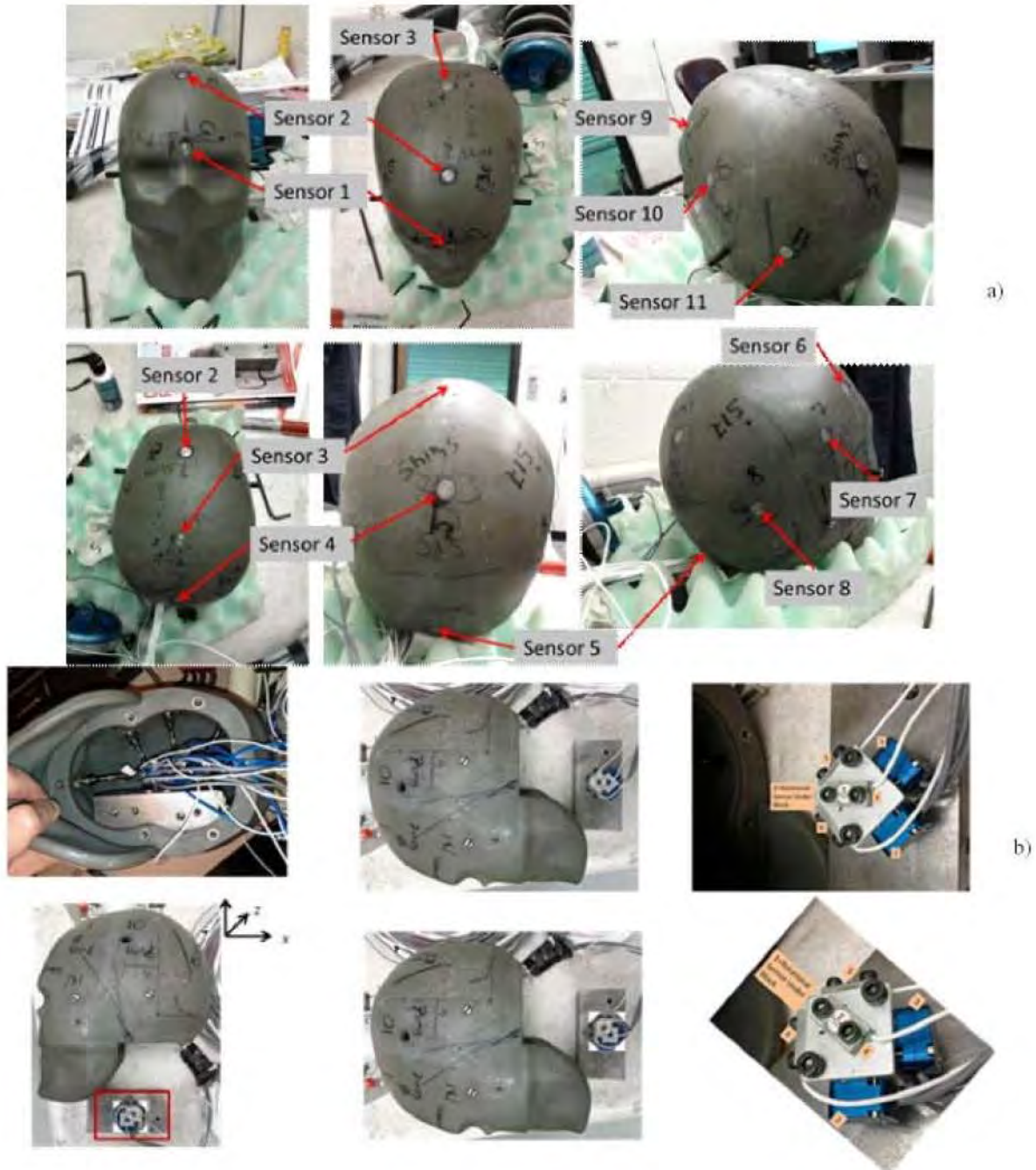


Figure 1: a) Pressure sensor locations on the RED head; b) Linear acceleration and angular rate sensors on a mounting block placed at the center of gravity of the RED head.



Table 1: Sensor part numbers, channel numbers in NI-DAQ system, and calibration factors

Sl. No	Channel Number	Sensor Slot at NI-DAQ	Sensor Position*	LabView Description	Sensor	Calibration (mV/psi)
1	0	PXI1Slot5/ai0	X1	X1	PCB1157**	5.69E-03
2	1	PXI1Slot5/ai1	X2	X2	PCB1145***	5.69E-03
3	2	PXI1Slot5/ai2	1	HS-1	28786	9.85E-03
4	3	PXI1Slot5/ai3	2	HS-2	28654	9.95E-03
5	4	PXI1Slot5/ai4	3	HS-3	25528	9.63E-03
6	5	PXI1Slot5/ai5	4	HS-4	28289	1.03E-02
7	6	PXI1Slot5/ai6	5	HS-5	28523	1.04E-02
8	7	PXI1Slot5/ai7	6	HS-6	23354	9.99E-03
9	8	PXI1Slot6/ai0	7	HS-7	28652	1.03E-02
10	9	PXI1Slot6/ai1	8	HS-8	28655	9.72E-02
11	10	PXI1Slot6/ai2	9	HS-9	25523	1.01E-02
12	11	PXI1Slot6/ai3	10	HS-10	28763	1.09E-02
13	12	PXI1Slot6/ai4	11	HS-11	28763	1.09E-02
14	13	PXI1Slot6/ai5	CG (in X-Y)	ARS	DTS 18K	1.03E-03
15	14	PXI1Slot6/ai6	CG (in X)	Lin4	LinearAccs	8.33E-03
16	15	PXI1Slot6/ai6	CG (in Y)	Lin5	LinearAccs	8.33E-03

* The positions of the numbered sensors and the linear acceleration/angular rate sensors are specified in Figure 1. The positions of X1 and X2 are shown in Figure 2 below.

** PCB1153 was used for the long duration tests inside 28” shock tube.

*** PCB1158 was used for the long duration tests inside 28” shock tube.

3.2 RED head placement

3.2.1 Case I: RED head inside 28" shock tube

Figure 2 illustrates schematically the configuration of UNL 28" shock tube and the RED head positions for in-tube short and long duration pulse tests, respectively.

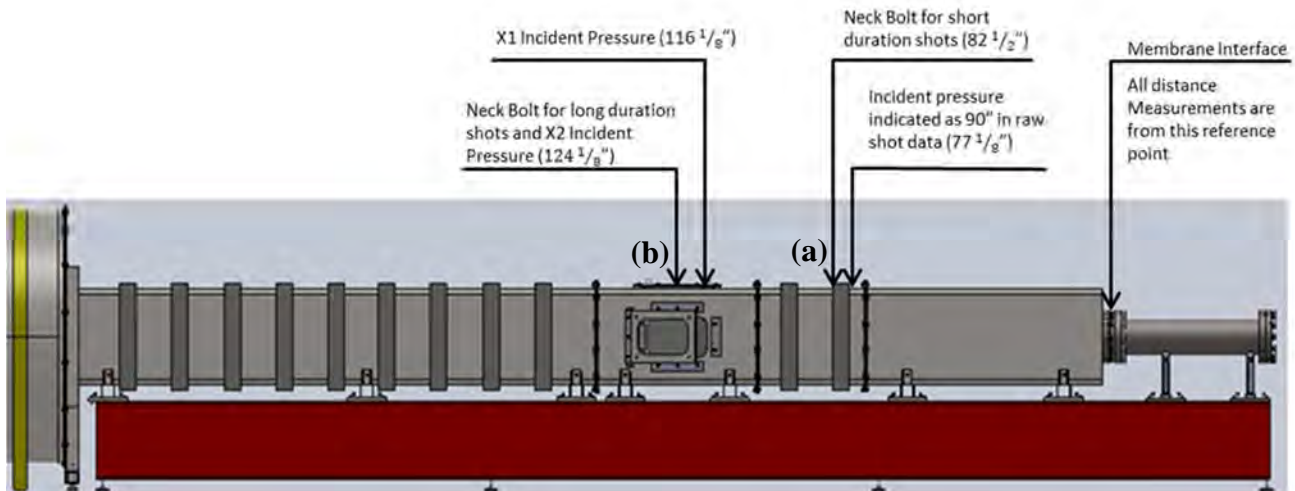


Figure 2: The RED head locations inside the 28" shock tube: (a) position for short duration pulse, and (b) position for long duration pulse.

3.2.2 Case II: RED head outside 9" shock tube

Figure 3 shows the experimental configuration for testing the RED head outside UNL 9" shock tube. NATICK wedge base was used to align the nose tip with the tube center line.



Figure 3: Picture showing that the RED head was placed outside the 9" shock tube. The RED head nose tip was 1.5" from the tube muzzle and centered with the tube center line and in 0° position using the NATICK manufactured wedge base.

Figure 4 shows schematically D1 and D2 position, which result in 1.5 in. and 6.5 in. distances from the RED head nose tip to the tube muzzle, respectively. The shock tube blast test matrix is presented in Table 2.

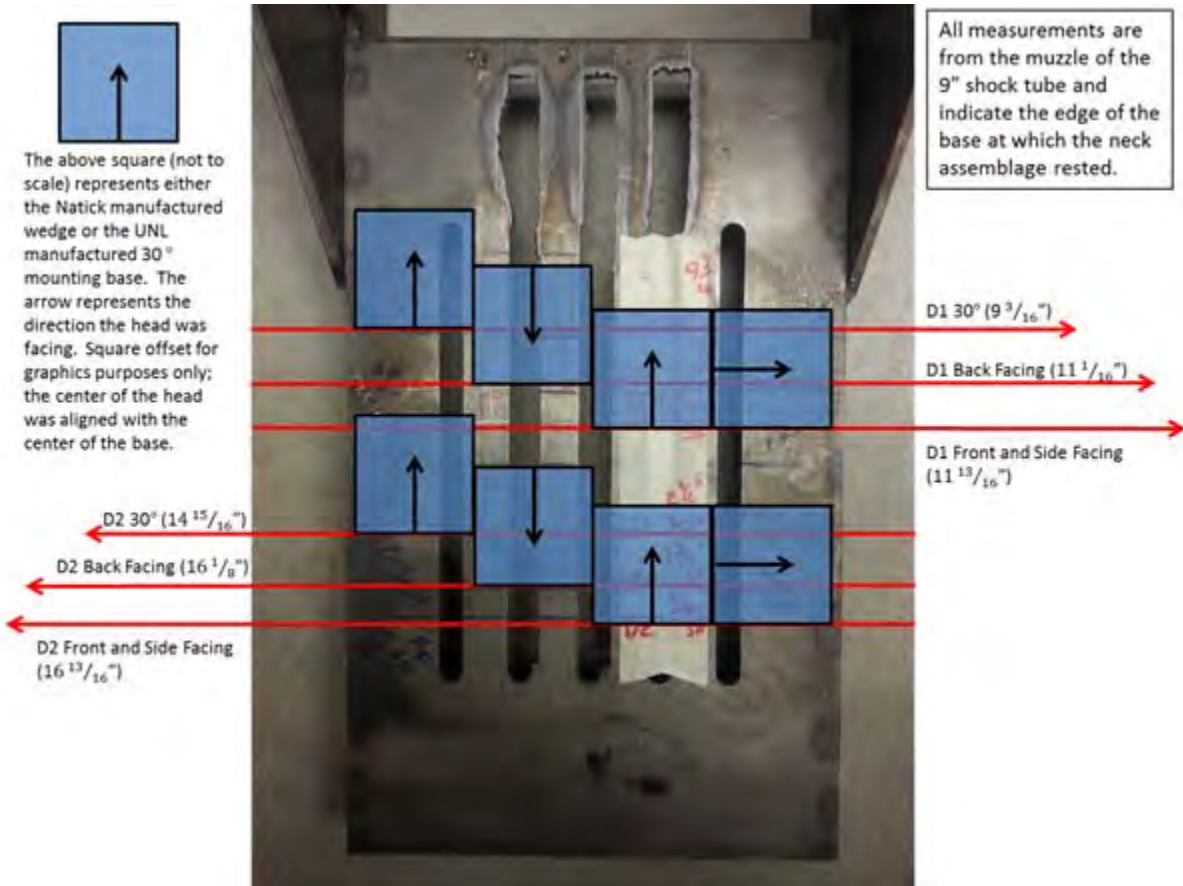


Figure 4: D1 and D2 positions for mounting the RED head outside the 9'' shock tube.

Table 2: Test matrix

Shock tube	Location/Pulse Duration	RED Head Placement
28"	Inside tube, 3 ms pulse	Front Facing Bare
	Inside tube, 5 ms pulse	Front Facing Bare
9"	Outside tube at 1.5" from muzzle	Front Facing Bare
	Outside tube at 6.5" from muzzle	Front Facing Bare



4 Results and Discussion

Table 3 summarizes the loading conditions used in the tests along with the shot logs. Helium gas was used in all the tests. The shock velocities measured in the tests are presented in Figure 5.

Table 3: Shot logs for Phase II tests (1 s data recording duration)

Sl. No	Blast No	Type of Test	Breech Length (in.)	Number of Membranes
1	3427	Long Duration With HS video	29.625	13
2	3428			
3	3429			
4	3430			
5	3431	Short Duration Without HS Video	12	14
6	3432			
7	3433			
8	3434			
9	3435			
10	3437	D1 Position with HS Video	35.625	5
11	3438			
12	3439			
13	3440			
14	3442			
15	3444	D2 Position with HS Video		
16	3445			
17	3446			

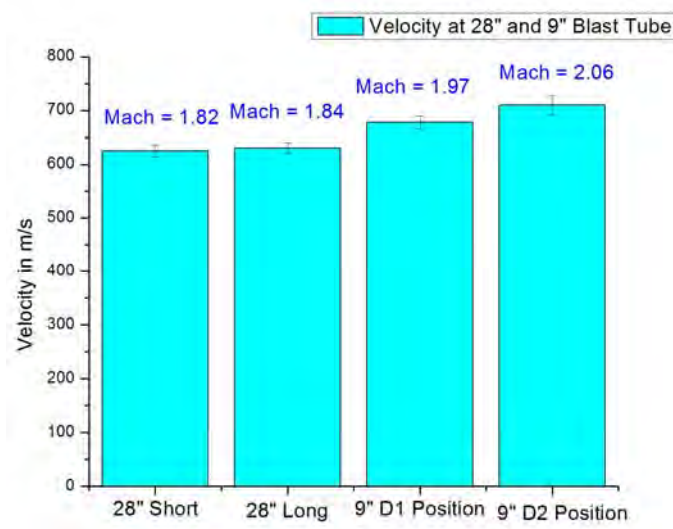


Figure 5: Shock velocities of the short and long duration blast loadings inside the 28” shock tube and the blast loadings at D1 and D2 positions outside the 9” shock tube.

4.1 Case I (a): RED head inside 28” tube with front bare head facing short pulse

A total of 5 tests intended to repeat the same loading condition were performed for this case. In Figure 6, the peak overpressures induced at various locations on the RED head by the 3-ms short duration blasts generated inside UNL 28” shock tube are presented along with those of the live-fire free-field blasts [1]. Though comparable, the two sets of data have statistically noticeable differences except for Sensor 4, where one error bar range is within the other. In this work, a power analysis was typically performed for a comparison with significant error bar overlapping to determine the chance for missing a difference (type II error). The chance is 59% for Sensor 4 comparison here. The primary reason for the difference is that the mean of the peak overpressures induced by the shock tube blasts is about 40% higher than that by the live-fire blasts as indicated by the measurements of Sensor 1 (the front most sensor). The difference between the results of the least intense shock tube blast and the most intense live-fire blast is much less significant. Overall the shock tube data capture the characteristic features of the live-fire data. The shock tube data from the sensors mounted along the two sides of the RED head also show the expected symmetry with respect to the sagittal plane, which is, however, absent in the live-fire results.

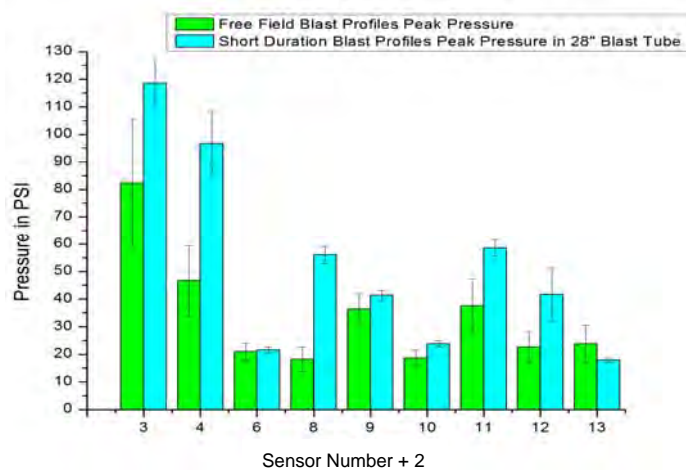


Figure 6: Peak overpressures induced on RED head by live-fire blasts and 3 ms blasts generated inside 28” shock tube.

Figure 7 shows the comparisons of the mean maximum positive and negative accelerations induced at the center of gravity of the RED head by the live-fire free-field blasts [1] and those by the 3-ms short duration blasts generated inside UNL 28” shock tube. Accelerometer 1 was aligned in X direction while Accelerometer 2 in Y direction. The differences between the two sets of data are statistically insignificant for the first three comparisons (from left) even though the chances for missing a difference are 94%, 77% and 69%, respectively. The difference is somewhat larger for the last comparison. Overall the two sets of data are in good agreement.

Figures 8 and 9 show respectively the acceleration profiles measured by Accelerometers 1 and 2 at the center of gravity of the RED head during a 3 ms duration blast loading generated inside the 28” shock tube. For Accelerometer 1 (aligned in X direction, Figure 8), the maximum positive and

negative values are 166 G and -163 G, respectively. For Accelerometer 2 (aligned in Y direction, Figure 9), the maximum positive and negative values are 127 G and -64 G, respectively. There are small but discernable slow secondary growths in both accelerations starting at about 10 ms after the initial shock loading. In the shock tube tests, large sample motion with the arrival of expanding flow of the pre-compressed driver gas at the RED head has been observed via high-speed video. The speed of the moving contact surface between the colder driver gas and hotter post-shock air is known to decrease with increasing distance and time. An estimate using 10 ms delay time gave an average speed of ~200 m/s, which is reasonable value since it is expected to peak at ~360 m/s.

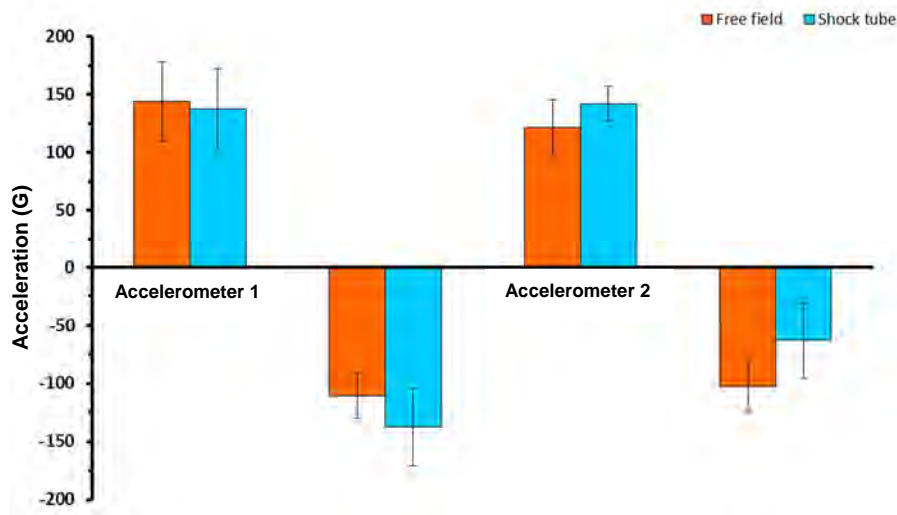


Figure 7: RED head mean maximum positive and negative accelerations induced by live-fire blasts and 3 ms blasts generated inside the 28” shock tube.

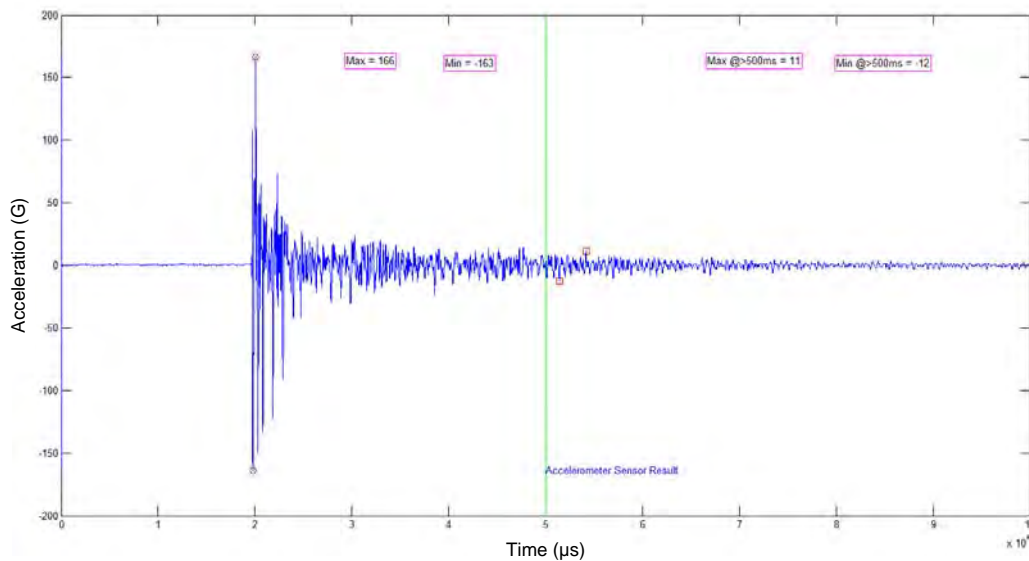


Figure 8: Linear acceleration history of RED head in X direction during a 3 ms blast loading inside the 28” shock tube.

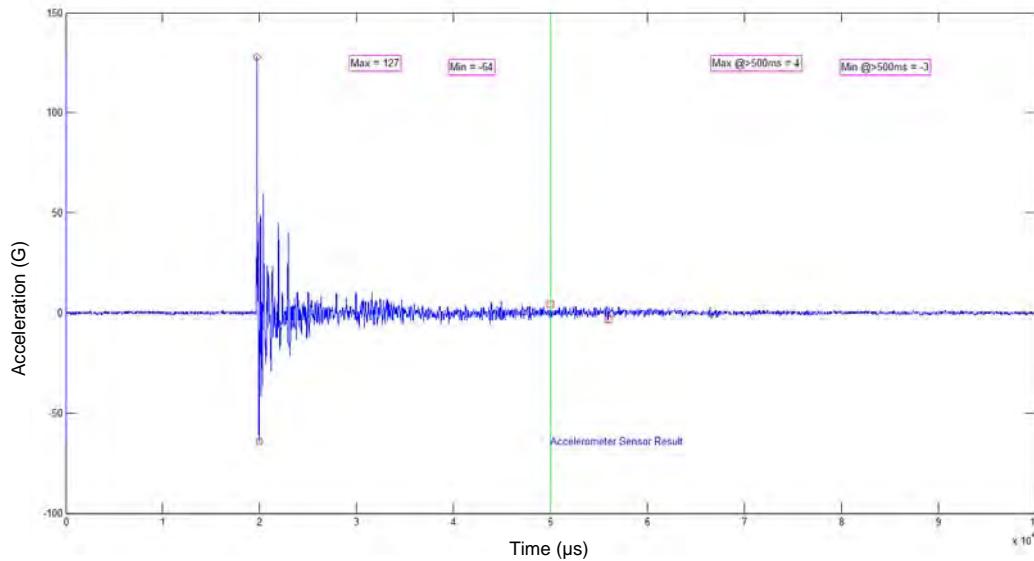


Figure 9: Linear acceleration history of RED head in Y direction during a 3 ms blast loading inside the 28'' shock tube.

The secondary response is seen to diminish quickly. Beyond 50 ms, the maximum positive and negative accelerations are 11 G and -12 G, respectively in X, and 4 G and -3 G, respectively in Y. Figure 10 shows the angular rate profile measured at the center of gravity of the RED head during the same test. The maximum positive and negative values are seen to be 1460 °/s and -1588 °/s, respectively. Small post-blast secondary dynamic event similar to those appeared in Figures 8 and 9 is again discernable. Beyond 50 ms, the maximums are 100 °/s and -116 °/s, respectively. The results shown in Figures 8-10 indicate that the post-blast RED head motion driven by the trailing expansion of the driver gas is non-impulsive and the resultant dynamic loading is insignificant.

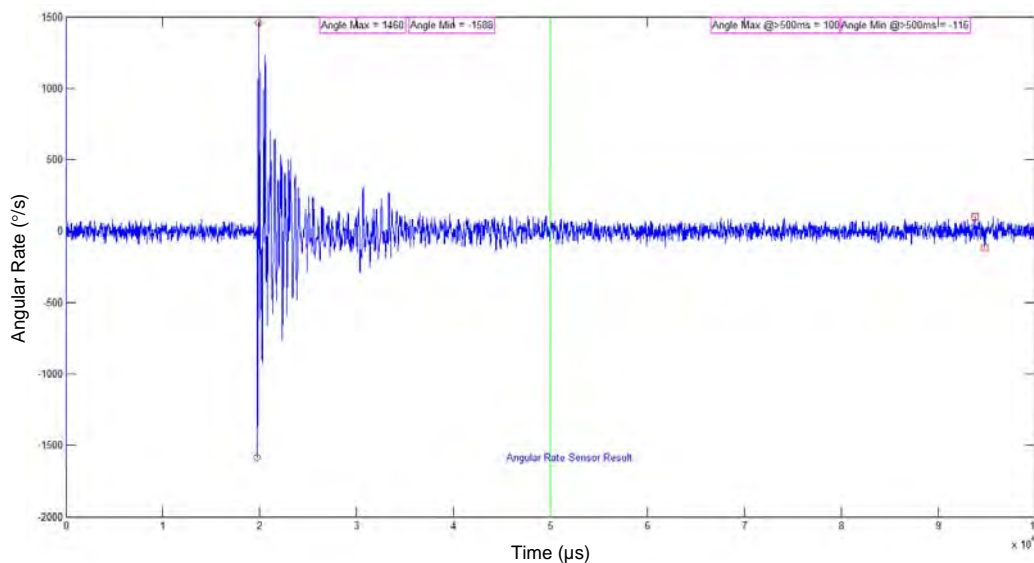


Figure 10: Angular rate history of RED head about Z axis during a 3 ms blast loading inside 28'' shock tube.

Figure 11 shows the comparisons of impulse densities (impulses per unit area) induced at various locations on the RED head by the live-fire free-field blasts [1] and those by the 3-ms short duration blasts generated inside the 28” shock tube. Clearly, there is a statistically significant difference in each comparison. Part of the difference comes from the peak overpressure difference between the two as discussed earlier. However, a significant portion of the difference is due to the fact that the shock tube blasts generated with pre-compressed helium gas decayed slower than the live-fire blasts. Therefore, this difference can be reduced in principle by further pulse shaping for faster post-peak overpressure decays or for shorter pulse durations than those generated with Case I (a) conditions.

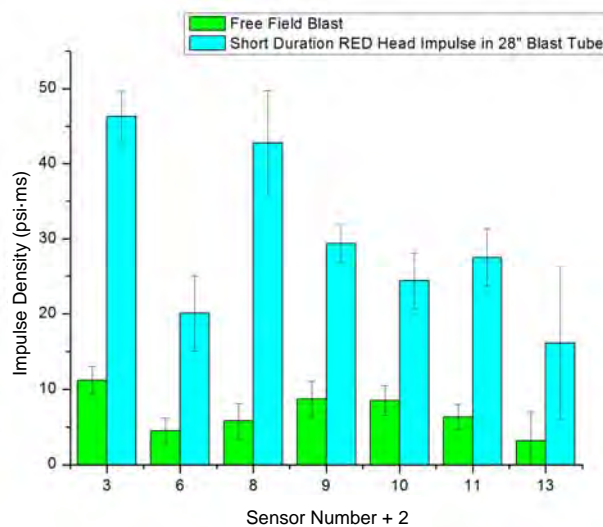


Figure 11: Impulse densities induced on RED head by live-fire blasts and 3 ms blasts generated inside 28” shock tube.

4.2 Case I (b): RED head inside 28” tube with front bare head facing long pulse

A total of 4 shock tube tests intended to repeat the same loading condition were conducted for this case. Figure 12 shows the comparisons of the mean maximum positive and negative accelerations induced at the center of gravity of the RED head by the 5-ms long duration blasts generated inside UNL 28” shock tube (the current case) and those by the 3-ms short duration blasts [Case I (a)]. A statistically significant difference is seen for both the positive and the negative accelerations in X direction (Accelerometer 1) and for the negative acceleration in Y direction (Accelerometer 2). The difference in the positive accelerations in Y direction is insignificant even though the chance for missing a difference is 86%. Compared to the maximum acceleration data of Case I (a), the current data fare worse in matching the live-fire accelerations (see also Figure 7).

Figures 13 and 14 show respectively the acceleration profiles measured by Accelerometers 1 and 2 at the center of gravity of the RED head during a Case I (b) test. For Accelerometer 1 (aligned in X direction), the maximum positive and negative values are 144 G and -192 G, respectively

(Figure 13). Beyond 50 ms, the maximums are 8 G and -8 G, respectively. For Accelerometer 2 (aligned in Y direction), the maximum positive and negative values are 237 G and -61 G, respectively (Figure 14). Beyond 50 ms, the maximums are 1 G and -2 G, respectively. Figure 15 shows the angular rate history measured at the center of gravity of the RED head during the same test. The maximum positive and negative values of the profile shown are 1833 °/s and -1547 °/s, respectively. Beyond 50 ms, the maximums are 107 °/s and -92 °/s, respectively. Small post-blast

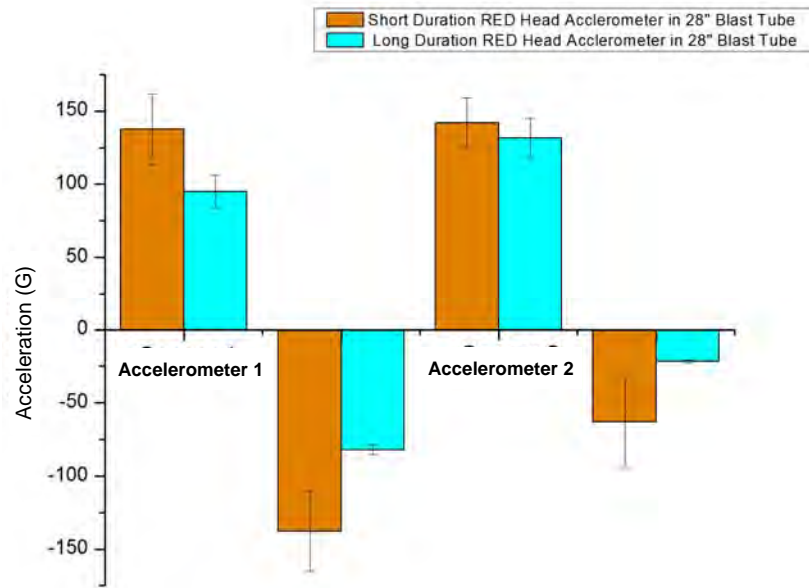


Figure 12: RED head mean maximum positive and negative accelerations induced by blasts generated inside 28” shock tube with Case I (a) and Case II (a) conditions.

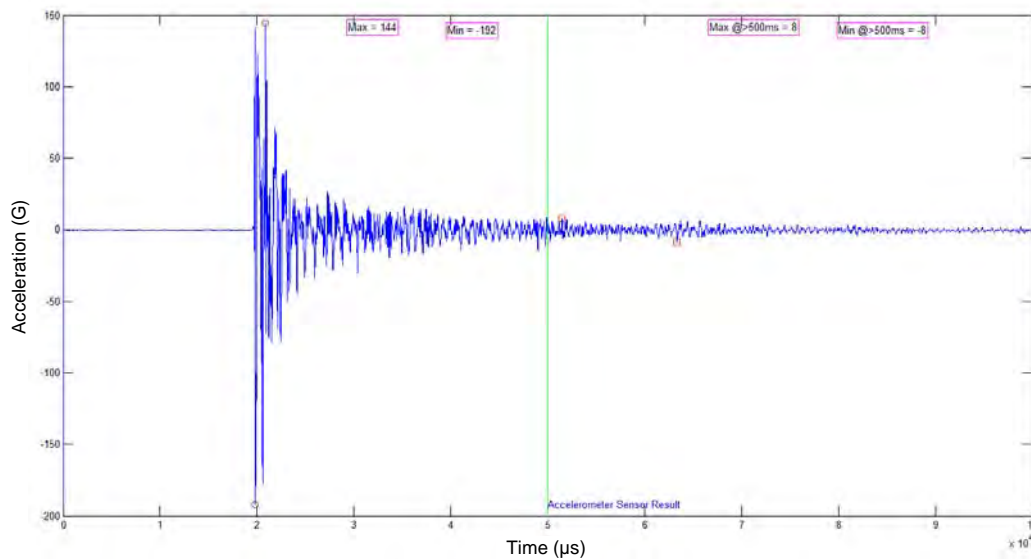


Figure 13: Linear acceleration history of RED head in X direction during a 5 ms blast loading inside 28” shock tube.

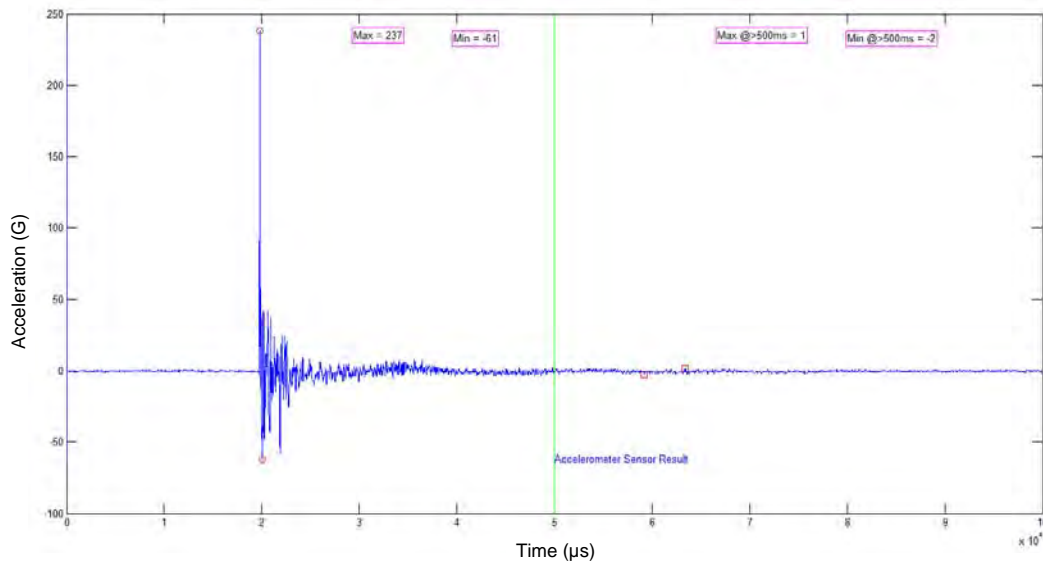


Figure 14: Linear acceleration history of RED head in Y direction during a 5 ms blast loading inside 28” shock tube.

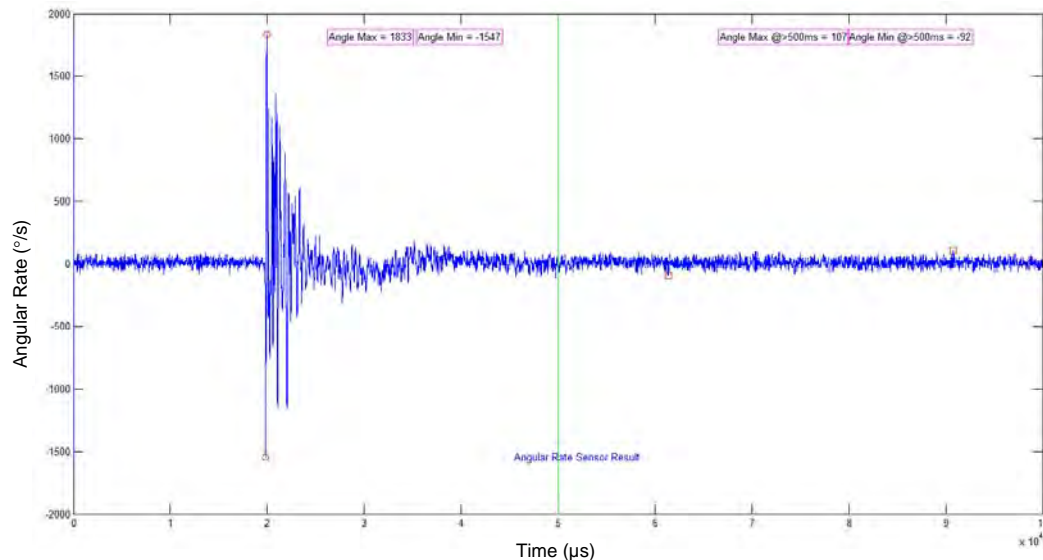


Figure 15: Angular rate history of RED head about Z axis during a 5 ms blast loading inside 28” shock tube.

secondary dynamic event is again discernable in the data shown in Figures 13-15. As a further evidence of its relation to the arrival of the expanding colder helium driver gas at the RED head behind the primary blast wave, the on-set time of the event in this case is seen to be 3~4 ms later than that in Case I (a), where the RED head was placed ~1 m closer to the breach. The average contact surface speed is expected to be slightly higher in the current case because of the more intense and longer loading. Again, this event appears to be non-impulsive and insignificant.

The overpressure and impulse density results of this series of tests will be presented later in comparisons with those of the tests where the RED head was placed outside UNL 9” shock tube.

4.3 Case II (a): RED head outside 9” tube at D1 position with front bare head facing

A total of 4 tests intended to repeat the same loading conditions were carried out for this case using UNL 9” shock tube. Placed at D1 position, the RED head is 1.5 in. from its nose tip to the shock tube muzzle. Figure 16 presents the peak overpressures induced at various locations on the RED head by the blasts generated using Case II (a) conditions in comparison with those obtained in Case I (a) tests (RED head inside 28” tube with front bare head facing 3 ms duration blasts). The loading parameters for the current series of tests were selected with the intention to match the peak overpressure at the front most sensor (Sensor 1) with that of Case I (a). However, the mean of the actual results is about 25% lower than the target value as indicated by the comparison for the sensor. The difference between the two sets of data for the rest of the sensors shown appears to be more or less consistent with this factor except for Sensor 7, for which one error bar range is within the other but the chance for type II error is 84%. Taking the loading level difference into account, the peak overpressure distribution generated with Case I (a) conditions on the RED head can be captured using Case II (a) testing conditions.

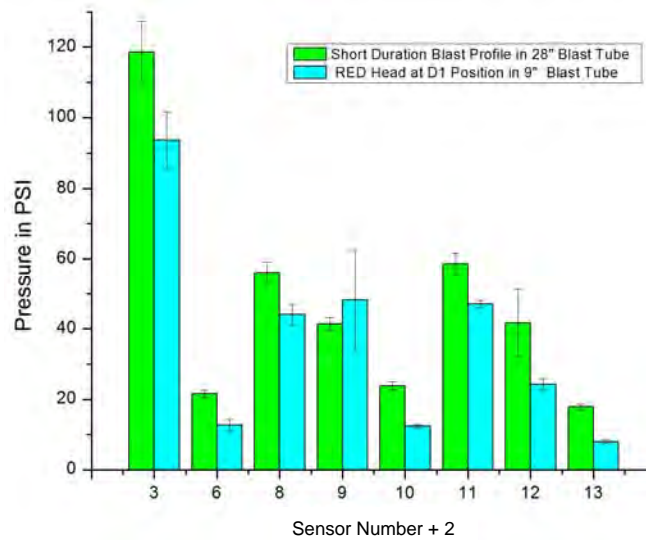


Figure 16: Peak overpressures induced on RED head by blasts generated with Case I (a) and Case II (a) conditions.

However, the comparisons of the impulse densities resulted from the two testing conditions at the same sensor locations give a very different picture as shown Figure 17. The mean impulse density at the front most sensor (Sensor 1) in the current case is 2.5 times as large as that in Case I (a) even though the peak overpressure at the same location is about 25% lower. Despite the very larger impulse density at Sensor 1, the impulse densities at the other sensor locations are drastically smaller, some by an order of magnitude, than those of Case I (a). The comparisons shown in Figures 16 and 17 suggest that the positive overpressure in each Case II (a) test diminished too fast as the blast was engulfing the RED head except in its front region. This is a very different dynamic loading characteristics than those of Case I (a) tests and the live-fire tests [1] (see also Figure 11).

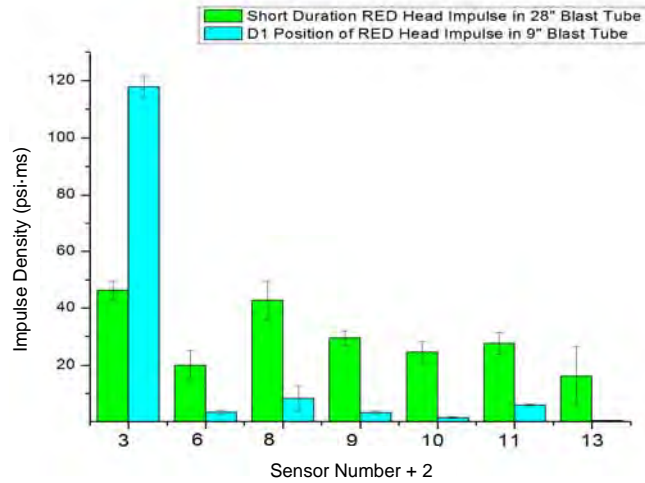


Figure 17: Impulse densities induced on RED head by blasts generated with Case I (a) and Case II (a) conditions.

In Figure 18, the peak overpressure results are further compared with those obtained in Case I (b) tests (RED head inside 28" tube with front bare head facing 5 ms duration blasts). The comparisons are mostly similar to those shown in Figure 16. In Figure 18, one error bar range is within the other for Sensor 6 and error bars are significantly overlapped for Sensors 7. But chances for the two results to have type II error are 80% and 82%, respectively. Figure 19 shows the comparisons of the impulse densities of the two cases. Note that the vertical scale starts at -10 here and that the chance of missing a difference is 69% for Sensor 4. Overall the results are not qualitatively different from those of Figure 17.

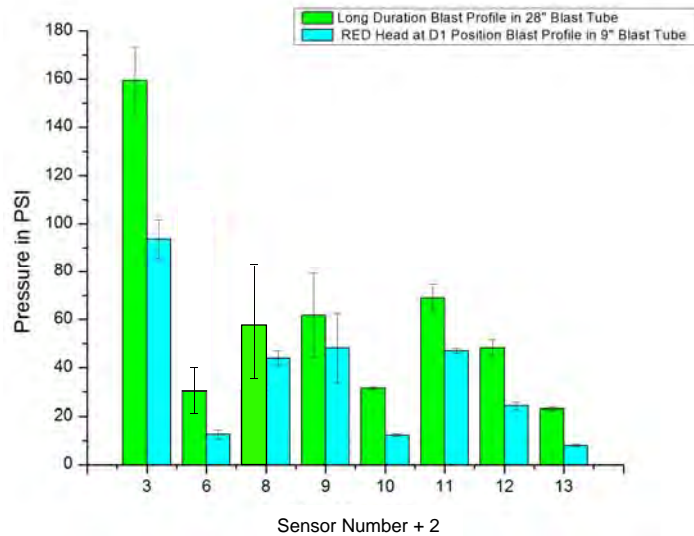


Figure 18: Peak overpressures induced on RED head by blasts generated with Case I (b) and Case II (a) conditions.

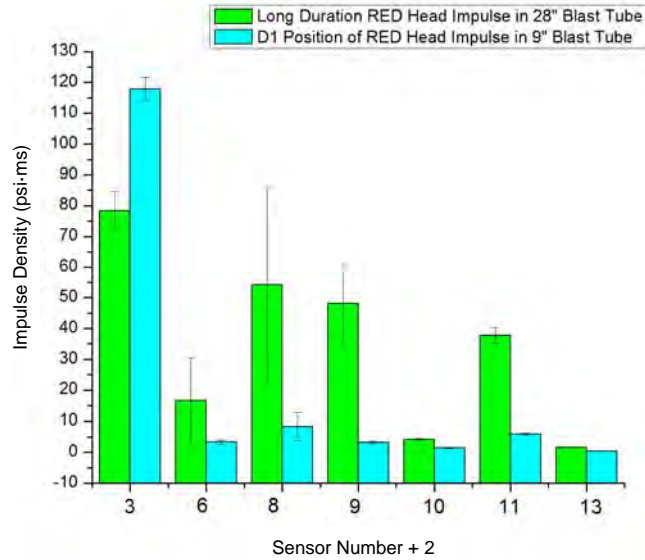


Figure 19: Impulse densities induced on RED head by blasts generated with Case I (b) and Case II (a) conditions.

Figures 20 and 21 show respectively the linear acceleration profiles measured by Accelerometers 1 and 2 at the center of gravity of the RED head during one of Case II (a) tests (RED head at D1 position outside the 9” tube). For Accelerometer 1 (aligned in X direction,), the maximum positive and negative values are 96 G and -83 G, respectively (Figure 20). Beyond 50 ms, the maximums are 1 G and -1 G, respectively. For Accelerometer 2 (aligned in Y direction), the maximum positive and negative values are 126 G and -22 G, respectively (Figure 21). Beyond 50 ms, the maximums are 1 G and -3 G, respectively. There is a noticeable sign of post-blast dynamic variation of the RED head motion in Y direction. It is likely caused by the unconfined flow outside the shock tube.

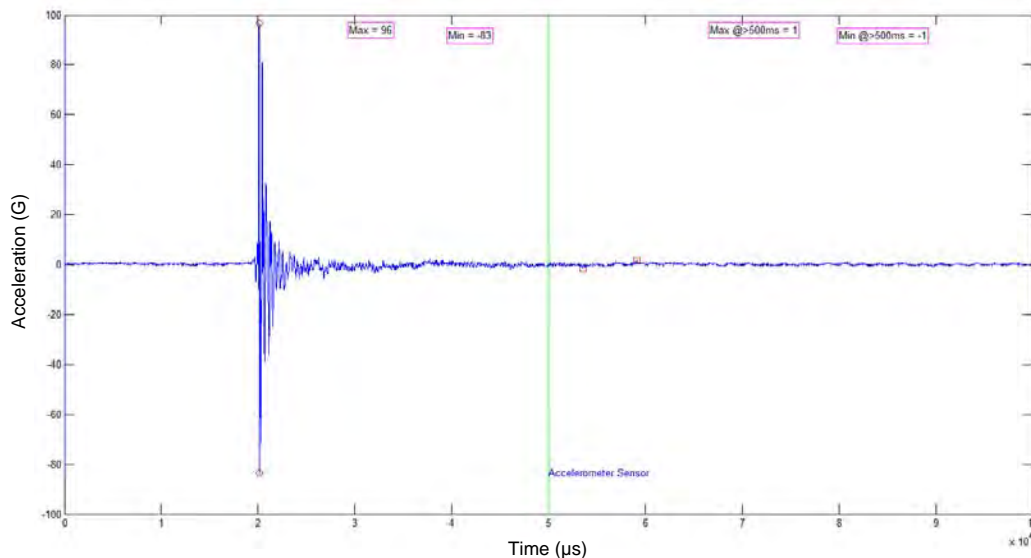


Figure 20: Linear acceleration history of RED head in X direction during a Case II (a) test (D1 position).

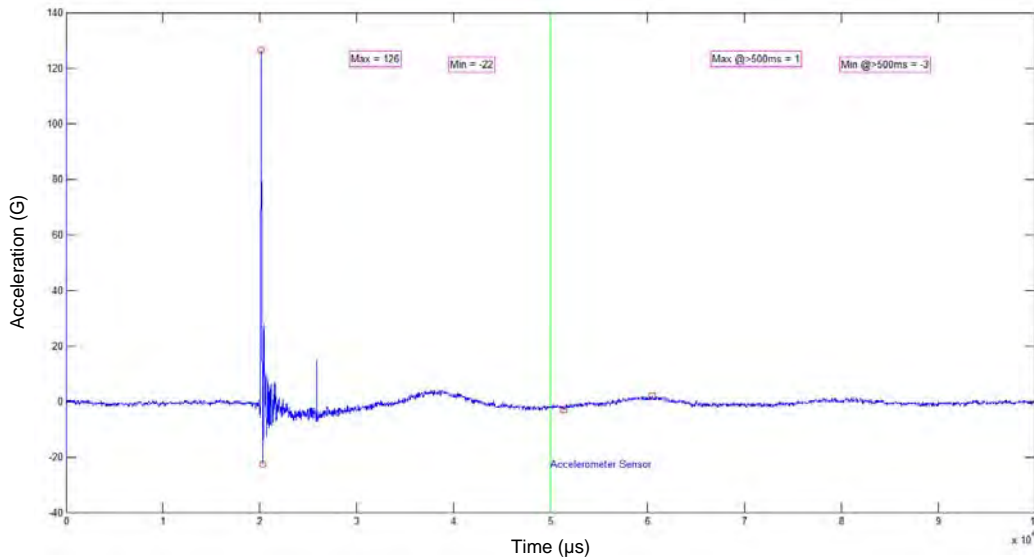


Figure 21: Linear acceleration history of RED head in Y direction during a Case II (a) test (D1 position).

Figure 22 shows the time history of angular rate measured at the center of gravity of the RED head during the same test. The maximum positive and negative values of the profile shown are 1527 °/s and -1839 °/s, respectively. Beyond 50 ms, the maximums are 127 °/s and -134 °/s, respectively. The post-blast dynamic variation of the RED head motion is more pronounced here. Though more visible than the in-tube tests, the post-blast secondary response in this case is again non-impulsive.

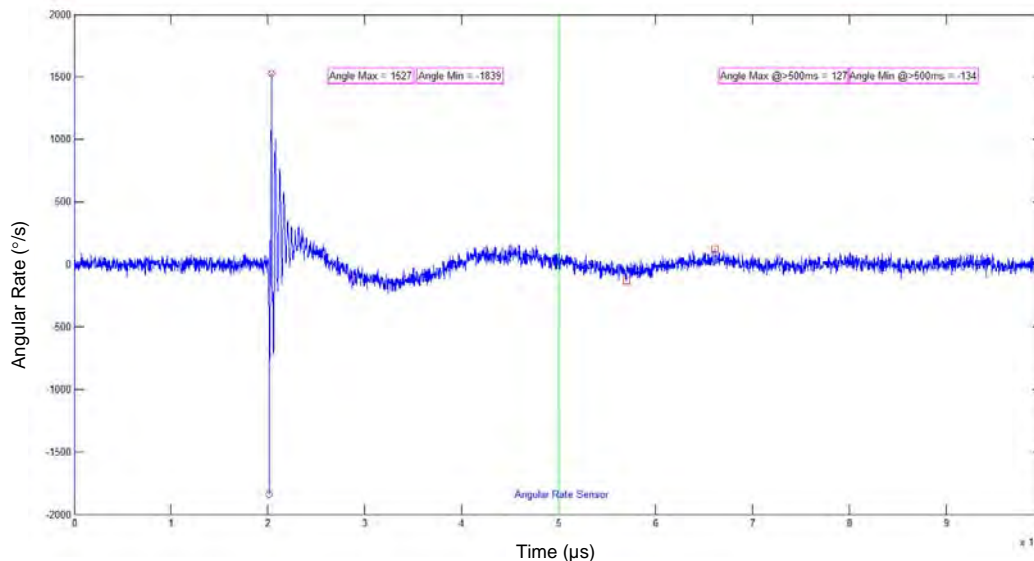


Figure 22: Angular rate history of RED head about Z axis during a Case II (a) test (D1 position).

Figure 23 presents the mean maximum positive and negative accelerations induced at the center of gravity of the RED head by the blasts generated with Case II (a) conditions (RED head at D1

position outside of the 9” tube) in comparison with those obtained under Case I (a) conditions (RED head inside the 28” tube facing 3 ms duration blasts). A statistically significant difference can be seen in both the positive and the negative accelerations in both X direction (Accelerometer 1) and Y direction (Accelerometer 2). Clearly, the acceleration data of Case II (a) do not match those of Case I (a), which agree very well with the live-fire acceleration data (see Figure 7).

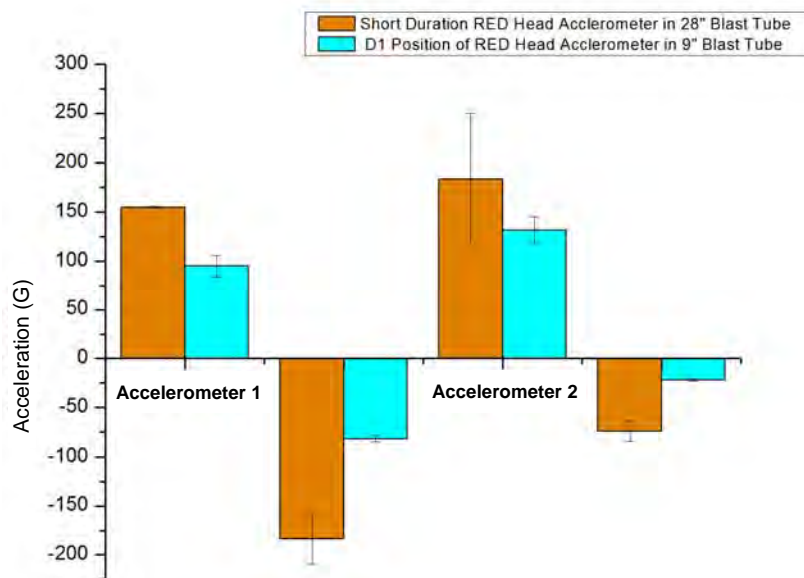


Figure 23: RED head mean maximum positive and negative accelerations induced by blasts generated with Case I (a) and Case II (a) conditions.

4.4 Case II (b): RED head outside 9” tube at D2 position with front bare head facing

A total of 4 tests intended to repeat the same loading condition were carried out for this case using UNL 9” shock tube. Placed at D2 position, the RED head is 6.5 in. from its nose tip to the shock tube muzzle. Figure 24 presents the peak overpressures induced at various locations on the RED head by the blasts generated with Case II (b) conditions in comparison with those of Case II (a) tests (RED head at D1 position outside the 9” tube). The comparisons with one error bar range being within the other are seen for Sensors 1, 4 and 9 even though they all have a 90% chance for missing a difference. The differences in the other comparisons are mostly small and become more noticeable only for Sensors 6 and 7. Overall the peak overpressures generated in the tests for the two cases are not significantly different. Figure 25 shows the comparisons of impulse densities of the two cases at various sensor locations in semi-logarithm scale. Except for Sensors 1, the difference is practically negligible even though power analyses indicated that the results of Sensors 4, 6, 7, and 8 have 65%, 66%, 95%, and 67% chances, respectively for type II error. The peak overpressure and impulse density results have no significant differences between the two cases.

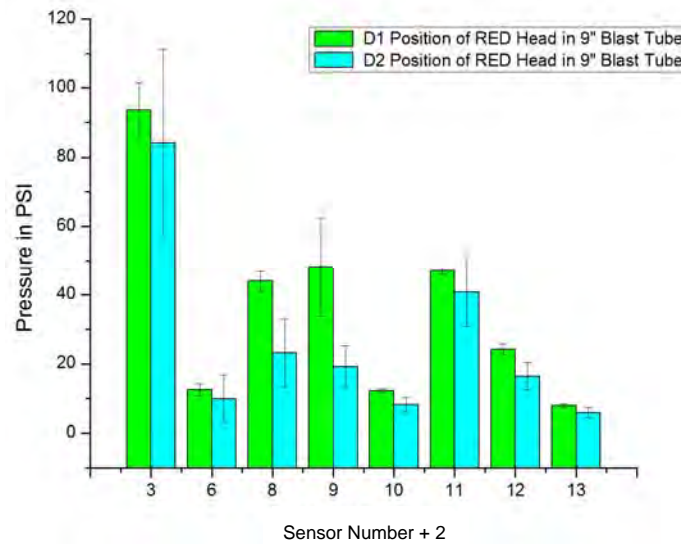


Figure 24: Peak overpressures induced on RED head by blasts generated with Case II (a) and Case II (b) conditions.

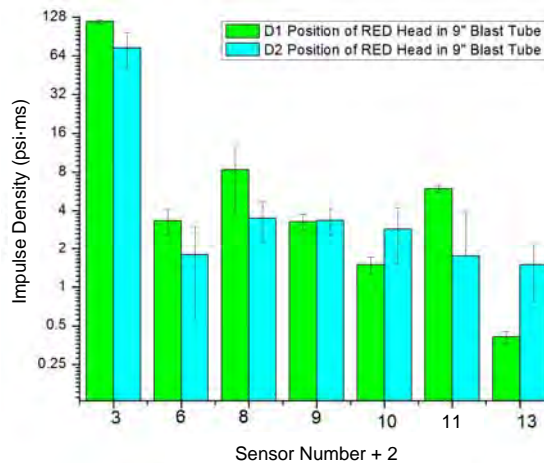


Figure 25: Impulses induced on RED head by blasts generated with Case II (a) and Case II (b) conditions.

Figures 26 and 27 show respectively the linear acceleration profiles measured by Accelerometers 1 and 2 at the center of gravity of the RED head during one of Case II (b) tests (RED head at D2 position outside the 9” tube). For Accelerometer 1 (aligned in X direction), the maximum positive and negative values are 36 G and -42 G, respectively (Figure 26). Beyond 50 ms, the maximums are 1 G and -1 G, respectively. For Accelerometer 2 (aligned in Y direction), the maximum positive and negative values are 44 G and -24 G, respectively (Figure 27). Beyond 50 ms, the maximums are 2 G and -1 G, respectively. Though non-impulsive and small, the post-blast dynamic variation of the RED head motion is visible not only in Y direction with lower frequency but also in X direction with higher frequency indicating stronger effects of the out-of-tube unconfined flow on the RED head than Case II (a), where the RED head was placed 5 in. closer to the tube muzzle.

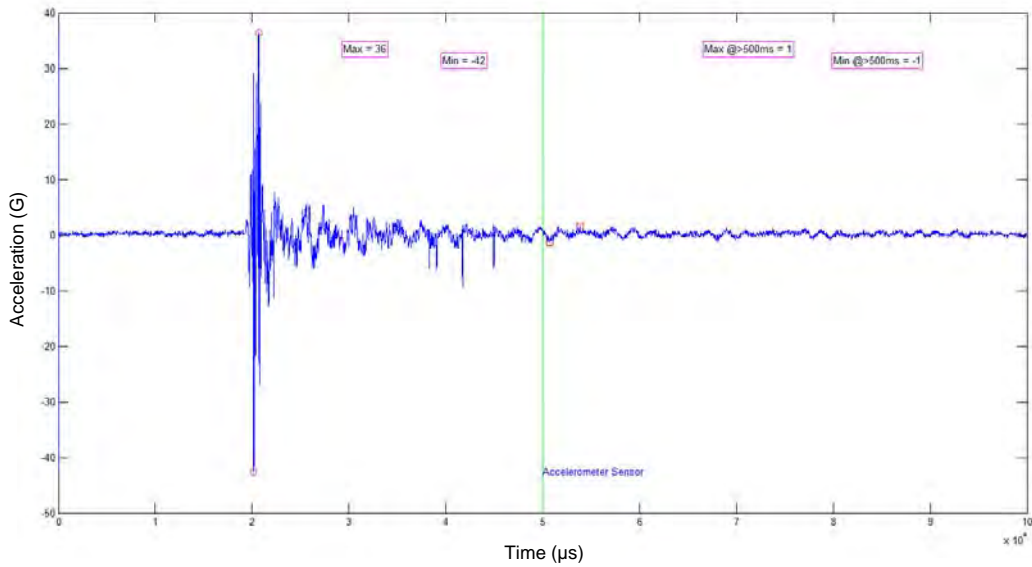


Figure 26: Linear acceleration history of RED head in X direction during a Case II (b) test (D2 position).

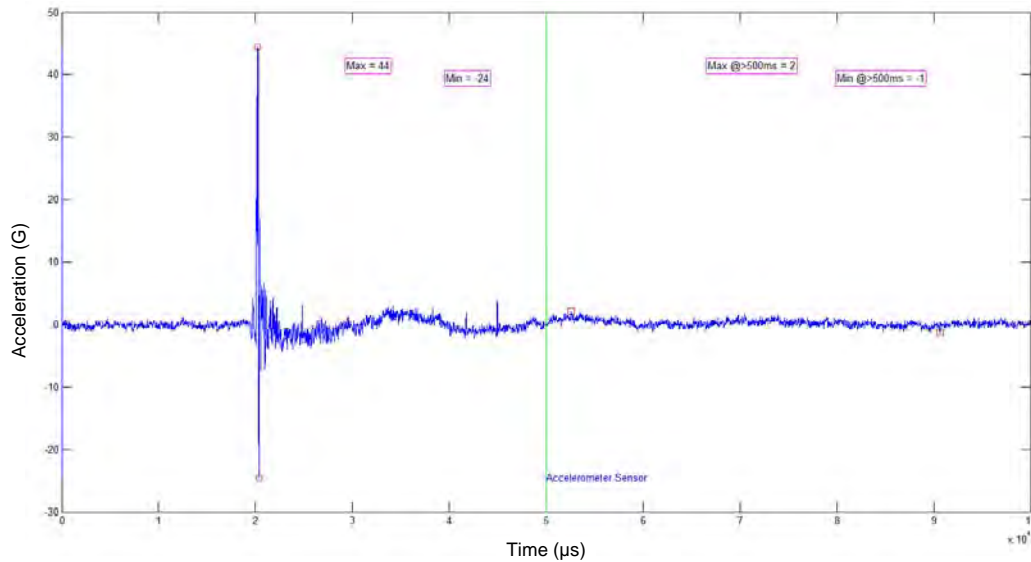


Figure 27: Linear acceleration history of RED head in Y direction during a Case II (b) test (D2 position).

Figure 28 shows the history of angular rate measured at the center of gravity of the RED head during the same test. The maximum positive and negative values in the profile shown are 568 °/s and -741 °/s, respectively. The maximum values after 50 ms are 103 °/s and -104 °/s, respectively. The post-blast dynamic variation of angular rate of the RED head is seen to be small and in lower frequency. The post-blast variations seen in Figures 26-28 are all non-impulsive and insignificant in magnitude compared to the RED head response to the primary blast loading.

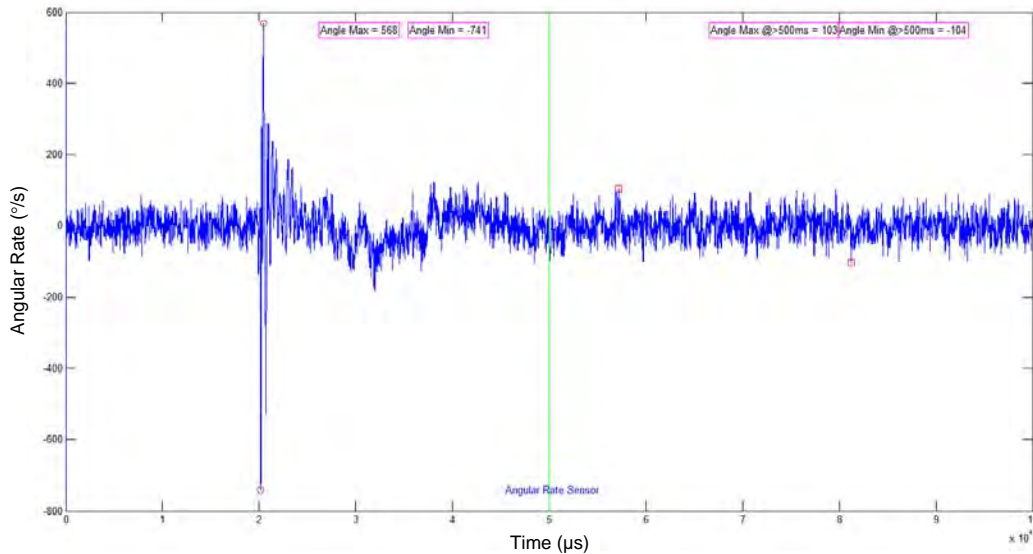


Figure 28: Angular rate history of RED head about Z axis during a Case II (b) test (D2 position).

Figure 29 presents the comparisons of the mean maximum positive and negative accelerations induced at the center of gravity of the RED head by the blasts generated with Case II (a) conditions (D1 position) and Case II (b) conditions (D2 position). In both X and Y directions, the maximum positive accelerations of Case II (b) are significantly lower than those of Case I (a), which are already lower than the targeted live-fire results (see Figures 7 and 23). The differences in the maximum negative accelerations are smaller in X direction (Accelerometer 1) and negligible in Y direction (Accelerometer 2). However, the latter has an 85% chance for missing a difference. Clearly, the maximum acceleration decreases with increasing RED head distance to the tube.

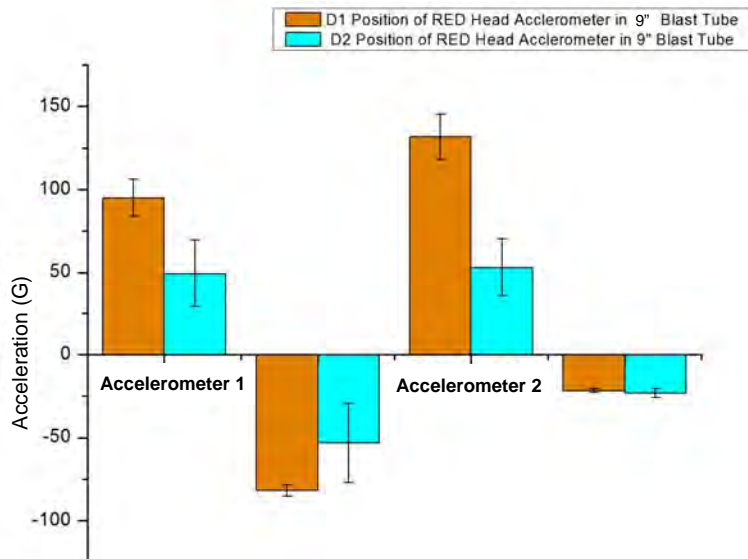


Figure 29: RED head mean maximum positive and negative accelerations induced by blasts generated with Case II (a) and Case II (b) conditions.

Figure 30 presents the maximum positive and negative angular rates at the center of gravity of the RED head in four comparisons (from left to right): between the data of the live-fire free-field blast tests [1] and those of Case I (a) (in-tube 3-ms blast tests), between the data of Case I (b) (in-tube 5-ms blast tests) and those of Case II (a) (blast tests at D1 out-of-tube position), between the data of Case I (a) and those of Case II (a), and between the data of Case II (a) and those of Case II (b) (blast tests at D2 out-of-tube position). The results of the live-fire tests are significantly lower than those of Case I (a) tests even though the linear acceleration results from the two are in very good agreement (see Figure 7). On the other hand, the results of Case II (b) tests, which did poorly in matching the targeted linear accelerations, are much closer to the targeted angular rates than those of the other shock tube tests presented. The differences in the RED head angular rates generated in the shock tube tests other than Case II (b) are small or negligible even though the chance for missing a difference is 91% for the positive rate comparisons between Case I (a) and Case II (a) and 86% for the negative rate comparison between the same pair. For a better matching with the live-fire angular rate data, a further tuning of the RED head tilt angle respect to the shock tube axis is needed.

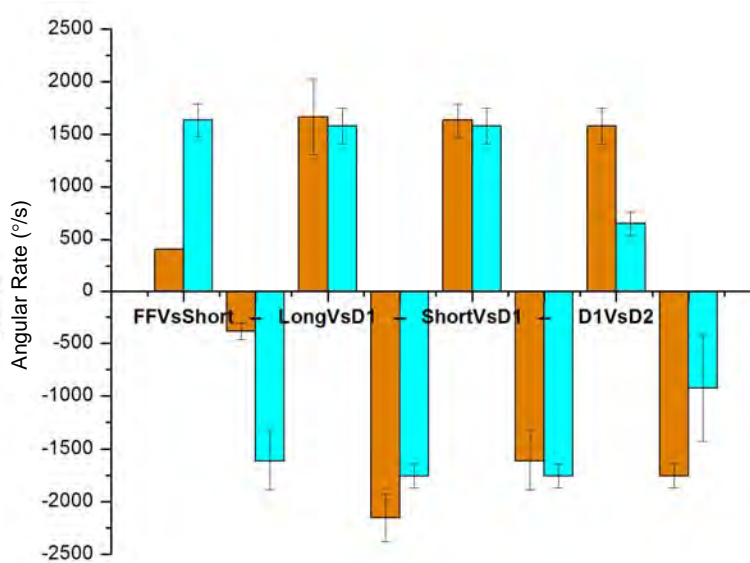


Figure 30: RED head mean maximum positive and negative angular rates for various blast loading conditions.

5 Closing Remarks

5.1 Peak Overpressure

The mean peak overpressures at the front most sensor (Sensor 1), which was directly against the blast wave, are seen to be significantly higher than those at the other sensors as expected. However, the difference between two mean peak overpressures at Sensor 1 is not necessarily scalable to that



between the corresponding mean peak overpressure distributions over the other sensors. For each shock tube test case presented, the overpressure distribution has a noticeable front-to-back amplitude decay in contrast to the live-fire data, in which sensor-to-sensor variations of the mean peak overpressures are small for the sensors mounted on the sides and the back of the RED head (see Figure 7). Furthermore, the ratio of the magnitude at the rear most sensor (Sensor 4) to that at the front most sensor (Sensor 1) is 28% for the live-fire data. For the in-tube tests, it is about 19%, which is a lower but still reasonable value. However, more pronounced reductions are seen for the out-of-tube tests: 14% for Case II (a) and 12% for Case II (b). Clearly, the lack of lateral inertia confinement to a blast exiting a shock tube diminishes its ability to sustain pressure as it engulfs the sample.

5.2 Impulse density

Impulse density is the time integration of the overpressure history over its positive duration and thus sensitive to both the peak overpressure and the overpressure decay profile. It is a more stringent measure for characterizing blast loading than the peak overpressure or the maximum acceleration (or G force). None of the shock tube blast tests presented in this report provides very good impulse density field match to those obtained from the live-fire blast tests. However, the impulse density fields generated by the blasts inside the 28" shock tube are more intense than those by the live-fire blasts everywhere (see Figure 11). The over simulation can therefore be reduced by further tuning the experimental conditions to achieve shorter pulse durations or faster post-peak decays than those of Case I (a) tests. On the other hand, there is no remedy for the difference between the impulse density fields generated by the blasts outside the 9" shock tube and those by the live-fire blasts because whereas the former are *an order of magnitude more intense* than the latter at the most front region, they are *less intense everywhere else* (see Figure 19 and Figure 11). In other words, an out-of-tube test designed to match the impulse density at the most front region will miss the targeted impulse density field completely elsewhere.

5.3 Acceleration and angular rate

According to U.S. Federal Motor Vehicle Safety Standard, the maximum peak acceleration threshold is 400 G. The maximum accelerations obtained from Accelerometers 1 and 2 are well within the safety limits for all the cases. The results for the angular rate of the RED head are similar. There is a good agreement in the RED head acceleration comparisons between the live-fire data and the data of the 3 ms blasts inside the 28" shock tube [Case I (a)]. However, compared to the latter, the maximum accelerations of the shock tube tests with the RED head being placed outside the 9" shock tube [Cases II (a) and (b)] are noticeably lower and decrease with increasing distance between the tube muzzle and the RED head. Shock tube testing with the sample being placed outside a tube of comparable cross-section size may not be able to generate the sample acceleration that mimics that attained under the live-fire free-field blast loading even if a good match is achieved for the peak overpressure in the most front region of the sample. Despite the



good comparisons of the maximum RED head accelerations between the live-fire data and the data of Case I (a), the comparisons of maximum positive and negative angular rates of the RED head are not as good between the two. For improved matching, the RED head tilt angle with respect to the shock tube axis needs to be further tuned in future.

Small post-blast secondary dynamic events can be identified in the linear acceleration and angular rate history data collected over the long period of time used in this work. These signals can be reasonably related to the visually observed large sample motions caused either by the interaction between the RED head and the expansion of the pre-compressed helium driver gas behind the primary blast wave or by that between the RED head and the laterally unconfined post-blast air flow outside the shock tube. It is important to note that beyond 50 ms the maximum RED head acceleration reading does not go above 12 G. Clearly, these post-blast secondary dynamic events are seen to diminish with increasing time. They are certainly non-impulsive and their resultant dynamic effects on the RED head are insignificant.

Reference

- [1] Namas Chandra, "Experimental Evaluation of Measurement Methodology for Primary Blast Loading Conditions," ARO/NATICK Final Report, University of Nebraska-Lincoln, 2013.